

การตรวจลักษณะเฉพาะทางไฟฟ้าของวัสดุอิเล็กทรอนิกส์ในเซลล์เชื้อเพลิงแบบออกไซด์ของแข็ง
ด้วยเทคนิคเอซีเอ็มพีแดนซ์สเปกโทรสโกปี



นางสาวอารีรักษ์ คำน้อย

สถาบันวิทยบริการ

จุฬาลงกรณ์มหาวิทยาลัย

วิทยานิพนธ์นี้เป็นส่วนหนึ่งของการศึกษาตามหลักสูตรปริญญาวิทยาศาสตรมหาบัณฑิต

สาขาวิชาเทคโนโลยีเซรามิก ภาควิชาวัสดุศาสตร์


คณะวิทยาศาสตร์ จุฬาลงกรณ์มหาวิทยาลัย

ปีการศึกษา 2548

ISBN 974-14-1847-7

ลิขสิทธิ์ของจุฬาลงกรณ์มหาวิทยาลัย

ELECTRICAL PROPERTY CHARACTERIZATION OF ELECTROLYTE MATERIALS IN SOLID OXIDE
FUEL CELLS BY AC IMPEDANCE SPECTROSCOPY



Miss Areerak Khamnoi

สภามหาวิทยาลัยบูรพาภิบาล
จุฬาลงกรณ์มหาวิทยาลัย
A Thesis Submitted in Partial Fulfillment of the Requirements
for the Degree of Master of Science Program in Ceramic Technology
Department of Materials Science

Faculty of Science

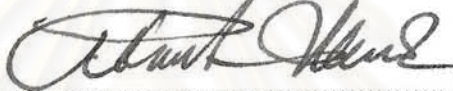
Chulalongkorn University

ISBN 974-14-1847-7

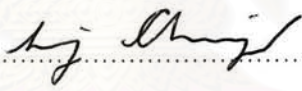
Academic year 2005


Thesis Title Electrical property characterization of electrolyte materials in Solid
Oxide Fuel Cells by AC-Impedance Spectroscopy
By Miss Areerak Khamnoi
Field of study Ceramic Technology
Thesis Advisor Associate Professor Supatra Jinawath, Ph.D.
Thesis Co-advisor Sumittra Charojrochkul, Ph.D.


Accepted by the Faculty of Science, Chulalongkorn University in Partial
Fulfillment of the Requirements for the Master 's Degree

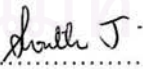

..... Dean of the Faculty of Science
(Professor Piamsak Menasveta, Ph.D.)

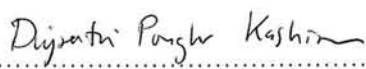
THESIS COMMITTEE


..... Chairman
(Associate Professor Saowaroj Chuayjuljit)


..... Thesis Advisor
(Associate Professor Supatra Jinawath, Ph.D.)


..... Thesis Co-advisor
(Sumittra Charojrochkul, Ph.D.)


..... Member
(Assistant Professor Sirithan Jiemsirilers, Ph.D.)


..... Member
(Dujreutai Pongkao Kashima, D. Eng.)

อารีรักษ์ คำน้อย : การตรวจลักษณะเฉพาะทางไฟฟ้าของวัสดุอิเล็กโทรไลต์ในเซลล์เชื้อเพลิงแบบ
ออกไซด์ของแข็งด้วยเทคนิคเอซิมพีแดนซ์สเปกโทรสโกปี (ELECTRICAL PROPERTY
CHARACTERIZATION OF ELECTROLYTE MATERIALS IN SOLID OXIDE FUEL CELLS
BY AC - IMPEDANCE SPECTROSCOPY) อ. ที่ปรึกษา: รศ.ดร. สุพัตรา จินาวัดน์,
อ. ที่ปรึกษาร่วม: ดร. สุมิตรา จรสโรจน์กุล, 112 หน้า. ISBN 974-14-1847-7.

อิทเทรียสเดบิลไลท์เซอร์โคเนียเป็นวัสดุที่ถูกนำมาใช้เป็นวัสดุอิเล็กโทรไลต์ในเซลล์เชื้อเพลิงแบบ
ออกไซด์ของแข็งเนื่องจากมีค่าการนำไฟฟ้าสูง (ประมาณ 0.1 ซีเมนต์ต่อเซนติเมตร ที่อุณหภูมิ 1000 องศา
เซลเซียส) ซึ่งเหมาะสมกับอุณหภูมิในการทำงานของเซลล์เชื้อเพลิงแบบออกไซด์ของแข็ง ในงานวิจัยนี้ได้
ทำการศึกษาลักษณะเฉพาะทางไฟฟ้าของอิทเทรียสเดบิลไลท์เซอร์โคเนียที่มีปริมาณอิทเทรียร้อยละ 3 8
และ 10 โดยโมล ซึ่งผงอิเล็กโทรไลต์ที่นำมาจากผู้ผลิตที่ต่างกัน ได้แก่ MEL DAIICHI และ TOSOH ทำการ
ตรวจสอบค่าการนำไฟฟ้าด้วยเทคนิคเอซิมพีแดนซ์สเปกโทรสโกปีในช่วงอุณหภูมิ 275 ถึง 600 องศา
เซลเซียส ความถี่ 0.05 ถึง 10^7 เฮิรตซ์ โดยค่าความต้านทานจากเกรน และขอบเกรนสามารถแสดงได้ด้วย
กราฟอิมพีแดนซ์ ซึ่งจากผลการทดลองพบว่าลักษณะของกราฟที่ได้แตกต่างกันตามแหล่งผู้ผลิตแม้ว่าจะ
เติมอิทเทรียในปริมาณที่เท่ากันก็ตาม ทั้งนี้อาจเกิดจากสิ่งเจือปนในสารตั้งต้นและสภาวะในการเผาขึ้นงาน
ได้ตรวจสอบองค์ประกอบของสารตั้งต้นด้วยเทคนิคเอกซเรย์ฟลูออเรสเซนซ์ (X-Ray Fluorescence
Technique) และดูโครงสร้างทางจุลภาคด้วยเทคนิคสแกนนิ่งอิเล็กตรอนไมโครสโกปี (Scanning
Electron Microscopy) จากผลการทดลองพบว่าการวิเคราะห์ผลจากเอซิมพีแดนซ์สเปกโทรสโกปีร่วมกับ
ผลโครงสร้างทางจุลภาคสามารถตรวจสอบสมบัติทางไฟฟ้าที่เหมาะสมของอิทเทรียสเดบิลไลท์เซอร์โคเนีย
ได้

สถาบันวิทยบริการ จุฬาลงกรณ์มหาวิทยาลัย

ภาควิชา.....วัสดุศาสตร์.....ลายมือชื่อนิติ.....จารย์กมล คำน้อย
สาขาวิชา.....เทคโนโลยีเซรามิก.....ลายมือชื่ออาจารย์ที่ปรึกษา.....สุพัตรา
ปีการศึกษา.....2548.....ลายมือชื่ออาจารย์ที่ปรึกษาร่วม.....

4672507423 : MAJOR CERAMIC TECHNOLOGY

KEY WORD: YSZ/ AC-IMPEDANCE SPECTROSCOPY / SOFC / ELECTROLYTE

AREERAK KHAMNOI: ELECTRICAL PROPERTY CHARACTERIZATION OF ELECTROLYTE MATERIALS IN SOLID OXIDE FUEL CELLS BY AC - IMPEDANCE SPECTROSCOPY. THESIS ADVISOR: ASSOC. PROF. SUPATRA JINAWATH, Ph.D. THESIS COADVISOR : SUMITTRA CHAROJROCHKUL, Ph.D. 112 pp. ISBN 974-14-1847-7.

Yttria - Stabilized Zirconia (YSZ) is an important solid electrolyte used in Solid Oxide Fuel Cells (SOFCs) due to its good electrical (0.1 siemens/cm at 1000⁰C) and mechanical properties. The electrical property of 3, 8 and 10 mol% Y₂O₃ - doped ZrO₂ were measured using AC-Impedance Spectroscopy, in the temperature range of 275 – 600⁰C and over the frequency range of 0.05 – 10⁷ Hz. From the impedance spectra, the bulk and grain boundary resistances of YSZ pellets from various suppliers (MEL, TOSOH, and DAIICHI) were significantly influenced by the containing impurities and the sintering conditions. The impurities in the starting powder were analyzed using X-Ray Fluorescence Technique (XRF), while the microstructure was investigated using Scanning Electron Microscope (SEM). The correlation between the electrical conductivity and sintering temperature from various electrolyte materials was developed. As a result, the AC-Impedance Spectroscopy technique in combination with microstructural investigation can be used to study the electrical property of YSZ effectively.

Department.....Materials Science..... Student's signature.....*Areerak*
 Field of study.....Ceramic Technology..... Advisor's signature.....*Supatra*
 Academic year...2005..... Co-advisor's signature.....*Sumittra*

ACKNOWLEDGEMENTS

First of all, I would like to express my gratitude to the financial support from the Office of the Atomic for Peace, Ministry of Science and Technology for my graduate study. Without them, the success of my graduate study would not have been possible. During my Master study, I also hold a deep gratitude to many people who have contributed to this research work and my success.

I would like to express special thanks to my advisors, Assoc. Prof. Dr. Supatra Jinawath from Chulalongkorn University and Dr. Sumittra Charojrochkul from National Metal and Materials Technology Center (MTEC) for their guidance, support, encouragement of the research work. Moreover, I spent 16 months to do experimental work at MTEC. Therefore, I would like to thanks all fuel cell researchers at MTEC who contributed to my success and are good friends of mine, namely, Dr. Rapeepong Suwanwarangkul, Hathaitip Mahaudom, Suda Wanakitti, Warunya Boonjob, Supatra Chewathanakup, and Touchakarn Boonyaprasit. I would also like to thank all researchers in Optical Microscopy and Image Analysis and Scanning Electron Microscope laboratories for preparing specimens and analyzing their microstructure, respectively.

All professors at the department of Materials Science, Faculty of Science are acknowledged for their help in providing knowledge for me during the course of my study.

All my friends at the Department of Materials Science and the Office of the Atomic for Peace are also acknowledged for their friendship, support and encouragement.

Last but not least, I would like to dedicate my thesis work to my family, without whom, this thesis work would not have so much meaning.

CONTENTS

	page
Abstract (Thai)	iv
Abstract (English)	v
Acknowledgements	vi
Contents	vii
List of Tables	ix
List of Figures	x
List of abbreviations.....	xiv
List of symbols	xv
Chapter I Introduction	1
Chapter II Literature Review	4
2.1 Fuel Cells Principle	4
2.2 Material for SOFCs	6
2.2.1 Electrolyte	7
2.2.2 Anode	9
2.2.3 Cathode	10
2.2.4 Interconnect	11
2.3 AC Impedance Spectroscopy Technique	12
2.3.1 Impedance Definition	13
2.3.2 Elementary Analysis of Impedance Spectra	17
Chapter III Experimental Procedure	22
3.1 Raw materials Characterization	22
3.2 Preparation of electrolyte materials	22
3.2.1 Equipments	22
3.2.2 Preparation	23
3.3 Characterization of Electrolyte Materials	25
3.3.1 Density	25
3.3.2 Microstructure of electrolyte materials	25
3.3.3 Measurement System for Impedance Spectroscopy	26

	page
Chapter IV Result and discussion	29
4.1 Investigation of 3Y MEL (3 mol%Y ₂ O ₃ -ZrO ₂ -MEL)	29
4.2 Investigation of 8Y MEL (8 mol%Y ₂ O ₃ -ZrO ₂ MEL)	36
4.3 Investigation of 8Y TOSOH (8 mol%Y ₂ O ₃ -ZrO ₂ TOSOH)	43
4.4 Investigation of 8Y DAIICHI (8 mol%Y ₂ O ₃ -ZrO ₂ DAIICHI)	50
4.5 Investigation of 10Y DAIICHI (10 mol%Y ₂ O ₃ -ZrO ₂ DAIICHI)	57
4.6 Discussion of the pellet impedance spectra	64
4.7 Characterization of electrolyte materials, prepared by tape casting	65
4.8 Summary	68
Chapter V Conclusion	72
Chapter VI Suggestions for the future work	74
References	75
Appendices.....	78
Appendix A.....	79
Appendix B.....	82
Biography	112

สถาบันวิทยบริการ
จุฬาลงกรณ์มหาวิทยาลัย

	page
Table 3.1 XRF and particle size distribution results for Ytria Stabilized Zirconia (YSZ)	22
Table 3.2 Preparation and characterization equipments	23
Table 3.3 Information of YSZ powder	24
Table 4.1 The X-Ray Fluorescence results of doped zirconia powder	30
Table 4.2 Conductivity and Activation energy at 800°C for 3 mol% Y ₂ O ₃ – ZrO ₂ (MEL)	34
Table 4.3 Conductivity and Activation energy at 800°C for 8 mol% Y ₂ O ₃ – ZrO ₂ (MEL)	41
Table 4.4 Conductivity and Activation energy at 800°C for 8 mol% Y ₂ O ₃ – ZrO ₂ (TOSOH)	48
Table 4.5 Conductivity and Activation energy at 800°C for 8 mol% Y ₂ O ₃ – ZrO ₂ (DAIICHI)	55
Table 4.6 Conductivity and Activation energy at 800°C for 10 mol% Y ₂ O ₃ – ZrO ₂ (DAIICHI)	62

LIST OF FIGURES

	page
Fig. 2.1 Schematic diagram of a Solid Oxide Fuel Cell operation	5
Fig. 2.2 The crystal structure of cubic zirconia, oxygen is blue, zirconium is green	8
Fig. 2.3 Variation of ionic conductivity of stabilized ZrO_2 with dopant concentration at 1080 K	10
Fig. 2.4 Schematic diagram of ideal impedance spectra	14
Fig. 2.5 Sinusoidal wave applied across the electrochemical cell	17
Fig. 2.6 Equivalent circuit model of R-C unit	18
Fig. 2.7 Schematic representation of Nyquist (a) plot and Bode plot (b)	18
Fig. 2.8 Impedance spectra of ceramic oxide and its equivalent circuit	18
Fig. 3.1 Flow chart of experimental procedures	24
Fig. 3.2 Schematic diagram of measurement system for the characterization of electrolyte materials using AC Impedance Spectroscopy	26
Fig. 3.3 An equivalent circuit and its corresponding impedance plot	27
Fig. 4.1 Impedance spectra of 3 mol% Y_2O_3 - ZrO_2 electrolyte after heat treatment at (a) $1500^\circ C$ and (b) $1550^\circ C$ (at various sintering time). All the measurements were taken at $400^\circ C$	31
Fig. 4.2 Impedance spectra of 3 mol% Y_2O_3 - ZrO_2 electrolyte after sintering for (a) 1 hour, (b) 2 hours, and (c) 4 hours at $1500^\circ C$ and $1550^\circ C$. All the measurements were taken at $400^\circ C$	32
Fig. 4.3 Arrhenius plots of the bulk and grain boundary conductivities for 3 mol% $Y_2O_3 - ZrO_2$ (MEL) sintered at $1500^\circ C$ (a) and $1550^\circ C$ (b) [for 1 hour, 2 hours and 4 hours].....	33
Fig. 4.4 SEM micrographs of 3Y MEL sintering at $1500^\circ C$ (a) and $1550^\circ C$ (b) for 4 hours	35
Fig. 4.5 The relative density of 3 mol% Y_2O_3 - ZrO_2 (MEL) sintering at $1500^\circ C$ and $1550^\circ C$	36

	page
Fig. 4.6 Impedance spectra of 8 mol% Y_2O_3 - ZrO_2 (MEL) electrolyte after sintering at a) 1500°C and (b) 1550°C (at various sintering time). All the measurements were taken at 400°C	38
Fig. 4.7 Impedance spectra of 8mol% Y_2O_3 - ZrO_2 (MEL) electrolyte after sintering for (a) 1hour, (b) 2 hours, and (c) 4 hours at 1500°C and 1550°C. All the measurements were taken at 400°	39
Fig. 4.8 Arrhenius plots of the ionic conductivity for 8 mol% Y_2O_3 - ZrO_2 (MEL) sintered at 1500°C(a) and 1550°C (b) [for 1 hour, 2 hours and 4 hours]	40
Fig. 4.9 SEM micrographs of 8 mol% Y_2O_3 - ZrO_2 (MEL)sintering at 1500°C (a) and 1550°C (b) for 4 hours	42
Fig. 4.10 The relative density of 8 mol% Y_2O_3 - ZrO_2 (MEL) sintering at 1500°C and 1550°C	43
Fig. 4.11 Impedance spectra of 8 mol% Y_2O_3 - ZrO_2 (TOSOH) electrolyte after sintering at (a) 1500°C and (b) 1550°C (at various sintering time). All the measurements were taken at 400°C	45
Fig. 4.12 Impedance spectra of 8 mol% Y_2O_3 - ZrO_2 (TOSOH) electrolyte after sintering for (a) 1 hour, (b) 2 hours, and (c) 4 hours at different temperature. All the measurements were taken at 400°C.....	46
Fig. 4.13 Arrhenius plots of the ionic conductivity for 8 mol% Y_2O_3 - ZrO_2 (TOSOH) sintered at1500°C (a) and 1550°C (b) [for1 hour, 2 hours and 4 hours	47
Fig. 4.14 SEM micrographs of 8 mol% Y_2O_3 - ZrO_2 (TOSOH) sintering at 1500°C (a) and 1550°C (b) for 4 hours	49
Fig. 4.15 The relative density of 8 mol% Y_2O_3 - ZrO_2 (TOSOH) sintering at 1500°C and 550°C	50
Fig. 4.16 Impedance spectra of 8 mol% Y_2O_3 - ZrO_2 (DAII CHI) electrolyte after sintering for (a) 1500°C and (b) 1550°C (at various sintering time). All the measurements were taken at 400°C	52

	page
Fig. 4.17 Impedance spectra of 8 mol% Y_2O_3 - ZrO_2 (DAIICHI) electrolyte after sintering for (a) 1 hour, (b) 2 hours, and (c) 4 hours at 1500°C and 1550°C. All the measurements were taken at 400°C	53
Fig. 4.18 Arrhenius plts of the ionic conductivity 8 mol% Y_2O_3 - ZrO_2 (DAIICHI) sintered at 1500°C (a) and 1550°C (b) at 1 hour, 2 hours and 4 hours	54
Fig. 4.19 SEM micrographs of 8 mol% Y_2O_3 - ZrO_2 (DAIICHI) sintering at 1500°C (a) and 1550°C (b) for 4 hours	56
Fig 4.20 The relative density of 8 mol% Y_2O_3 - ZrO_2 (DAIICHI) sintering at 1500°C and 1550°C	56
Fig. 4.21 Impedance spectra of 10mol% Y_2O_3 - ZrO_2 (DAIICHI) electrolyte after sintering at (a) 1500°C and (b) 1550°C for (at various sintering time). All the measurements were taken at 400°C	59
Fig. 4.22 Impedance spectra of 10 mol% Y_2O_3 - ZrO_2 (DAIICHI) electrolyte after sintering for (a) 1 hour, (b) 2 hours, and (c) 4 hours at 1500°C and 1550°C. All the measurements were taken at 400°C	60
Fig. 4.23 Arrhenius plots of the ionic conductivity for 10 mol% Y_2O_3 - ZrO_2 (DAIICHI) sintered at 1500°C (a) and 1550°C (b)1 hour, 2 hours and 4 Hours	61
Fig. 4.24 SEM micrographs of 10 mol% Y_2O_3 - ZrO_2 (DAIICHI) sintering at 1500°C (a) and 1550°C (b) for 4 hours	63
Fig. 4.25 The relative density of 10 mol% Y_2O_3 - ZrO_2 sintering at 1500°C and 1550°C	64
Fig. 4.26 Impedance spectra of pellets electrolyte from various suppliers (DAIICHI, MEL and TOSOH) after sintering at 1550°C for 4 hours. Impedance spectra were taken at 400°C	65
Fig 4.27 Impedance spectra of 8 mol% Y_2O_3 - ZrO_2 MEL, TOSOH and DAIICHI electrolyte (tape casting) after sintering for 4 hours at 1500°C All the measurements were taken at 400°C	66

	page
Fig 4.28 Arrhenius plots of the bulk and grain boundary conductivities for 8 mol% $Y_2O_3 - ZrO_2$ sintered at $1500^\circ C$ for 4 hours.(tape casting).....	67
Fig 4.29 SEM micrographs of 8 mol% $Y_2O_3-ZrO_2$ sintering at $1500^\circ C$ for 4 hours, [MEL (a), TOSOH (b), and DAIICHI (c)] (tape casting)	68
Fig 4.30 Impedance spectra of 8 mol% $Y_2O_3-ZrO_2$ MEL, TOSOH and DAIICHI electrolyte after sintering for 4 hours at $1500^\circ C$ (prepared by pellet and tape casting). All the measurements were taken at $400^\circ C$	71



สถาบันวิทยบริการ
จุฬาลงกรณ์มหาวิทยาลัย

LIST OF ABBREVIATIONS

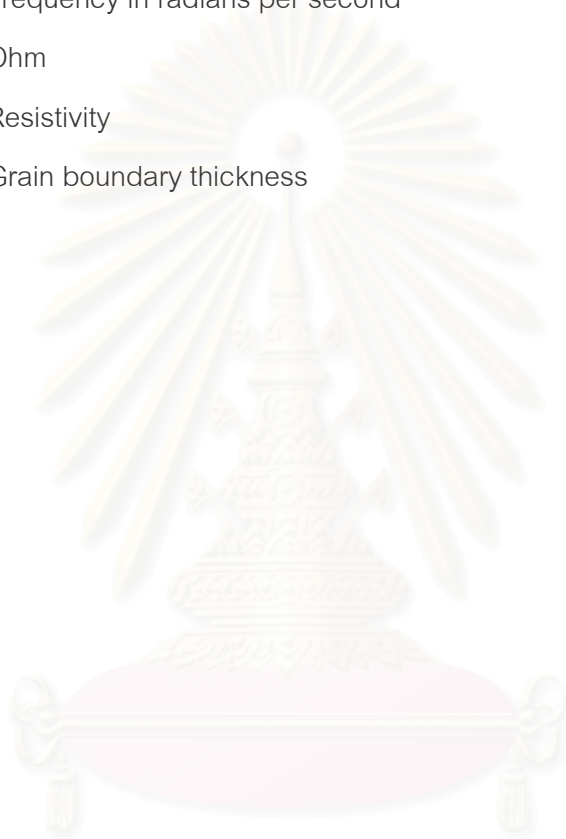
AC	Alternate Current
AFC	Alkaline Fuel Cell
DC	Direct Current
LSM	Lanthanum Strontium Manganite
MCFC	Molten Carbonate Fuel Cell
PAFC	Phosphoric Acid Fuel Cell
PEMFC	Proton Exchange Membrane Fuel Cell
SOFC	Solid Oxide Fuel Cell
YSZ	Ytria Stabilized Zircnia



สถาบันวิทยบริการ
จุฬาลงกรณ์มหาวิทยาลัย

LIST OF SYMBOLS

f	frequency
σ	Electrical conductivity
μ	Micron
θ	Phase shift in radians
ω	Frequency in radians per second
Ω	Ohm
ρ	Resistivity
δ	Grain boundary thickness



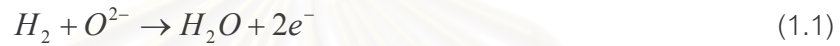
สถาบันวิทยบริการ
จุฬาลงกรณ์มหาวิทยาลัย

CHAPTER I

INTRODUCTION

Fuel cells are electrochemical devices that convert chemical reaction directly to electric power and heat by electrochemical combination of a fuel with an oxidant [1-3]. The basic physical structure or building block of a fuel cell consists of an electrolyte layer in contact with a porous anode and cathode on either side.

The oxidation of hydrogen at an anode is as follows:



The oxygen reduction at a cathode:



A fuel cell has components and characteristics similar to a typical battery, but differs in several aspects. A battery is an energy storage device that the maximum energy available is determined by the amount of chemical reactant stored. The battery will cease to produce electrical energy when the chemical reactants are consumed (i.e., discharged). In a secondary battery, the reactants are regenerated by recharging, which involves putting energy into the battery from an external source. The fuel cell, on the other hand, is an energy conversion device that theoretically has the capability of producing electrical energy for as long as the fuel and oxidant are supplied to the electrodes.

The primary feature of a fuel cell is its high conversion efficiency, up to 45 – 60%. A fuel cell converts a chemical energy of fuel directly into electrical energy. Thus, the usual losses involved in conversion of fuel to heat, to mechanical energy and then to electrical energy are avoided.

Emissions of pollutants from fuel cells are several orders of magnitude lower than those produced by conventional power generators. Production of undesirable emissions such as NO_x, SO_x, and particulates is either negligible or undetectable for fuel cells systems. According to the potential in reducing the environmental impact and geopolitical consequences of use of fossil fuels, fuel cells have emerged as tantalizing alternatives to combustion engines. In addition to high efficiency and low emissions, fuel cells are attractive for modular and distributed generation nature, with zero noise pollution. They will also play an essential role in the future hydrogen economy [1].

Among the different types of fuel cells, the high temperature fuel cell with a solid electrolyte is name a Solid Oxide Fuel Cell (SOFC).The use of solid electrolyte in SOFC eliminates material corrosion and liquid electrolyte management problems. The conductivity requirement for solid electrolyte necessitates high operating temperatures (600° – 1000°C). SOFC is particularly interesting because of three reasons. Firstly, it is among the highest degree of conversion efficiency. Secondly, the direct uses of natural gas or hydrocarbon fuels without expensive reforming (internal reforming) are possible. Finally, the waste heat at high temperature can be further utilized in many different ways to improve the overall efficiency. Due to the mentioned advantages, the SOFC is being studied and developed for its application in the stationary energy conversion. During the past years, further potential applications have been added to the areas of the distributed power generator and electric vehicles.

The most common materials for the SOFC are oxide ion conducting, yttria stabilized zirconia (YSZ) as an electrolyte, strontium-doped lanthanum manganite (LSM) as a cathode, nickel/YSZ as an anode , and doped lanthanum chromite or high-temperature metals as an interconnect. The main features of the SOFC are all solid-state construction and high temperature operation. Improvements are needed in the design of electrodes structure, the selection of suitable electrolytes, and the development of compatible materials to support the reactions [4].

The electrolyte of the SOFC is an oxygen conductor. The electrolyte conducts ions between the anode and cathode. The electrolyte carries the ions produced at the

cathode to the anode to balance the charge from the electron flow and complete the electrical circuit. The electrolyte also separates the fuel from the oxidant. The electrolyte must be stable in both reducing and oxidizing environments, and must have sufficiently high ionic conductivity with low electronic conductivity at the cell operating temperature. In addition, the electrolyte must be dense enough to prevent gas cross leakage [2-5].

An Impedance Spectroscopy (IS) is a non-destructive method for evaluation of a wide range of materials, including corrosion inhibitors, batteries and fuel cells. An Impedance Spectroscopy is a tool for investigating the electrical and electrochemical properties of materials and systems. The investigator typically compares or fits the impedance data to an equivalent circuit. IS is becoming a popular analytical tool in materials research and development as it involves a relatively simple electrical measurement that can readily be automated and whose results may often be correlated with many complex materials variables. The typical variables include effect of mass transport, rates of chemical reactions, corrosion and dielectric properties to defects, microstructure, and compositional influences on the conductance of solids [6].

In this thesis, the electrical characterization of the electrolyte materials of SOFC has been carried out using an AC impedance spectroscopy technique. Electrolyte material used in this study is yttria stabilized zirconia (3, 8, and 10mol% Y_2O_3 in ZrO_2 , YSZ).

Objectives of this thesis are the followings:

1. to characterize electrical property of electrolyte materials of SOFC using an AC-Impedance Spectroscopy technique,
2. to identify good preparation conditions for optimal electrical property of YSZ electrolyte, and
3. to correlate between the mechanism of electrical conductivity with the experimental results.

CHAPTER II

LITERATURE REVIEW

2.1 Fuel Cells Principle

2.1.1 Principle

Fuel Cells are energy conversion devices that produce electricity and heat by electrochemical combination of a fuel with an oxidant. The primary components of a fuel cell are an ion conducting electrolyte, a cathode, and an anode, as shown schematically in Fig. 2.1. A Fuel (e.g. hydrogen) is fed to the anode where it is oxidized and electrons are released to the external circuit. Oxidant (e.g. oxygen) is fed to the cathode where it is reduced and electrons are accepted from the external circuit. The electrons flow from the anode to the cathode through the external circuit that producing direct electric current. Direct chemical combustion is prevented by the electrolyte that separates the fuel (H_2) from the oxidant (O_2). Although the electrolyte serves as a barrier to gas diffusion, but will let ions migrate across [2-3, 5].

The oxidation of hydrogen at an anode is as follows:



The oxygen reduction at a cathode:



The overall reaction:



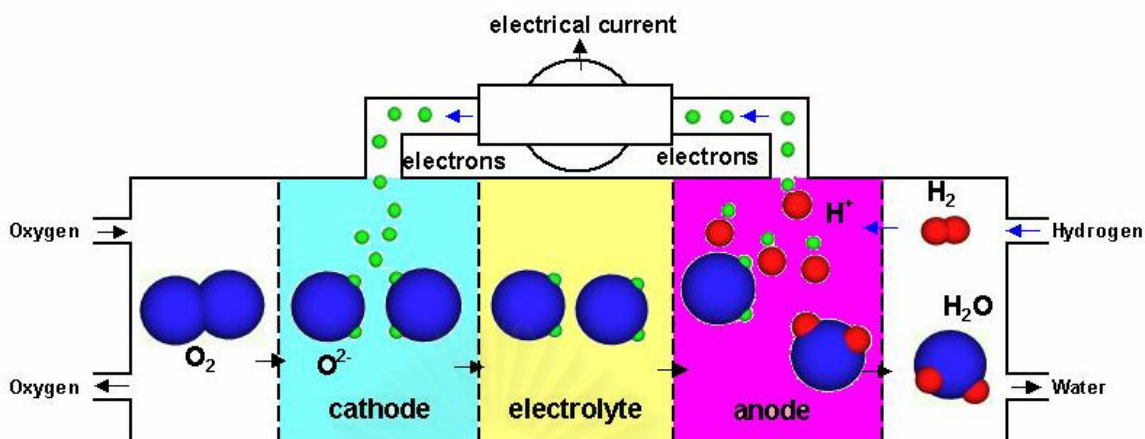


Fig.2.1: Schematic diagram of a Solid Oxide Fuel Cell operation

2.1.2 Types of Fuel Cells

The different types of fuel cells are named according to their electrolyte materials [4]. The Alkaline Fuel Cell (AFC) uses a concentrated solution of potassium hydroxide (KOH) in water as an electrolyte. Hydroxyl ions (OH^-) migrate from the cathode to the anode in these fuel cells. Hydrogen gas supplied to the anode reacts with the OH^- ions to produce water. The reaction releases electrons, which provide electric power. The operation temperature is in the range of 50 – 200°C. The AFC was used on the Apollo space shuttle and Orbiter spacecraft. The AFC suffers from one major problem that the strong alkaline electrolyte reacts with CO_2 , which eventually reduces the electrolyte conductivity. This means that pure oxygen and hydrogen must be used.

The Phosphoric Acid fuel Cell (PAFC) operates at temperatures of 200°C, using H_3PO_4 as an electrolyte. The PAFC was the first to be produced commercially, which operates at 200°C. Stationary units range from 50 to 200 kW in capacity. The platinum catalyst in the carbon-based electrodes is expensive. Carbon monoxide and sulphur, which are contaminants in hydrogen from fossil fuels, can significantly decrease the

lifetime of electrode. Since the acid is used as an electrolyte, the components in the cell need to be corrosion-resistant, that increases the cost.

The Proton Exchange Membrane Fuel Cell (PEMFC) is called Polymer Electrolyte Fuel Cell (PEFC). The PEMFC uses thin polymer membrane as an electrolyte. The polymer membrane coated with a thin layer of platinum catalyst to enhance the electrochemical reaction. The PEMFC operates at low temperature about 50 to 100°C, which makes them suitable for use in portable devices, car, and home. The platinum used to coat the electrolyte is expensive, and after less than two years of operation, the electrolyte has to be replaced. The electrolyte must be kept optimally saturated with water, and the hydrogen must be very pure. The need to increase the lifetime and lower the cost are the main barriers to wide spread use of the PEMFC.

The Molten Carbonate Fuel Cell (MCFC) is a high temperature fuel cell using molten salts of sodium or lithium as electrolytes. The MCFC is developed for used as a stationary power plant. The operation temperature is between 600 and 800°C. The MCFC is disadvantageous comparing to SOFC because of the need to work with corrosive liquid rather than a solid electrolyte.

The Solid Oxide Fuel Cell (SOFC) uses a ceramic material as an electrolyte. The materials for SOFC are Ytria Stabilized Zirconia (YSZ) as an electrolyte, Strontium-doped Lanthanum Manganite (LSM) as a cathode, nickel/YSZ as an anode , and doped Lanthanum Chromite or high-temperature metals as an interconnect. The operation temperature is between 800 and 1000°C. Very high operation temperatures allow the internal reforming of hydrogen fuels to occur without the need of precious metal catalysts. Due to high operating temperatures, SOFCs are suitable for residential applications as stationary units. The needs for low-cost materials that are durable at high temperatures are the main technical and economical challenges.

2.2 Materials for SOFCs

An SOFC single cell consists of an oxide electrolyte sandwiched between an anode and a cathode. SOFC are not typically operated as a single unit, they are connected in electrical series to build up voltages. A series of cells is referred to as a stack in which an interconnect joins the anode of one cell to the cathode of the next cell. The principle components of SOFC are an electrolyte, an anode, a cathode, and an interconnect [3-5]. Each of these components serves several functions in the fuel cell and must meet certain requirements.

2.2.1 Electrolyte [3, 5, 7, 8]

The electrolyte for SOFC conducts oxygen ions from the cathode site to the anode site. The electrolyte serves as a barrier to gas diffusion, but will let ions migrate across it. The requirements for the electrolyte in the SOFC are:

- 1) Stability, the electrolyte must be chemically, morphologically, and dimensionally stable in both reducing atmosphere on the anode side and oxidizing atmosphere on the cathode side.
- 2) Conductivity, the electrolyte have sufficiently high ionic with low electronic conductivity at the cell operating temperature. The electrolyte conductivity must not be changed significantly over prolonged periods.
- 3) Compatibility: The electrolyte must be chemically compatible with the other cell components during fabrication as well as under operation.
- 4) Thermal expansion: the thermal expansion of the electrolyte must match from room temperature to operation temperature and fabrication temperatures those of other cell components to avoid cracking and delaminating during fabrication and thermal cycle operation.

- 5) Porosity: the electrolyte must be dense to prevent gas cross leakage. The electrolyte material must be impervious to both oxidant and fuel gases between room temperature and operating temperature.

Present SOFCs use Ytria Stabilized Zirconia (YSZ) as an electrolyte. Doped ceria has been suggested as an alternative electrolyte for low temperature SOFC. Other oxygen conductors have been proposed as electrolyte materials for SOFC, especially for reduced operation temperature.

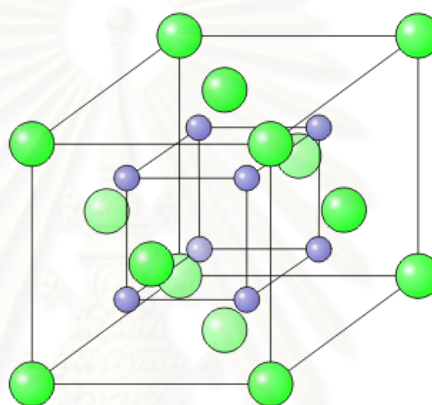


Fig 2.2: The crystal structure of cubic zirconia, oxygen is blue, zirconium is green [8].

Zirconia exhibits three polymorphs. At room temperature, it has a monoclinic (m) crystal structure. The monoclinic structure changes to tetragonal (t) above 1170°C and to cubic (c) fluorite structure above 2370°C (Fig 2.2). The monoclinic-tetragonal transformation is associated with a large volume change (3 to 5%). The cubic phase exists up to the melting point of 2680°C . However, an addition of certain aliovalent oxides can stabilize the cubic fluorite structure of zirconia from room temperature to its melting point. The most commonly used stabilizing oxide for zirconia are CaO, MgO, Y_2O_3 , Sc_2O_3 , and certain rare-earth oxides. Stabilization of zirconia is accomplished by direct substitution of divalent or trivalent cations of appropriate size for the host lattice cation Zr^{4+} . This substitution not only stabilizes the cubic fluorite structure but also creates a large concentration of oxygen vacancies [6, 9].



The high oxygen vacancy concentration gives rise to high oxygen-concentration mobility. The ionic conductivity of stabilized zirconia depends on dopant and dopant concentration. The conductivity of stabilized zirconia varies with dopant concentration (Fig 2.3). For the zirconia – yttria system, the yttria concentration at which the conductivity maximum occurs at 8 mol% and then decrease. The decrease in the conductivity at high dopant concentrations is believed to be due to defect ordering, vacancy clustering, or electrostatic interaction [10-11]. At low Y_2O_3 concentrations, the average distance between defect complexes is large, and each oxygen – ion vacancy is trapped and immobilized inside the defect complex, resulting in low oxygen-ion conductivity. With increasing Y_2O_3 concentration, the defect complexes begin to overlap one another. The effective carrier concentration and migration path for oxygen-ion vacancies thus increase with accompanying increase in conductivity. A further increase in the Y_2O_3 concentration leads to the appearance of two-fold associate defect complexes ($Y'_{Zr}V_{O}^{\bullet\bullet}Y'_{Zr}$) [10].

สถาบันวิทยบริการ
จุฬาลงกรณ์มหาวิทยาลัย

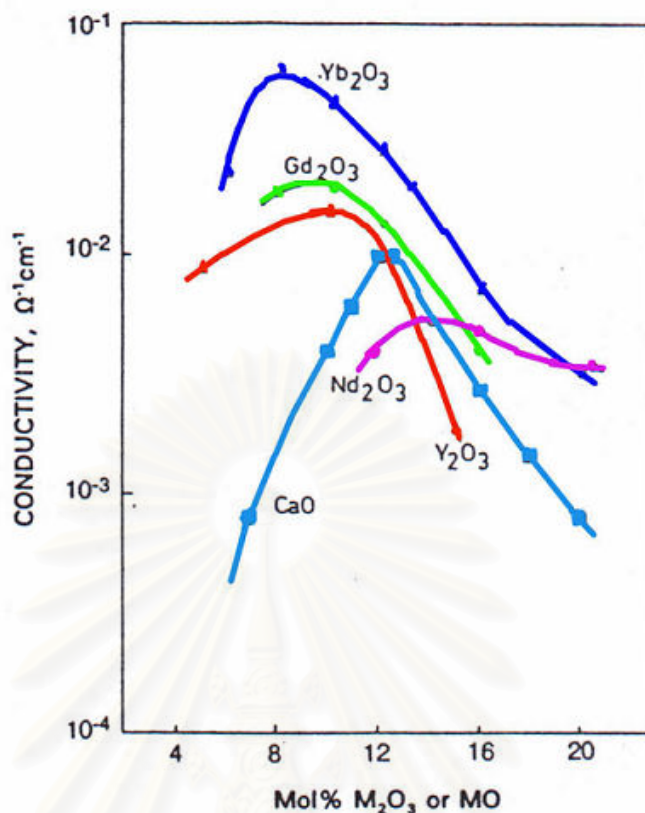


Fig.2.3: Variation of ionic conductivity of stabilized ZrO_2 with dopant concentration at 1080 K [12].

Doped ceria has been suggested as an alternative electrolyte for intermediate temperature SOFC. Ceria possesses the same fluorite structure as the stabilized zirconia. The oxygen vacancies are introduced by substituting Ce^{4+} with trivalent rare earth ions. The conductivity of doped ceria systems depends on the kind of dopant and its concentration. A typical dopant concentration in the CeO_2 - Sm_2O_3 systems shows the maximum conductivity at around 10 mol% Sm_2O_3 . Ceria-based oxide ion conductors are reported to be purely ionic conductivity at high oxygen partial pressure. At lower oxygen partial pressure, this material becomes partially reduced. This leads to electronic conductors in the large volume fraction of the electrolyte extending from the anode side. When a cell is constructed with such an electrolyte with electronic conduction, electronic current flows through the electrolyte even at open circuit, and the terminal voltage is somewhat lower than the theoretical value [5].

2.2.2 Anode [3, 5]

The anode as the part of the SOFC where the electrons are released is obviously crucial for a high performance of the fuel cell. In particular, the following specific properties are required for the anode

- 1) Sufficient porosity: the porosity of the anode must be tailored with regard to mass transport considerations as well as mechanical strength.
- 2) Stability: the anode must be chemically, morphologically, and dimensionally stable at operating temperature in the fuel gas environment; it must also be tolerant towards contaminants.
- 3) Conductivity: a maximum electrical conductivity under a large variety of operating conditions is desired to minimize the ohmic losses.
- 4) Compatibility: the anode must be chemically, thermally, and mechanically compatible with the other fuel cell components during fabrication as well as under operation.
- 5) Activity: the anode must have a high catalytic activity for the oxidation of the fuel gas.

Nickel - Yttria Stabilized Zirconia (Ni-YSZ) cermet (cermet = mixture of ceramic and metal) is currently the state-of-the-art material for SOFC anode. Because of the reducing conditions of the fuel gas, metals can be used as SOFC anode. Since the composition of the fuel changes during the operation of the fuel cell, suitable metals must be non-oxidized not only at the fuel inlet conditions but also at the more oxidized conditions of fuel outlet. At the operating temperature of 1000°C for the YSZ-based SOFC, suitable metals are limited mainly to nickel, cobalt, and noble metals. Nickel is most commonly used because of its low cost when compared with other metals such as, cobalt, platinum, and palladium. To maintain the porous structure of nickel over long period at 1000°C and provide other desired properties for anode, a nickel metal is often dispersed on the surface of an YSZ support. The function of the YSZ support in the anode is to support the nickel-metal particles, to inhibit coarsening of the metallic

particles at the fuel cell operating temperature and to provide an anode thermal expansion coefficient acceptably close to those of the other cell components.

2.2.3 Cathode [2-3, 5]

The cathode operates in an oxidizing environment of air or oxygen at high temperature ($\sim 1000^\circ\text{C}$) and participates in the oxygen reduction reaction,



The oxygen in a gas phase is reduced to oxygen ions, consuming two electrons in the process. The requirements of cathode are the followings:

- 1) Sufficient porosity, the porosity of the cathode must be tailored with regard to mass transport considerations as well as mechanical strength.
- 2) High electronic conductivity
- 3) High catalytic activity, the cathode must have a high catalytic activity for oxygen reduction
- 4) Chemical compatibility with electrolyte and interconnect during fabrication as well as under operation.
- 5) Compatible coefficient of thermal expansion with the other components during fabrication as well as under operation.

Because of the high operating temperature of the SOFC, only noble metals or electronic conducting oxides can be used as cathode materials. Noble metals, such as platinum, palladium, or silver, are unsuitable for practical applications because of prohibitive cost and insufficient long-term stability due to vaporization of silver. Several doped oxides and mixed oxides have been proposed and investigated. The material of choice for the cathode is lanthanum manganite. In order to satisfy all of the requirements listed above, the lanthanum manganite is doped with alkaline or rare earth cations. At present, strontium-doped lanthanum manganite (LSM) is the most commonly used.

2.2.4 Interconnect [2-3, 5]

The requirements of the interconnect are as follows:

- 1) Dense to prevent gas cross leakage in the fuel cell system
- 2) Adequate electronic conductivity in the dual atmosphere at the operating temperature.
- 3) Chemical compatibility with the anode and the cathode during the fabrication and operation temperature.
- 4) Compatible coefficient of thermal expansion with other cell components.

The materials that satisfies all of these requirements and widely used in SOFC is alkaline earth doped lanthanum chromite. This material like is like a cathode material, with perovskite structure and p-type conductivity due to the small polaron hopping mechanism. The important difference between the lanthanum manganite and the lanthanum chromite is the ability of chromite to survive highly reducing as well as oxidizing atmospheres.

2.3 AC Impedance Spectroscopy Technique

The electrical properties of solid oxide electroceramics are evaluated by their conductivity. Four basic techniques are usually applied; two-probe DC, four-probe DC, fixed frequency AC and impedance spectroscopy [6,14]. The two-probe DC method determines the total resistance due to the sample and to the electrode materials. The four-probe technique gives only the resistance of the sample, which makes it useful for characterization of a single crystal. For polycrystalline materials, the measured value is the sum of the bulk resistance (R_b) and the grain boundary resistance (R_{gb}). Since the R_{gb} is strongly dependent with impurities and processing parameters such as; sintering temperature, and cooling rates, the electrode contribution can be overcome also by the fixed AC method, which is usually performed in the frequency range of 1 – 20 kHz. In this case an instability and uncertainty of the results can be obtained when the measurements are performed at different temperatures. At lower temperatures the single

frequency point may determine R_b , while at higher temperatures the value could respond to bulk and grain boundary resistance ($R_b + R_{gb}$)(Fig 2.4). The increasing demand for separation of the bulk from the grain boundary conductivity inspired Bauerle [14] to perform detailed investigations for the solution of this problem by impedance spectroscopy. After this successful introduction, which ensured the distinguishing between the bulk, grain boundary and electrode effect, impedance spectroscopy was quickly applied as a sophisticated method for conductivity characterization of different electroceramic materials such as; conductors, semiconductors, dielectric ceramics etc.

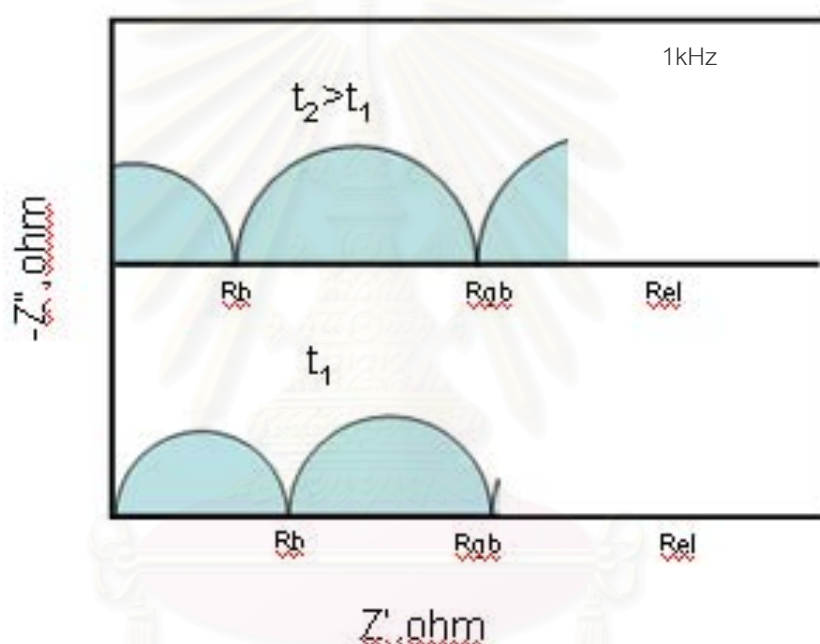


Fig 2.4: Schematic diagram of impedance spectra.

2.3.1 Impedance Definition [6]

Electrochemical impedance theory is a well-developed branch of AC theory that describes the response of a circuit to an alternating current or voltage as a function of frequency.

In DC theory the resistance is defined by Ohm's Law:

$$E = IR \quad (2.5)$$

where; E = potential in Volts, V,

I = current in Amperes, A, and

R = resistance in Ohm, Ω

In AC theory, where the frequency is non-zero, the analogous equation is:

$$E = IZ \quad (2.6)$$

As in Eq.2.1, E and I are defined as a potentials and a current, respectively. Z is defined as impedance, the AC equivalent of resistance. Impedance values are also measured in ohms (Ω). The resistors, capacitors, and inductors impede the flow of electrons in AC circuits, in which the impedance is expressed as a complex value. The resistance is the real component and combined capacitance and inductance is the imagination component. The impedance is usually measured by applying an AC potential to an electrochemical cell and measuring the current through the cell, when applying a sinusoidal potentials excitation. The response to this potential is an AC current signal containing the excitation frequency and its harmonics. The ratio of voltage to current (V/I) is known as an impedance, which is therefore a complex resistance. The impedance varies with the frequency of applied voltage, in a way that is related to the properties of the materials.

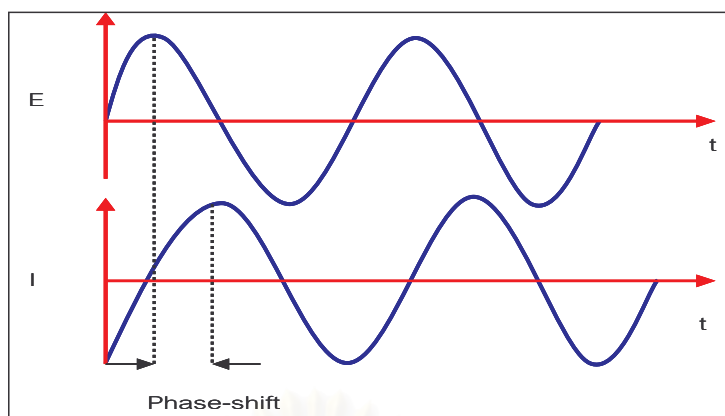


Fig 2.5: Sinusoidal wave applied across the electrochemical cell

The potential sine wave can be described by the equation:

$$E(t) = E_0 \cos(\omega t) \quad (2.7)$$

and the current:

$$I(t) = I_0 \cos(\omega t + \theta) \quad (2.8)$$

where;

$E(t)$ = instantaneous potentials, V,

$I(t)$ = instantaneous current, A,

θ = phase shift in radians,

t = time in second, s,

ω = frequency in radians per second = $2\pi f$, and

f = frequency in Hertz, Hz

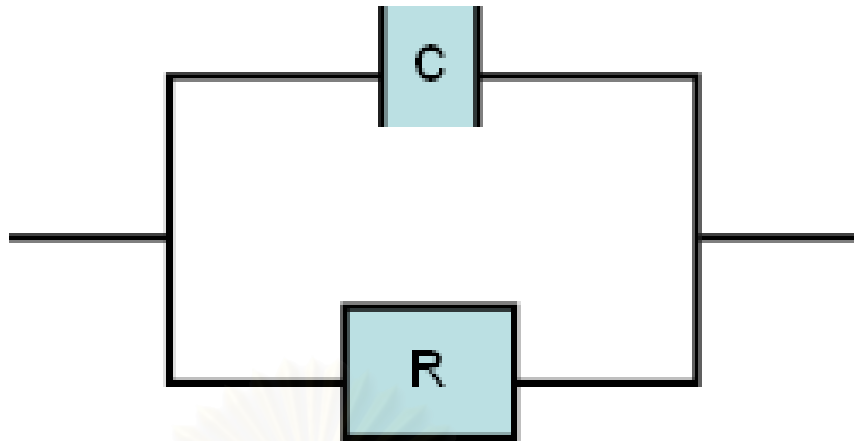


Fig 2.6: Equivalent circuit model of R-C unit

The Impedance of the resistive element R is $Z_R = R$ and the impedance of the capacitive element C is $Z_C = \frac{1}{i\omega C}$. The equivalent circuit model of an RC unit is shown in Fig 2.6. According to the parallel connection of R and C, the total impedance is:

$$\frac{1}{Z} = \frac{1}{R} + i\omega C \quad (2.9)$$

Having solved this equation for Z as well as for separated expressions for the real and for the imagination part, the total impedance becomes:

$$Z = \frac{R}{1 + R^2 C^2 \omega^2} - \frac{R^2 C \omega}{1 + R^2 C^2 \omega^2} i \quad (2.10)$$

where

$$Z' = \text{real}(Z) = \frac{R}{1 + R^2 C^2 \omega^2} \quad (2.11)$$

and

$$Z'' = \text{imaginary}(Z) = \frac{R^2 C \omega}{1 + R^2 C^2 \omega^2} \quad (2.12)$$

The Impedance Spectra can be plotted in the Nyquist representation where the negative imaginary part of the impedance, Z'' is plotted versus the real part of the impedance, Z' . The Impedance Spectra can also be plotted in Bode representation where the absolute impedance, $|Z|$, as well as the phase shift, θ are plotted versus the angular frequency, ω . Both representations contain, in principle, the same information and can be transferred to each other (Fig 2.7).

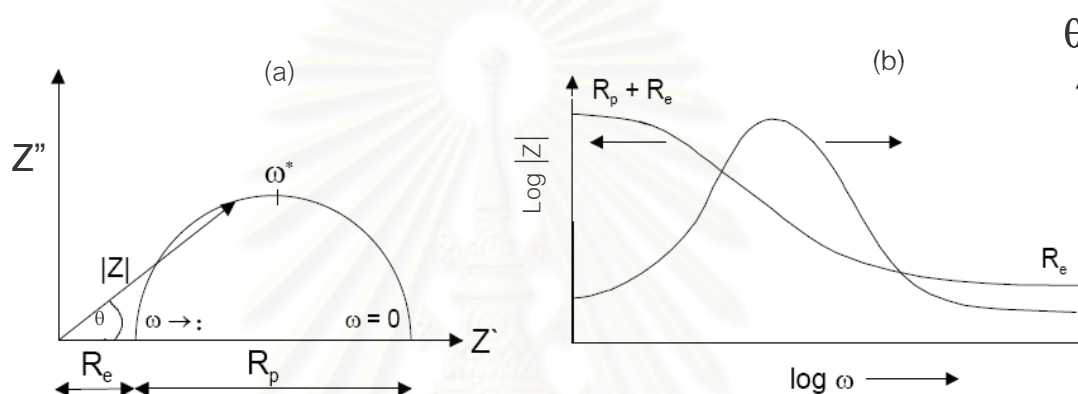


Fig 2.7: Schematic representation of Nyquist plot (a) and Bode plot (b).

The relaxation frequency is defined as the maximum frequency of the Z'' versus Z' curve. The maximum is mathematically defined as

$$\frac{dZ''}{dZ'} = 0 \quad (2.13)$$

The derivative can be written as

$$\frac{dZ''}{dZ'} = \frac{dZ''}{d\omega} \cdot \frac{d\omega}{dZ'} \quad (2.14)$$

A reasonable solution for the relaxation frequency, ω^* , is then

$$\omega^* = \frac{1}{RC} \quad (2.15)$$

2.3.2 Elementary Analysis of Impedance Spectra

The Nyquist plot of a ceramic oxide consists of three semicircles as shown in Fig 2.8. Its corresponding equivalent circuit includes the three parallel R-C elements, connected in series. A detailed analysis has been performed for elucidation of physical meaning of each semicircle by Bauerle [14]. It was found, that the first semicircle corresponds to the bulk properties, the second one corresponds to the grain boundaries, while the last one is due to the electrode response. Polycrystalline materials with uniform composition of grains and grain boundaries show only one bulk and one grain boundary semicircle regardless of the fact whether the grains and the grain boundaries are of uniform thickness or not. This conclusion comes from the independence of the characteristic time constant on the thickness

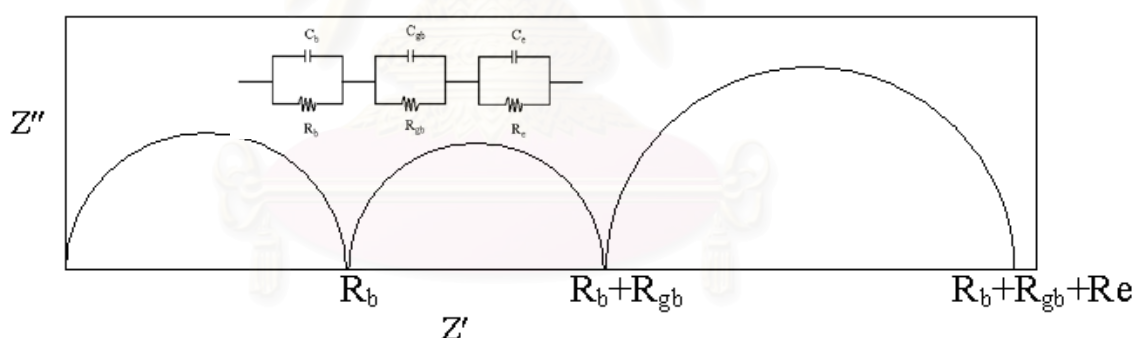


Fig 2.8: Idealized impedance spectra of ceramic oxide and its equivalent circuit.

The Impedance investigations of the conductivity are operating with the first two semicircles, since they are corresponding to the bulk and the grain boundary properties. The bulk properties are sensitive to the chemical composition, internal porosity, presence of additional phases. The grain boundary contribution is influenced by the sample purity, doping concentration, aging, grain size, porosity and space charge [15-16].

The interpretation of the first two high semicircles in the Nyquist plots of polycrystalline electroceramics with bulk and grain boundary properties ensures quantitative evaluation of their resistance (R_b and R_{gb}) and capacitance (C_b and C_{gb}).

The bulk conductivity was calculated from;

$$\sigma_{bulk} = \frac{L}{R_{bulk} A} \quad (2.16)$$

σ_{bulk} = the bulk conductivity, s/cm,

R_{bulk} = the bulk resistance, Ω ,

A = the cross-sectional area, cm^2 , and

L = the thickness of the sample, cm.

The specific grain boundary conductivity σ_{gb} was from;

$$\sigma_{gb} = \frac{L \delta_{gb}}{R_{gb} A d_g} \quad (2.17)$$

δ_{gb} is being the grain boundary thickness, which can be calculated from the capacitance according to Guo and Maier [14-18].

$$\delta_{gb} = \frac{d_g C_{bulk}}{C_{gb}} \quad (2.18)$$

replace (2.18) to (2.17);

$$\sigma_{gb} = \frac{LC_{bulk}}{R_{gb} A C_{gb}} \quad (2.19)$$

d_g = the average grain size, μm , and

C_{bulk} and C_{grain} = the bulk and grain capacitance, F

Haeing et al [11] were used impedance spectroscopy technique to characterize the degradation of the electrical conductivity in stabilized zirconia systems. They have shown that annealing at 1000 °C reduces the electrical conductivity of 8 mol% Yttria-Stabilised Zirconia (8YSZ), known as a good performing material for Solid Oxide Fuel Cells (SOFCs) electrolytes. This decrease in electrical conductivity by ageing for 1000 hours was not observed for doped zirconia with higher yttria contents.

Guo and Maier [17] have shown that the activation energy for the grain boundary resistivity of the sample 8YSZ (~1.16eV) is slightly higher than that for the bulk resistivity (~1.05eV). The difference between the two activation energies increases with decreasing dopant concentration, mainly because of the marked decrease of the activation energy for the bulk resistivity.

The impedance investigations may contribute to the optimization of materials, including selection of chemical composition, purity of the initial components, sintering conditions (atmosphere, sintering temperature, cooling rate), as well as the fundamental investigation of the conductivity mechanism.



สถาบันวิทยบริการ
จุฬาลงกรณ์มหาวิทยาลัย

CHAPTER III

EXPERIMENTAL PROCEDURE

In this thesis, AC-Impedance Spectroscopy is used to determine the ionic conductivity of YSZ electrolyte.

3.1 Raw materials and Characterization

3.1.1 Starting materials

The starting materials from various suppliers are listed as shown in Table 3.1. The particle size distribution of all starting materials was characterized using a particle size analyzer (Malvern, Master sizer S). The composition of all powder was characterized using X-ray Fluorescence Technique (Philips, PM 2510).

Table 3.1 XRF and particle size distribution results for Yttria Stabilized Zirconia (YSZ)

Materials	PSD (μm)	Concentration (% weight)					
		ZrO ₂	Y ₂ O ₃	HfO ₂	SiO ₂	As ₂ O ₃	Cl
3Y MEL	0.70 – 1.57	93.54	4.55	1.56	-	-	-
8YMEL	0.82 – 5.01	86.07	12.54	1.38	-	-	-
8Y TOSOH	0.12 – 3.12	84.92	13.49	1.40	-	-	0.19
8Y DAIICHI	0.20 – 0.91	85.64	12.67	1.37	-	0.33	-
10Y DAIICHI	0.12 – 6.40	83.28	15.38	1.34	-	0.35	-

3.2 Preparation of Electrolyte Materials

3.2.1 Equipments

The equipment for preparation and characterization of electrolyte materials are summarized in Table 3.2.

Table 3.2 Preparation and characterization equipments

Apparatus	Company	Model
1. Muffle Furnace	Lenton Thermal Designs, England	UAF 18/5
2. Balance and Density Kit	A&D company, Japan	GR-200
3. Grinder/Polisher	Wirtz Buehler, Germany	-
4. Optical Microscope	ZEISS	Axiotech
5. Ultrasonic Cleaner	Crest Ultrasonics Corp.	True sweep 275D
6. Hydraulic Press	Carver, INC.USA	M
7. Particle size Analyzer	Malvern, USA	Master sizer S
8. X-Ray Fluorescence Analyzer	Philips	PW 2510
9. X-Ray Diffractometer	Jeol	JDX-3530
10. Scanning Electron Microscope	Jeol	JSM-5410
11. Digital micrometer	Mitutoyo, Japan	-
12. Impedance Spectroscopy	Solartron analytical	Solartron SI 1260(Impedance/Gain -phase analyzer)

3.2.2 Preparation

The commercial YSZ powders were from MEL (Magnesium Elektron, England), DAIICHI (Japan), and TOSOH (Japan). The pellets of approximately 300 mg were prepared by uniaxial pressing (Carver, Hydraulic press) in a stainless steel die at 60 MPa. The diameter of green pellet is 13 mm. They were then sintered in a muffle furnace with a heating rate of 3°C/min to 1500°C and 1550°C with soaking time of 1, 2 and 4 hours, respectively. The sintered samples were furnace cooled at a cooling rate of 5°C/min. The sintered pellets are of 10 mm diameter and 0.2 mm thick.

Table 3.3: Information of YSZ powder

Code	Composition of Y_2O_3 in ZrO_2	Purity	Supplier
3MEL	3 mol %	99.9%	MEL
8MEL	8 mol %	99.9%	MEL
8TOSOH	8 mol %	99.9%	TOSOH
8DAIICHI	8 mol %	99.9%	DAIICHI
10DAIICHI	10 mol %	99.9%	DAIICHI

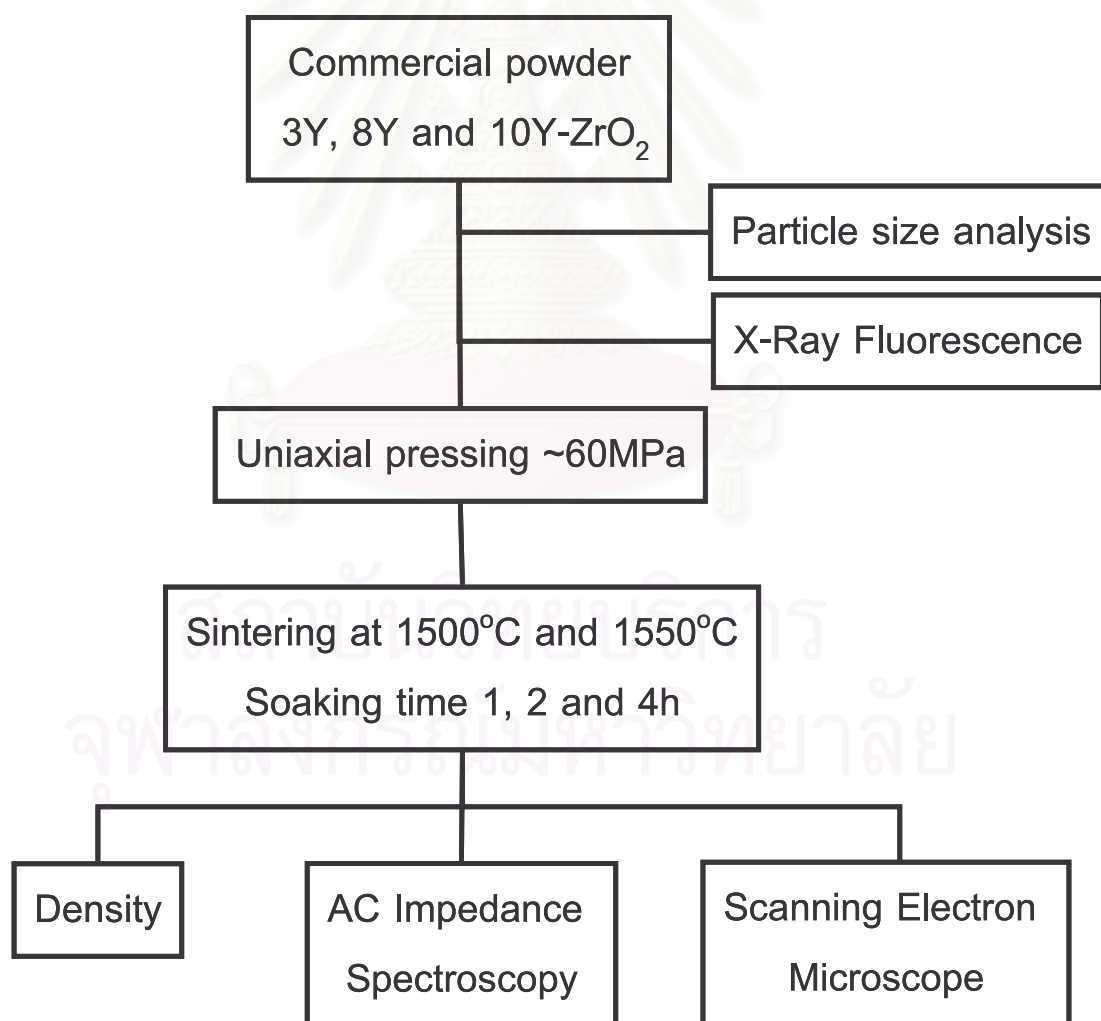


Fig 3.1: Flow chart of experimental procedures.

3.3 Characterization of Electrolyte Materials

3.3.1 Density

The bulk density of the sintered pellets was measured using an Archimedes technique ASTM C 373 -88 [18]. The sintered samples were heated in an oven at 100°C followed by cooling in a desiccator. The dry mass, D was measured to the nearest 0.01 gram. The samples were placed in a pan in distilled water and boiled for 5 hours. After boiling for 5 hours, the specimens were soaked in water at room temperature for 24 hours. After the impregnation of test specimens, the mass, S , was measured to the nearest 0.01 gram of each specimen while suspended in water. Then, excess water was removed from the surface using cotton cloth and then the saturated mass, M , was measured to the nearest 0.01 gram.

In the following calculations, the assumption is made that 1 cm³ of water weighs 1 gram. The exterior volume, V , (cm³), can be calculated as follows:

$$V = M - S \quad (3.1)$$

The bulk density, B , (g/cm³), of a specimen is quotient of its dry mass divided by the exterior volume, include pores can be calculated as follows:

$$\text{Bulk density} = \frac{D}{M - S} \quad (3.2)$$

3.3.2 Microstructure of electrolyte materials

The microstructure of the electrolytes were characterized using a Scanning Electron Microscope (SEM)(Jeol, JSM-5410).The electrolyte pellets, after impedance spectroscopic measurement, were polished using SiC paper and diamond suspension and then ultrasonically cleaned. The polished-pellets were thermally etched

at 50°C less than the sintering temperature for 5 minutes [19]. The etched-pellets were carbon sputtered prior to the microstructural examination.

3.3.3 A Measurement System for Impedance Spectroscopy

The setup of the AC-Impedance Spectra measurement system is as shown in Fig.3.2. The system consists of the Frequency Response Analyzer, (FRA) (SOLARTRON 1260 Impedance/Gain-phase analyzer), sample holder, a data analyzer and a tube furnace. The electrolyte pellets for AC-Impedance Spectroscopy measurement had their surfaces polished with SiC paper and ultrasonically cleaned. Then the pellet-electrolytes were coated with gold paste on both sides as electrodes and fired at 800°C for 1 hour. The samples were loaded inside the sample holder. The impedance spectra were collected in the frequency range of 0.05 Hz to 10⁷ Hz, within the temperatures range of 275 – 600°C under air atmosphere. The impedance of the sample was measured at 25°C interval with increasing temperature at the rate of 3°C/min using a controlled program furnace. The impedance spectra plot between real part (Z') and imaginary part (Z'') is called Nyquist plot.

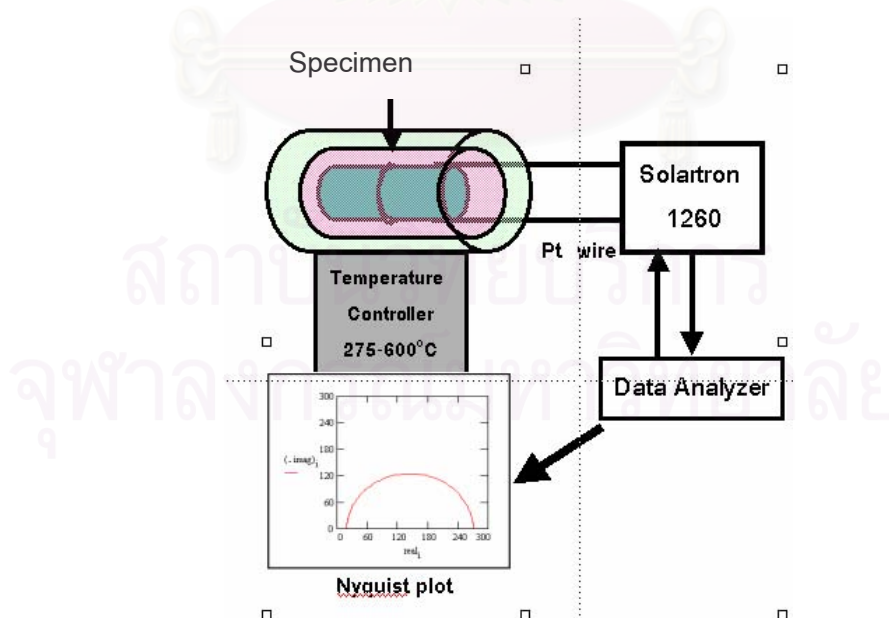


Fig. 3.2: Schematic diagram of measurement system for the characterization of electrolyte materials using AC Impedance Spectroscopy.

In general, the AC Impedance of an ionic conductor measured by a two-probe method contains contributions from the bulk, grain boundaries and electrode/electrolyte interfaces, which can be reflected in a complex plane by three successive semicircles, as shown in Fig.3.3. The frequency increases from the right to the left across the plot. The arc at the high frequency end of the spectrum represents the bulk resistivity(R_b); the arc at the middle of the spectrum is a consequence of the grain boundary effect (R_{gb}) while the low-frequency arc is assigned to the electrode response(R_e). Typical geometry-normalised capacitances for bulk and grain boundary components are in the order of $10^{-12} \text{ Fcm}^{-1}$ and to 10^{-8} Fcm^{-1} , respectively. In general, the circuit elements representing the response of the electrode depends on the electrochemical reaction occurring at the sample electrode interface but usually has a capacitive components with a values between 10^{-7} and 10^{-5} Fcm^{-1} . [20]

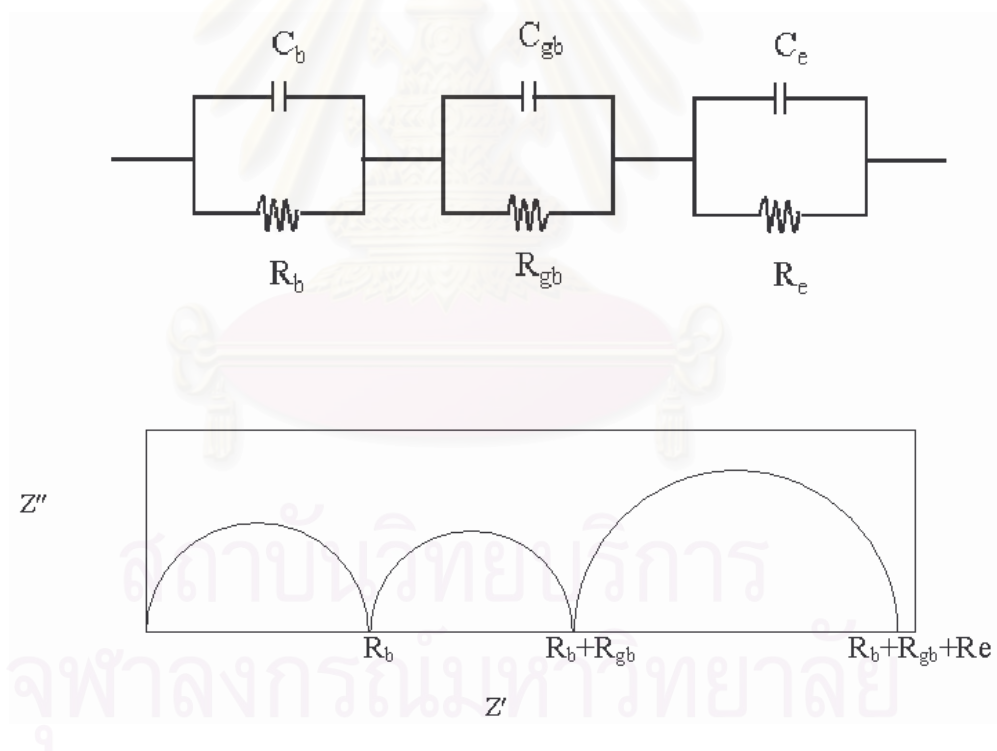


Fig. 3.3: An equivalent circuit and the corresponding impedance plot

The calculation of the electrolyte materials is based on the Ohm's law;

$$V = IR, R = \frac{V}{I} \quad (3.2)$$

and
$$R = \rho \frac{L}{A} \quad (3.3)$$

$$\rho = \frac{RA}{L} \quad (3.4)$$

$$\sigma = \frac{1}{\rho} = \frac{L}{RA} \quad (3.5)$$

Where; V = applied voltage, V,
 I = current, A,
 R = resistance in Ohm, Ω
 ρ = resistivity in Ohm.centimeter, Ω .cm,
 σ = conductivity in siemens.centimeter, s/cm,
 L = sample thickness in centimeter, cm, and
 A = the cross-sectional area centimeter square, cm^2

According to the Arrhenius equation [21], the conductivity of electrolyte materials can be expressed as;

$$\sigma_T = \left(\frac{A}{T}\right) \exp\left(\frac{-Ea}{RT}\right) \quad (3.6)$$

$$\ln \sigma_T T = -\frac{Ea}{RT} + \ln\left(\frac{A}{T}\right) \quad (3.7)$$

where; Ea = activation enthalpy for ionic conductivity, J/mol,

T = absolute temperature, K,

R = gas constant, 8.314 J/K mol, and

A = the pre-exponential factor.

From Eq (3.7). $\ln(\sigma T)$ versus $1000/T$ is plotted to determine the electrical conductivity of the electrolyte at 800°C and the activation energy.

CHAPTER IV

RESULTS AND DISCUSSION

In this thesis, the electrolyte materials for SOFC consist of 3, 8 and 10 mol% Y_2O_3 - ZrO_2 . The 3 mol% Y_2O_3 - ZrO_2 has higher mechanical strength at both room temperature and fuel cell operation temperature (700 – 1000°C) in comparison with the fully stabilized zirconia (8 -10 mol% Y_2O_3). However the fully stabilized zirconia has higher electrical conductivity at 800 - 1000°C [5]. Therefore the 3, 8 and 10 mol% Y_2O_3 from various suppliers were characterized in several aspects as follows, particle size distribution (PSD) of powder using laser diffraction technique, the purity of materials using X-Ray Fluorescence technique (XRF), electrical conductivity using AC-Impedance Spectroscopy, microstructure investigating using Scanning Electron Microscopy (SEM), and density of sintered electrolyte using Archimedes method.

4.1 Investigation of 3Y MEL (3 mol% Y_2O_3 - ZrO_2 -MEL)

4.1.1 Particle size distribution

The particle size distribution of 3 mol% Y_2O_3 - ZrO_2 (MEL) was shown in Table 3.3; the curve distribution was shown in APPENDIX A. The mean particle size of 3 mol% Y_2O_3 - ZrO_2 (MEL) was 0.70 μm , in the particle size distribution ranging from 0.13 to 1.57 μm .

4.1.2 X-Ray Fluorescence

The Electrical conductivity of the ceramic electrolyte was influenced by the processing and the purity of raw materials [22-26]. The composition of 3 mol% Y_2O_3 - ZrO_2 (MEL) characterized from XRF was shown in Table 4.1. The presence of 1.56 wt % HfO_2 in the raw powder was detected.

Table 4.1: The X-Ray Fluorescence results of doped zirconia powder.

Materials	Suppliers	Concentration (weight %)					
		ZrO ₂	Y ₂ O ₃	HfO ₂	SiO ₂	As ₂ O ₃	Cl
3mol % Y ₂ O ₃ -ZrO ₂	MEL	93.54	4.55	1.56	-	-	-
8mol % Y ₂ O ₃ -ZrO ₂	MEL	86.07	12.54	1.38	-	-	-
8mol % Y ₂ O ₃ -ZrO ₂	TOSOH	84.92	13.49	1.40	-	-	0.19
8mol % Y ₂ O ₃ -ZrO ₂	DAIICHI	85.64	12.67	1.37	-	0.33	-
10mol % Y ₂ O ₃ -ZrO ₂	DAIICHI	83.28	15.38	1.34	-	0.35	-

4.1.3 AC-Impedance Spectra

The impedance spectra are plotted between the imaginary part of the impedance as a function of the real part of the impedance, also called Nyquist plots or Cole Cole plots. All the impedance spectra of the electrolyte pellets sintered at 1500°C and 1550°C described in this thesis were measured at 400°C. This temperature is high enough to detect both bulk and grain boundary contributions to the conductivity of O²⁻ ion migration. Fig. 4.1 shows the impedance spectra of 3 mol% Y₂O₃-ZrO₂ (MEL) electrolyte pellets after sintering at 1500°C and 1550°C for 1, 2 and 4 hours. The impedance spectra show that real components decrease with increasing the soaking time at all sintering temperatures. The decrease of real part of the impedance corresponds to an increase of electrical conductivity of the electrolyte pellet. The impedance spectra after heat treatment at three fixed times at different sintering temperatures were shown in Fig 4.2. The electrical conductivity of the electrolyte pellets are strong temperature dependent. The impedance spectra were simulated with RC equivalent circuit as presented in Fig.3.3 to determine the resistance and capacitance of materials constituent. Simulation was carried out using a non-linear least square fit method with less than 5% error. The electrical conductivities were determined from Eq (3.5). Arrhenius plots Eq (3.7) between the conductivity and the reciprocal of absolute temperature was shown in Fig 4.3.

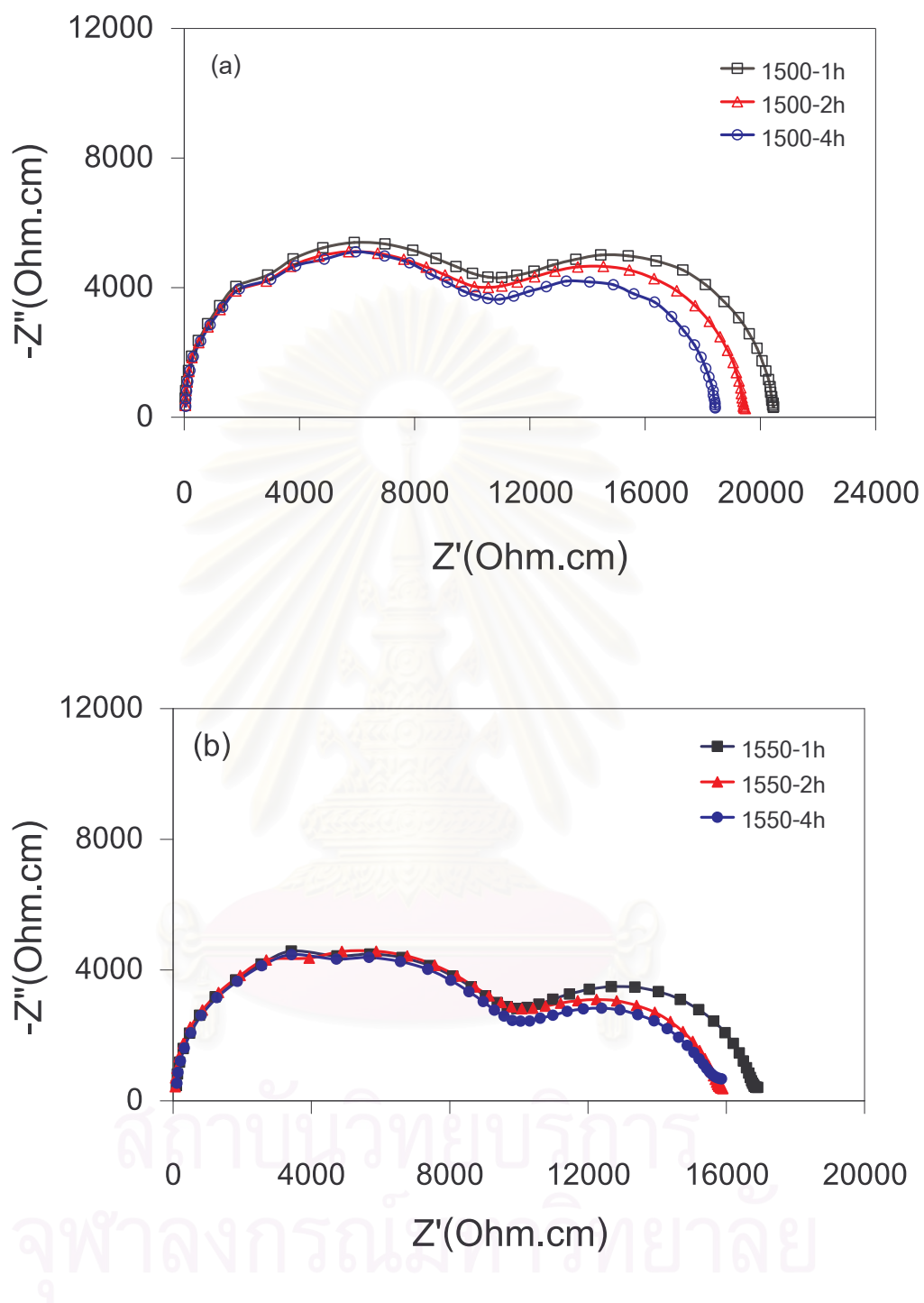


Fig 4.1: Impedance spectra of 3 mol% $\text{Y}_2\text{O}_3\text{-ZrO}_2$ electrolyte after sintering at (a) 1500°C and (b) 1550°C (at various sintering times). All the measurements were taken at 400°C.

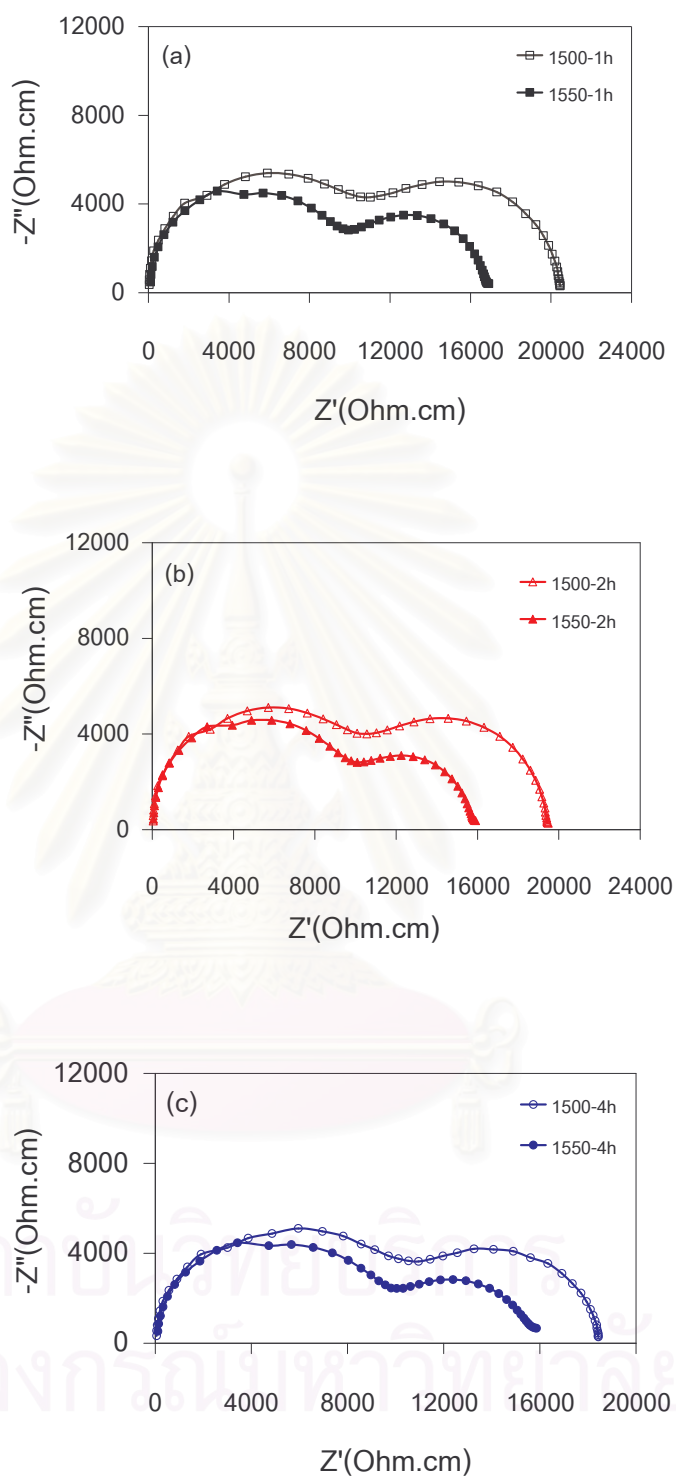


Fig: 4.2: Impedance spectra of 3 mol% $\text{Y}_2\text{O}_3\text{-ZrO}_2$ electrolyte after sintering for (a) 1 hour, (b) 2 hours, and (c) 4 hours at 1500°C and 1550°C. All the measurements were taken at 400°C.

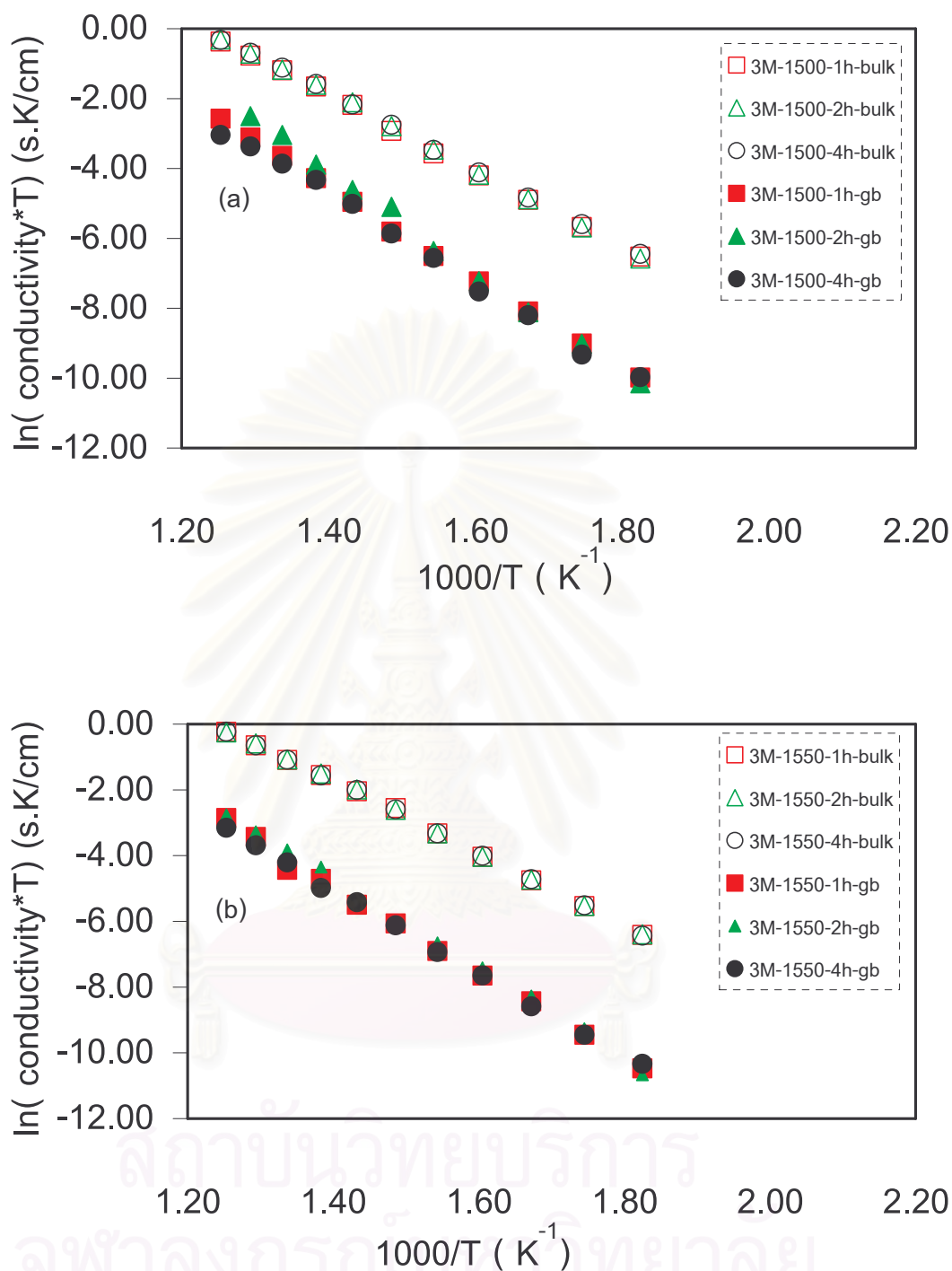


Fig 4.3: Arrhenius plots of the bulk and grain boundary conductivities for 3 mol% Y_2O_3 – ZrO_2 (MEL) sintered at 1500°C (a) and 1550°C (b) [for 1 hour, 2 hours, and 4 hours]

Fig 4.3 shows Arrhenius plots of the bulk conductivity and the grain boundary conductivity of 3 mol % $Y_2O_3 - ZrO_2$ (MEL) in various sintering conditions. The conductivities are shown as a function of temperature. The slopes represent the activation energy for oxygen ion migration [6]. The slopes of the bulk conductivity results are similar for all specimens. In the specimen sintered at $1550^\circ C$ for 2 hours the grain boundary slope is the highest, and hence the activation energy. The slope of the Arrhenius plots implied to the stability of electrolyte materials. The activation energy of the bulk conduction was smaller than that of the grain boundary. These results are similar to the previous research [6, 15-16]. The activation energies calculated from $\ln \sigma T - 1/T$ are shown in Table 4.2. The conductivities at $800^\circ C$ are calculated and extrapolated from Arrhenius Eq (3.8). The bulk conductivities are greater than grain boundary conductivities. The highest conductivity was obtained from the pellet that was sintered at $1550^\circ C$ for 4 hours.

Table 4.2: Conductivity and Activation energy at $800^\circ C$ for 3 mol% $Y_2O_3 - ZrO_2$ (MEL).

Sintering temperature($^\circ C$)	Sintering time (h)	Conductivity(S/cm)		Activation energy(eV)	
		bulk	gb	bulk	gb
1500	1	0.0207	0.0045	0.94	1.13
	2	0.0227	0.0021	0.96	1.05
	4	0.0237	0.0032	0.94	1.10
1550	1	0.0248	0.0029	0.94	1.13
	2	0.0258	0.0023	0.94	1.17
	4	0.0271	0.0022	0.94	1.09

4.1.4 Microstructure

The microstructural images of 3 mol% $Y_2O_3 - ZrO_2$ (MEL) at various sintering temperatures were presented in Fig. 4.4. The specimens were thermally etched at $50^\circ C$ below sintering temperatures for 5 minutes to enhance the appearance of grain boundaries [19]. Microstructure of the sintered specimens at 4 hours for the $1500^\circ C$ and

1550°C was depicted in Fig 4.4. The microstructure showed uniform and narrow grain size distribution with no abnormal grain growth. The average grain size calculated using image analysis technique was 0.8 μm . Small pores were detected in both specimens, but the specimens sintered at 1550°C showed less pores than that sintered at 1500°C. The excess porosity is expected to reduce the effective cross-section area of the specimen, possibly reducing the total conductivity [35]. Therefore the specimen in Fig 4.4b showed higher ionic conductivity than that in Fig 4.4a.

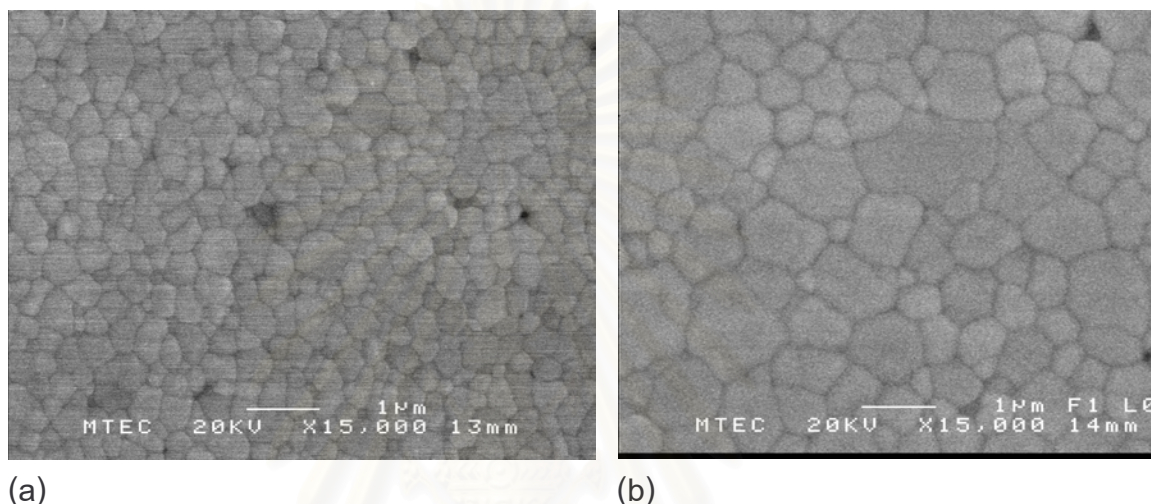


Fig 4.4: SEM micrographs of 3 mol%Y₂O₃-ZrO₂(MEL) sintering at 1500°C (a) and 1550°C (b) for 4 hours.

4.1.5 Density

The relative density of the sintered electrolyte was shown in Fig 4.5. It was shown that the relative density increased with increasing of sintering time.

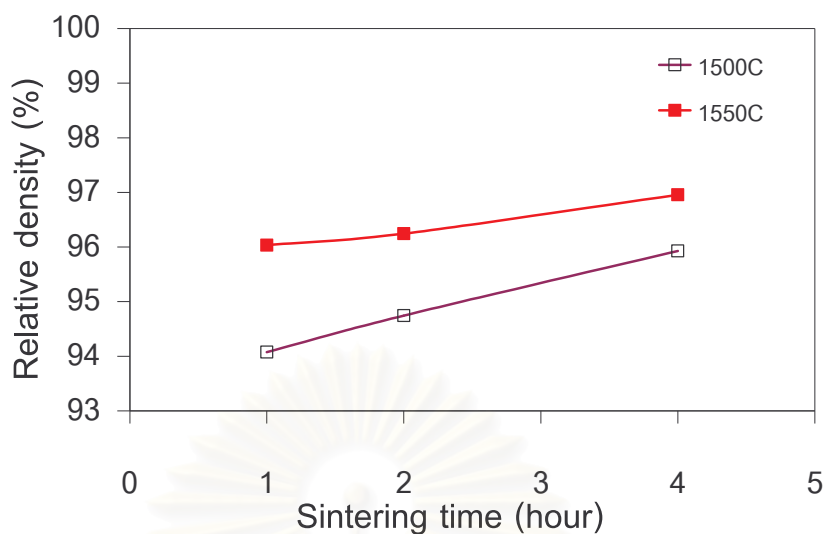


Fig 4.5: The relative density of 3 mol% Y_2O_3 - ZrO_2 (MEL) sintering at 1500°C and 1550°C.

4.2 Investigation of 8Y MEL (8 mol% Y_2O_3 - ZrO_2 MEL)

4.2.1 Particle size distribution

The particle size distribution of 8 mol% Y_2O_3 - ZrO_2 (MEL) powder was shown in Table 3.3. The curve distribution is shown in APPENDIX A. The average particle size of 8 mol% Y_2O_3 - ZrO_2 (MEL) is 3.30 μm , in the size distribution ranging from 0.82 to 50.1 μm .

4.2.2 X-Ray Fluorescence

The Electrical conductivity of the ceramic electrolyte was influenced by the processing and the purity of raw materials [22-26]. The composition of 8 mol% Y_2O_3 - ZrO_2 (MEL) characterized from XRF was shown in Table 4.1. The presence of 1.38 wt % HfO_2 in the raw powder was detected.

4.2.3 AC-Impedance Spectra

The impedance spectra measured at 400°C for 8 mol% Y_2O_3 - ZrO_2 (MEL) electrolyte pellets after sintering at 1500°C for 1, 2 and 4 hours were shown in Fig 4.6(a). The impedance spectra showed that the resistance of the real components decrease with increasing the sintering time at all investigated temperatures. The decrease of real part of the impedance corresponds to an increase of electrical conductivity of the electrolyte pellets. The grain boundary resistance (R_{gb}) was smaller than the bulk resistance (R_b). This result was different from the 3 mol% Y_2O_3 - ZrO_2 (MEL) system. The grain boundary resistance decreasing depended on the Y_2O_3 content [6]. The impedance results of the pellets sintered at 1550°C were shown in Fig 4.7(b). The grain boundary resistance decreases with increasing of soaking time, while the bulk resistance shows no significant difference in the shape. The impedance spectra after heat treatment at three fixed soaking times from different sintering temperatures are shown in Fig 4.8. The impedance spectra of 8 mol% Y_2O_3 - ZrO_2 (MEL) indicated the dependency of electrical conductivity with sintering temperature. The electrical conductivities were calculated from Eq (3.5). Arrhenius plots between the conductivity and the reciprocal of absolute temperature is shown in Fig 4.8.

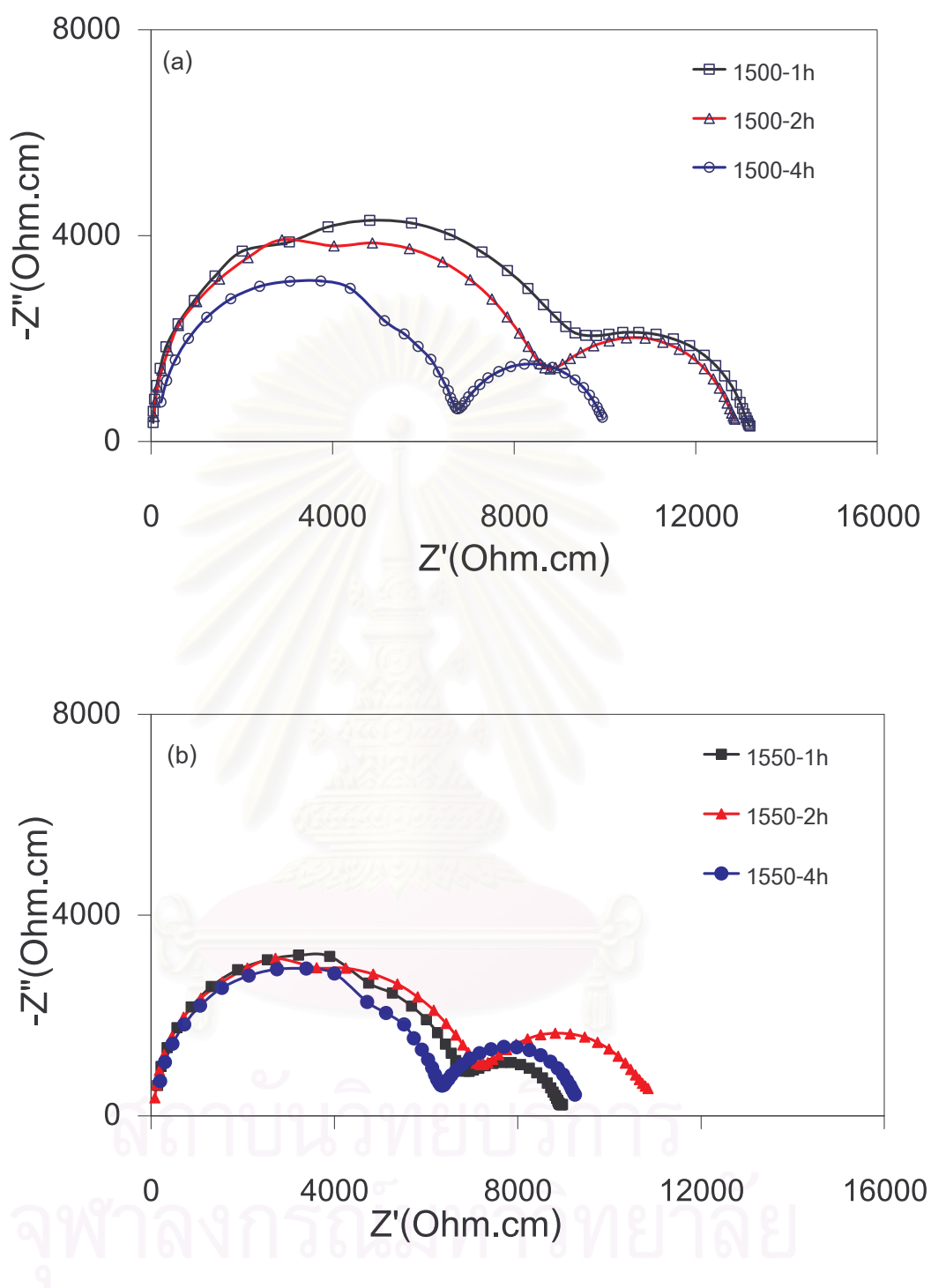


Fig 4.6: Impedance spectra of 8 mol% $\text{Y}_2\text{O}_3\text{-ZrO}_2$ (MEL) electrolyte after sintering for (a) 1 hour, (b) 2 hours, and (c) 4 hours at 1500°C and 1550°C. All the measurements were taken at 400°C.

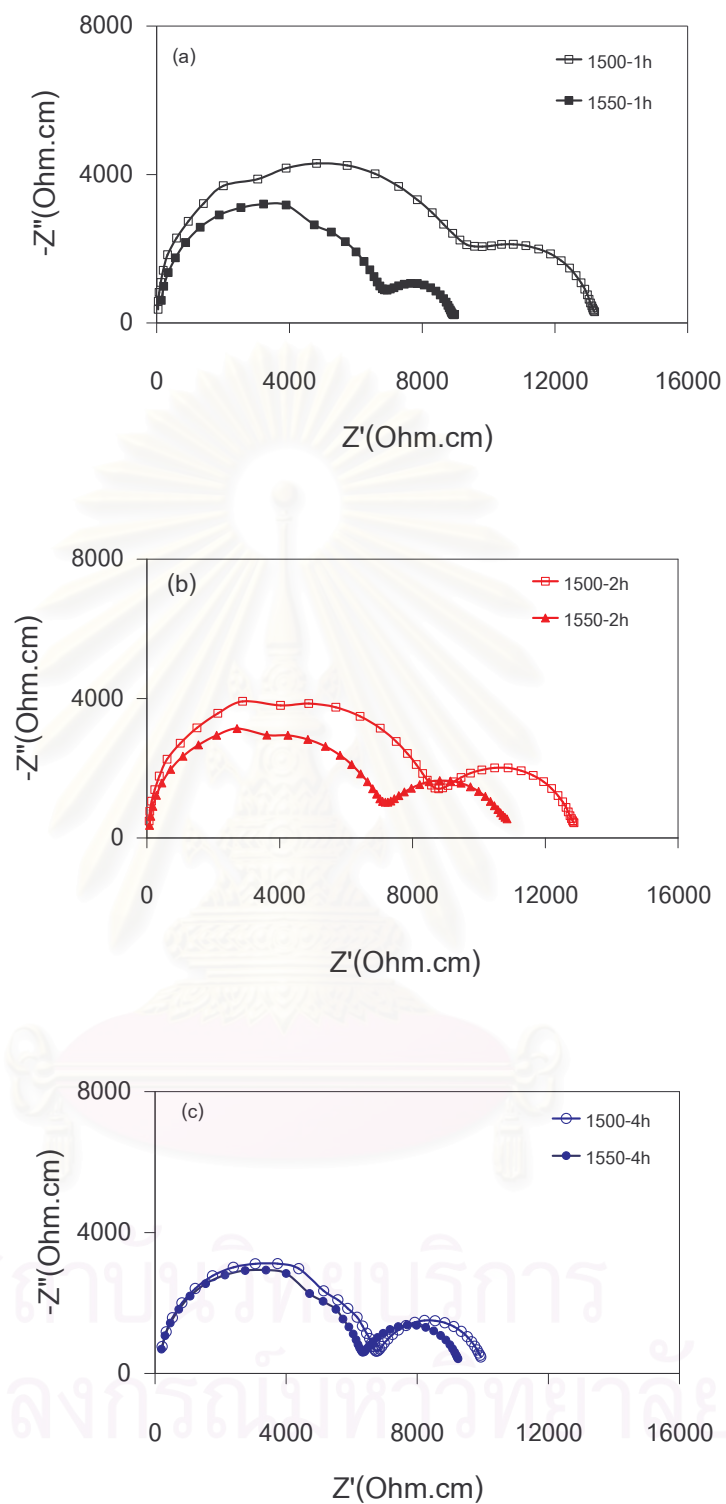


Fig 4.7: Impedance spectra of 8 mol% $\text{Y}_2\text{O}_3\text{-ZrO}_2$ (MEL) electrolyte after sintering for (a) 1 hour, (b) 2 hours, and (c) 4 hours at 1500°C and 1550°C. All the measurements were taken at 400°C.

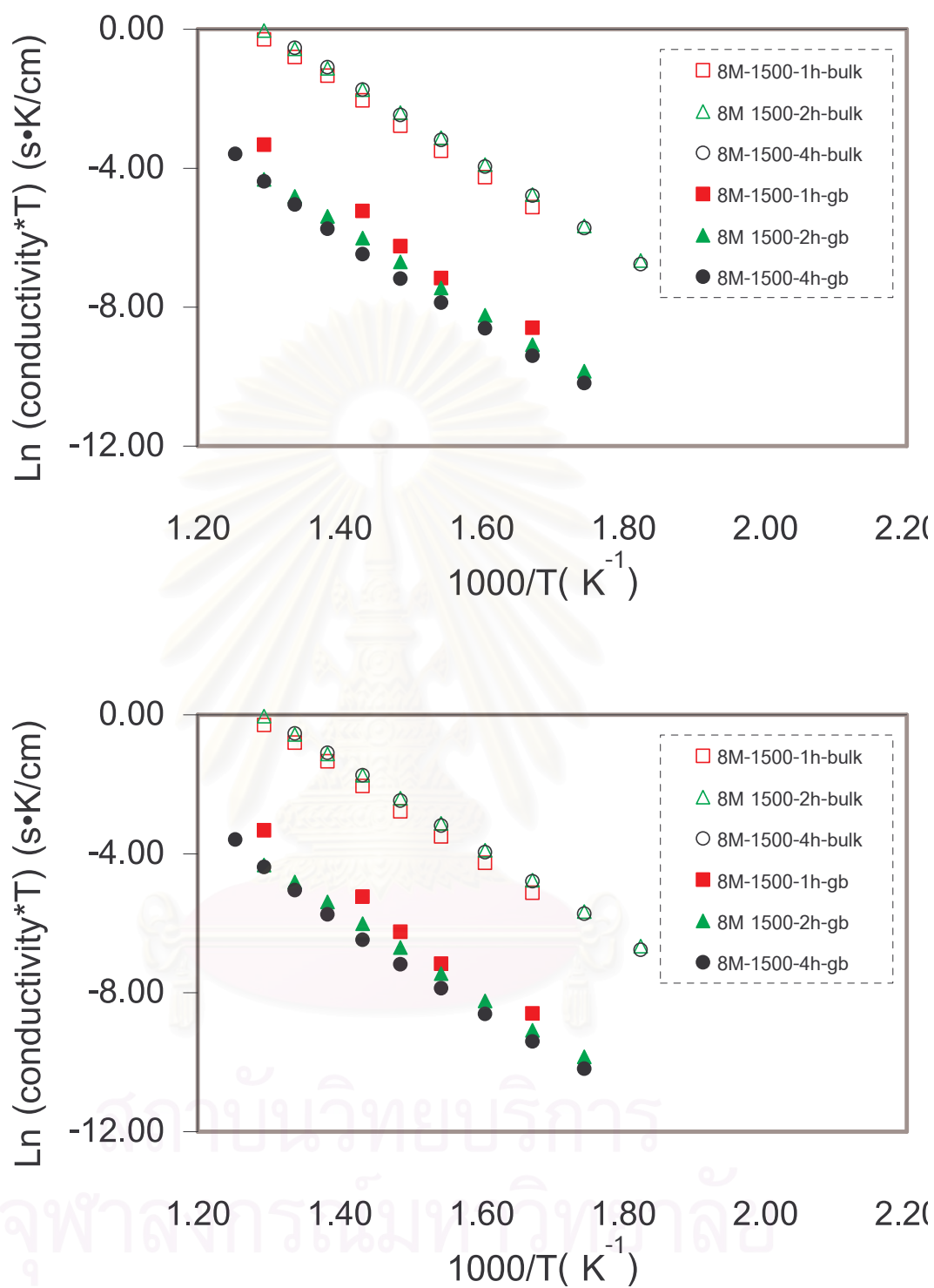


Fig 4.8: Arrhenius plots of the bulk and grain boundary conductivities for 8 mol% Y_2O_3 – ZrO_2 (MEL) sintered at 1500°C (a) and 1550°C (b) [for 1 hour, 2 hours, and 4 hours]

Arrhenius plots of the bulk conductivity and the grain boundary conductivity of 8 mol% Y_2O_3 - ZrO_2 (MEL) in various sintering conditions were shown in Fig 4.8. The conductivities are shown as a function of temperature. The temperature operation stability of the bulk ionic conductivities for all specimens are the same, because the slopes for all specimens are quite similar. The slope of the bulk conductivities is less steep than that of the grain boundary conductivities, which indicates that the activation energies of the grain boundary conductivity are higher than the bulk conductivity. The oxygen ion migration passed the grain boundary is very difficult because of the grain boundary blocking effect [16-17, 28-29]. The activation energies calculated from the Arrhenius plots were shown in Table 4.3, The activation energy values were determined from the impedance data over the temperature range of 300°C to 550°C for the bulk and the grain boundary conductivities. The conductivities of the specimens are calculated and extrapolated from Arrhenius Eq (3.7) as shown in Table 4.3. The highest bulk conductivity was obtained from the pellet that was sintered at 1500°C for 4 hours. The activation energy of the bulk conductivity was smaller than that of the grain boundary

Table 4.3: Conductivity and Activation energy at 800°C for 8 mol% Y_2O_3 – ZrO_2 (MEL).

Sintering temperature(°C)	Sintering time (h)	Conductivity(S/cm)		Activation energy(eV)	
		bulk	gb	bulk	gb
1500	1	0.0713	0.0054	1.11	1.3
	2	0.0.840	0.0011	1.08	1.08
	4	0.0.960	0.0013	1.10	1.14
1550	1	0.0.891	0.0015	1.10	1.14
	2	0.0932	0.0012	1.10	1.17
	4	0.0969	0.0015	1.10	1.14

4.2.4 Microstructure

The microstructural images of 8 mol% $Y_2O_3 - ZrO_2$ (MEL) at various sintering temperatures were presented in Fig. 4. The specimens were thermally etched at $50^\circ C$ below sintering temperature for 5 minutes to enhance the appearance of grain boundaries [19]. The average grain size of the specimens after sintering for 4 hours at $1500^\circ C$ and $1550^\circ C$ were $4.2 \mu m$ and $4.6 \mu m$, respectively. There were numerous pores in the grains and at the grain boundaries, but these are isolated and do not present a continuous path through the sample. During The Final stage of sintering, in addition to an elimination of pores, a general coarsening of the microstructure by grain growth occurs. During this process the average grain size increases with time as the smaller grains are consumed by larger grains [30-31]. The grain size is a major factor determining the electrical property of ceramics. Guo and Zhang [16] have shown that the electrical property of YSZ is a function of grain size.

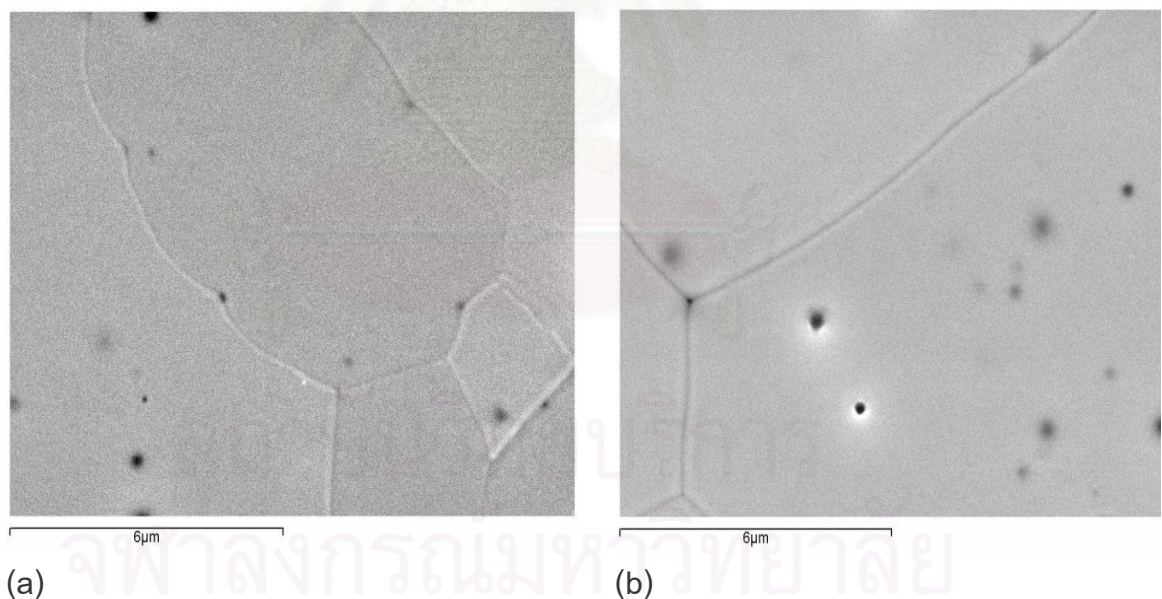


Fig 4.9: SEM micrographs of 8 mol% $Y_2O_3 - ZrO_2$ (MEL) sintering at $1500^\circ C$ (a) and $1550^\circ C$ (b) for 4 hours

4.2.5 Density

The relative densities of sintered electrolyte specimens were shown in Fig 4.10. The relative density increased with increasing sintering temperature from 1500°C to 1550°C. The relative density of specimens increases from 92.5 to 96.3% for sintering temperature at 1500°C for the soaking time one hour, two hour, and four hours. The relative density increases from 96.3 to 97.8% for the specimens sintered at 1550°C from one hour to four hours

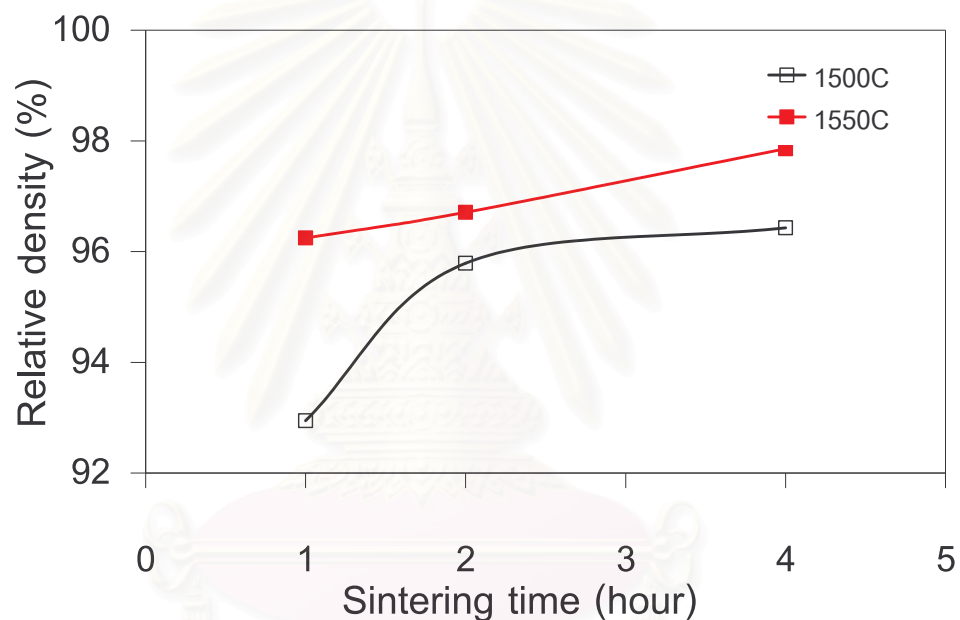


Fig 4.10: The relative density of 8 mol% Y_2O_3 - ZrO_2 (MEL) sintering at 1500°C and 1550°C.

4.3 Investigation of 8Y TOSOH (8 mol% Y_2O_3 - ZrO_2 TOSOH)

4.3.1 Particle size distribution

The particle size distribution of 8 mol% Y_2O_3 - ZrO_2 (TOSOH) was shown in Table 3.3; the curve distribution was shown in APPENDIX A. The mean particle size of 8Y TOSOH powder is 1.74 μm , in the size distribution ranging from 0.12 to 3.12 μm

4.3.2 X-Ray Fluorescence

The composition of 8Y TOSOH characterized from XRF was shown in Table 4.1. The presence of 1.40 wt % HfO_2 and 0.19 wt % Cl in the raw powder was detected.

4.3.3 AC-Impedance Spectra

The impedance spectra of 8 mol% $\text{Y}_2\text{O}_3\text{-ZrO}_2$ (TOSOH) electrolyte pellets after sintering at 1500°C and 1550°C for 1, 2 and 4 hours are shown Fig 4.11 to compare the sintering temperature effect. All the measurement temperatures were taken at 400°C . The impedance spectra showed only one semicircle at high frequency. The observed semicircle can be identified as a bulk property. This assertion is supported by the capacitance associated with it (5×10^{-11} F). As these spectra are unusual, it is suspected to be caused by impurities. From the XRF results, hafnium and chloride were detected. At 1500°C ; the bulk resistance was not different after changing the sintering time. For the bulk resistance, the sintering time was not significant. The conductivities of 8 mol% $\text{Y}_2\text{O}_3\text{-ZrO}_2$ (TOSOH) were influenced by the bulk resistance. At 1550°C , the sintering time was significant. The electrical conductivities were determined from Eq (3.5). Then use the Arrhenius Eq (3.7) was used to plot the dependence of the conductivity on the reciprocal of temperature as shown on Fig 4.13.

สถาบันวิทยบริการ
จุฬาลงกรณ์มหาวิทยาลัย

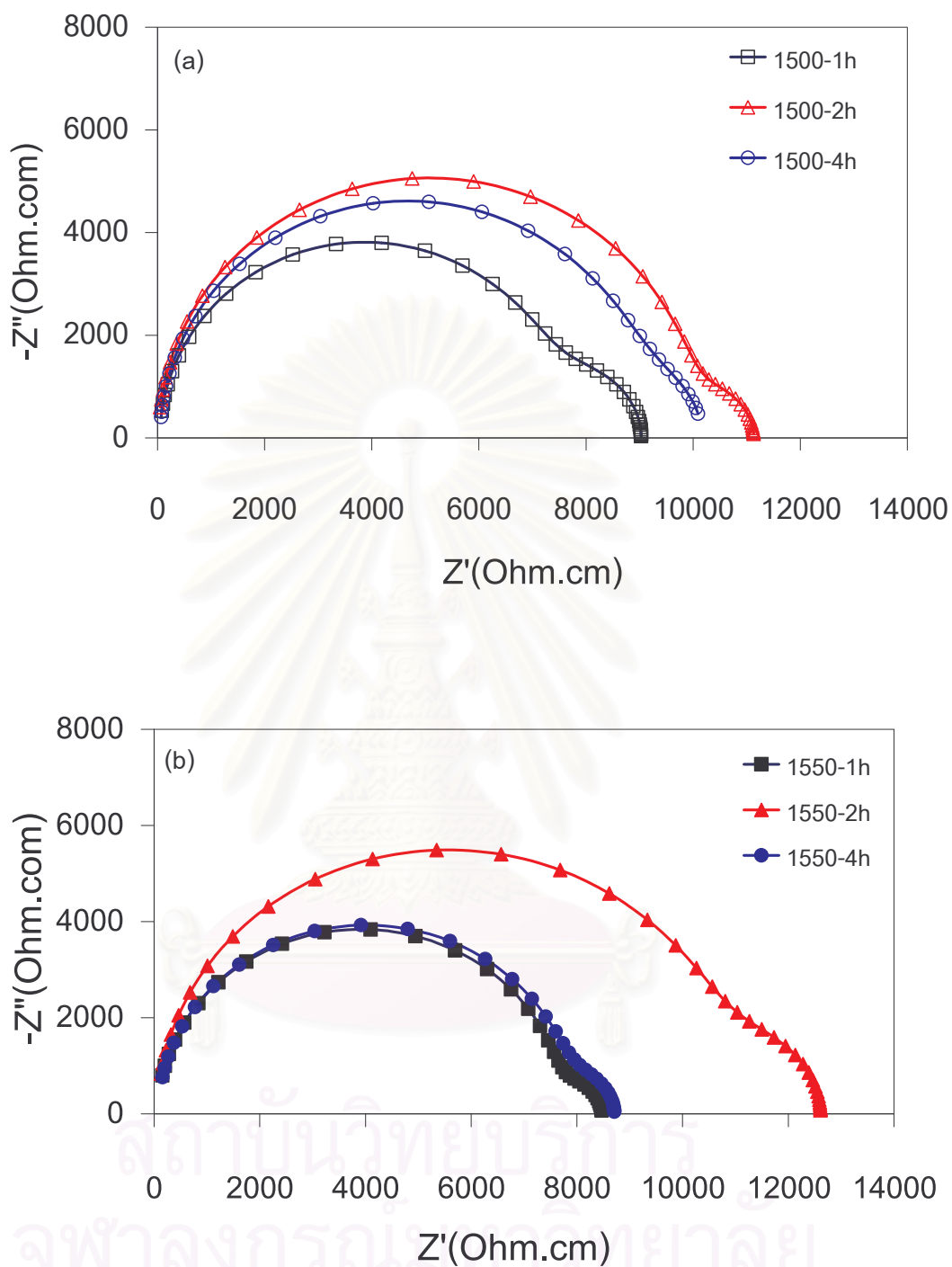


Fig 4.11: Impedance spectra of 8mol%Y₂O₃-ZrO₂ (TOSOH) electrolyte after sintering for (a) 1 hour, (b) 2 hours, and (c) 4 hours at 1500°C and 1550°C. All the measurements were taken at 400°C.

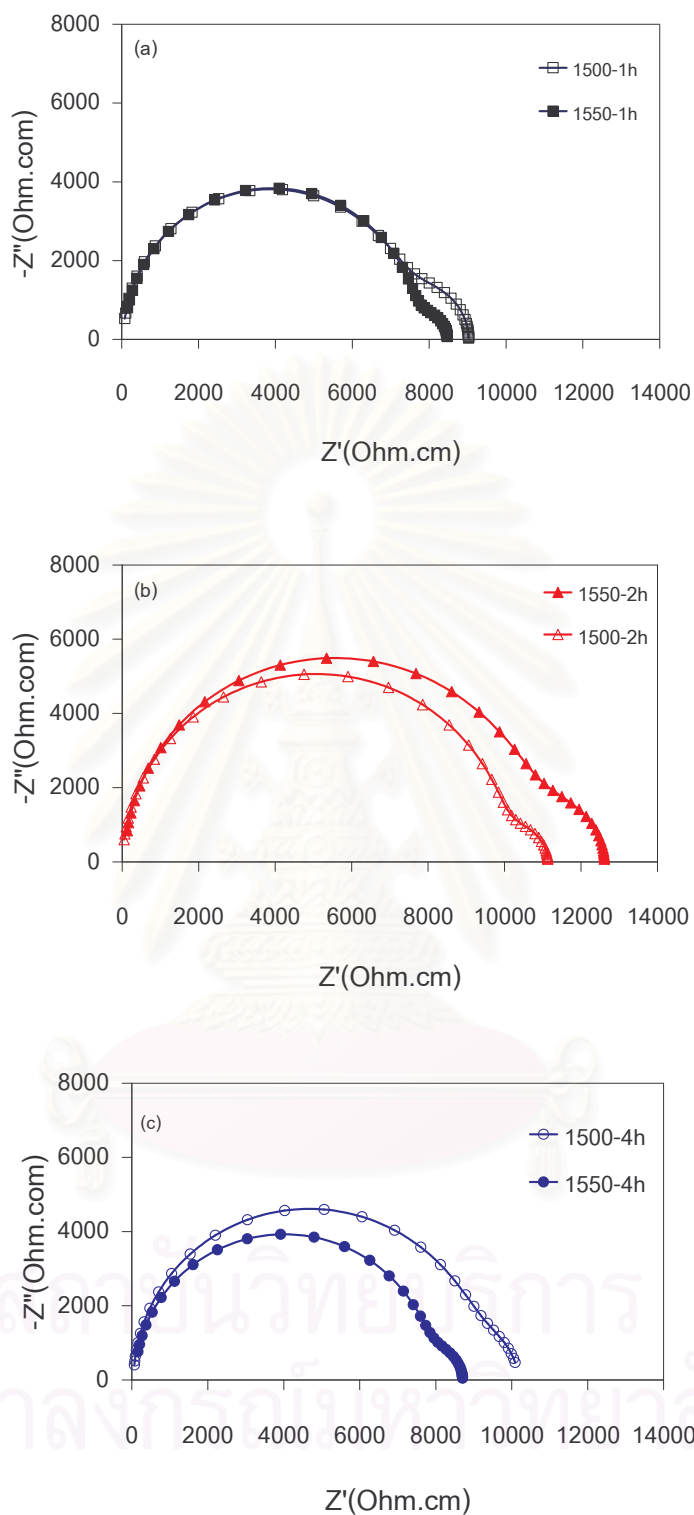


Fig 4.12: Impedance spectra of 8 mol%Y₂O₃-ZrO₂ (TOSOH) electrolyte after sintering for (a) 1 hour, (b) 2 hours, and (c) 4 hours at 1500°C and 1550°C. All the measurements were taken at 400°C.

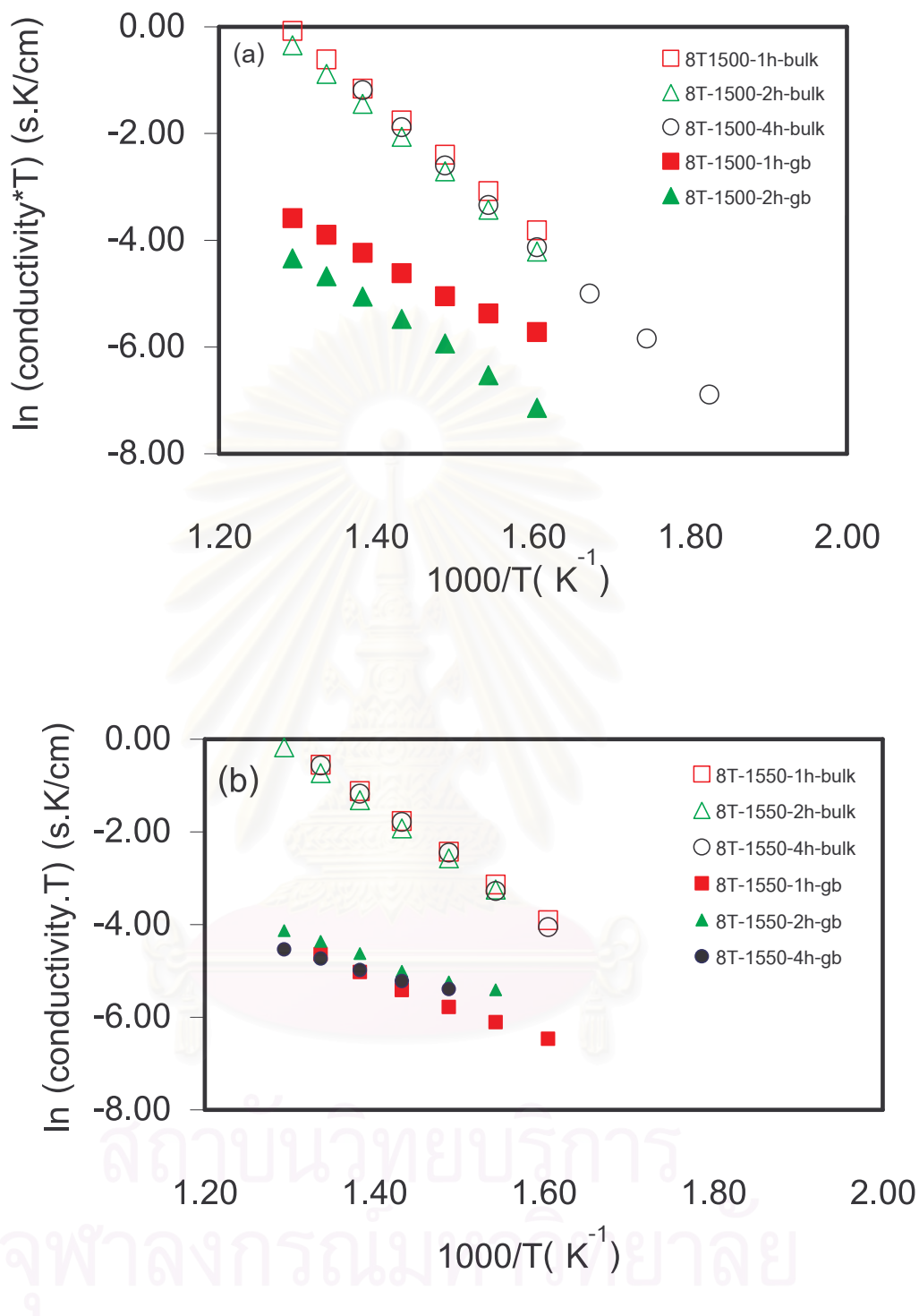


Fig 4.13: Arrhenius plots of the bulk and grain boundary conductivities for 8 mol% Y_2O_3 - ZrO_2 (TOSOH) sintered at 1500°C (a) and 1550°C (b) [for 1 hour, 2 hours, and 4 hours]

Fig 4.13 shows Arrhenius plots for the bulk and the grain boundary conductivities of 8 mol% $Y_2O_3 - ZrO_2$ (TOSOH). It can be seen from Fig 4.13 that the bulk and the grain boundary conductivities of the specimen sintered at different temperatures follows fairly well the Arrhenius relationship. The bulk and the grain boundary increase gradually as the sintering temperatures increase. The activation energies are shown in Table 4.4. The ionic conductivities at $800^\circ C$ were calculated and extrapolated from the Arrhenius relationship, and are shown in Table 4.4. The highest conductivity from this system was the specimen that was sintered at $1550^\circ C$ for 4 hours.

Table 4.4: Conductivity and Activation energy at $800^\circ C$ for 8 mol% $Y_2O_3 - ZrO_2$ (TOSOH).

Sintering temperature($^\circ C$)	Sintering time (h)	Conductivity(S/cm)		Activation energy(eV)	
		bulk	gb	bulk	gb
1500	1	0.0650	0.0003	1.03	0.60
	2	0.0581	0.0003	1.07	.078
	4	0.0879	ND	1.11	ND
1550	1	0.0854	0.0001	1.08	0.58
	2	0.0643	0.0001	1.06	0.46
	4	0.0919	0.0001	1.12	0.75

4.3.4 Microstructure

The microstructure of 8 mol% $Y_2O_3 - ZrO_2$ (TOSOH) is shown in Fig. 4.14. There were numerous spherical pores in Fig 4.14(a) more than in Fig 4.14(b). The lower sintering temperature showed more pores in the specimen with large amount of grain growth. During The Final stage of sintering, in addition to the elimination of pores, a general coarsening of the microstructure by grain growth occurs. During this process the average grain size increases with time as the smaller grains are consumed by larger grains [30-31]. The average grain sizes of $1500^\circ C$ and $1550^\circ C$ for the sintering times of

4 hours are 3.1 and 3.0 μm . The pores initially existed within the bulk and/or at the grain boundary which contribute to the change in the actual path of oxygen ions within the bulk and/or at grain boundaries. The existence of the pores weakens the conduction path between grains, causing these pores to impede the movement of the oxygen ions. With increasing of the sintering temperatures, these pores are continuously eliminated and density is increased. Therefore, the effective area of contact between the grains are improved, and the oxygen ions becomes mobile, resulting in an enhancement of the oxygen ion conductivity [22].

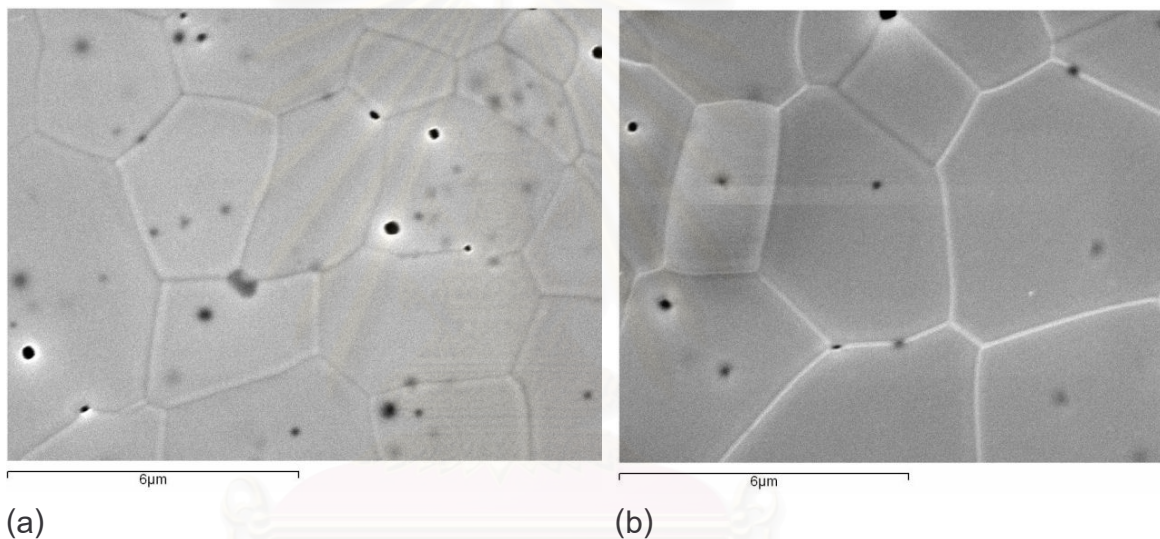


Fig 4.14: SEM micrographs of 8 mol% $\text{Y}_2\text{O}_3\text{-ZrO}_2$ (TOSOH) sintering at 1500°C (a) and 1550°C (b) for 4 hours

4.3.5 Density

The relative density of the electrolyte specimens were increased with increasing sintering temperature and sintering time as shown in Fig 4.15.

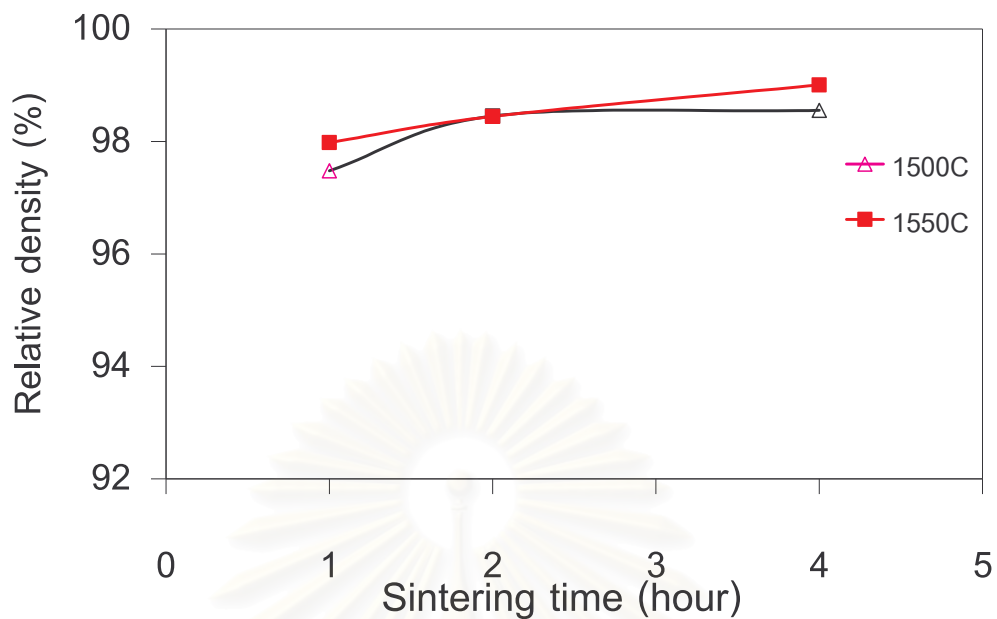


Fig 4.15: The relative density of 8 mol% Y_2O_3 - ZrO_2 (TOSOH) sintering at 1500°C and 1550°C.

4.4 Investigation of 8Y DAIICHI (8 mol% Y_2O_3 - ZrO_2 DAIICHI)

4.4.1 Particle size distribution

The mean particle size of 8 mol% Y_2O_3 - ZrO_2 (DAIICHI) is 0.89 μm , in the size distribution ranging from 0.59 to 1.39 μm . The curve distribution is shown in APPENDIX A.

4.4.2 X-Ray Fluorescence

The composition of 8 mol% Y_2O_3 - ZrO_2 (DAIICHI) characterized from XRF was shown in Table 4.1. The presence of 1.33 wt % HfO_2 and 0.33 wt % of As_2O_3 in the raw powder was detected.

4.4.3 AC-Impedance Spectra

The impedance spectra of 8 mol%Y₂O₃ - ZrO₂ (DAIICHI) as a function of sintering time at 1500°C and 1550°C are shown in Fig 4.16. All measurements were taken at 400°C that the two semicircles were closely overlapped. These results may come from the impurity [32]. The XRF presented only hafnium and arsenic. Kayan et al [33] suggested that the small amount of As₂O₃ increases the electrical conductivity of MnO₂. In this case the arsenic can be the grain boundary modifier to reduce the grain boundary resistance the same way as with alumina [34]. The bulk resistance decreased with increasing the sintering time at both sintering temperatures (Fig 4.16). The impedance measurements at different temperature (350-600°C) were shown in Appendix B. The bulk resistance disappeared at 500°C but a small semicircle of grain boundary appeared instead. The electrical conductivity of the electrolyte pellets are strong temperature dependent. The electrical conductivities were determined from Eq (3.5). Then the Arrhenius equation Eq (3.7) was used to plot the dependence of the conductivity on the reciprocal of absolute temperature.

Arrhenius plots of the bulk conductivity were shown in Fig 4.18. The bulk conductivity results are similar for all specimens. The activation energies calculated from $\ln\sigma T$ versus $1/T$ plot were presented in Table 4.5.

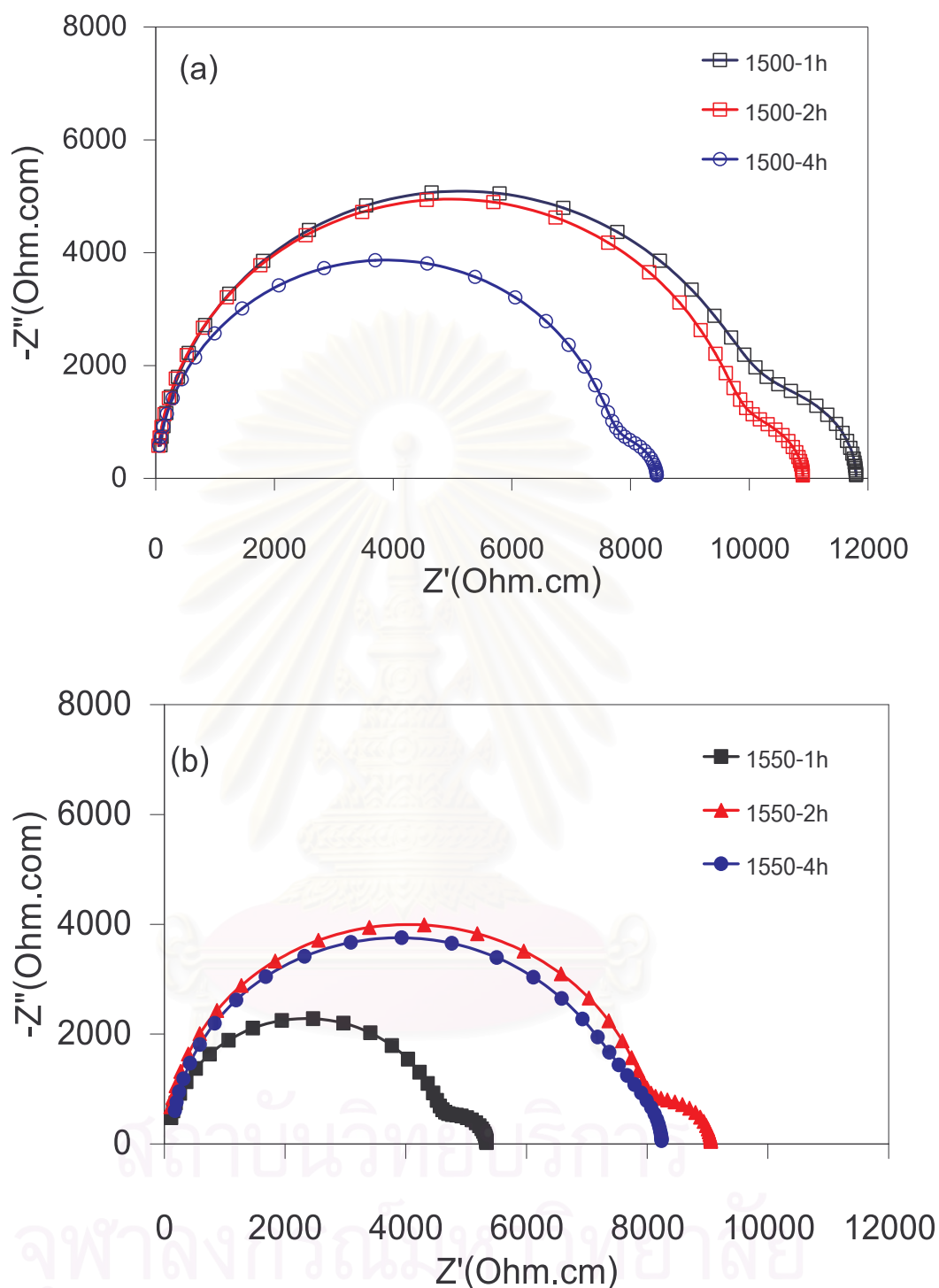


Fig 4.16: Impedance spectra of 8mol%Y₂O₃-ZrO₂ (DAIICHI) electrolyte after sintering at (a) 1500°C and (b) 1550°C (at various sintering time). All the measurements were taken at 400°C.

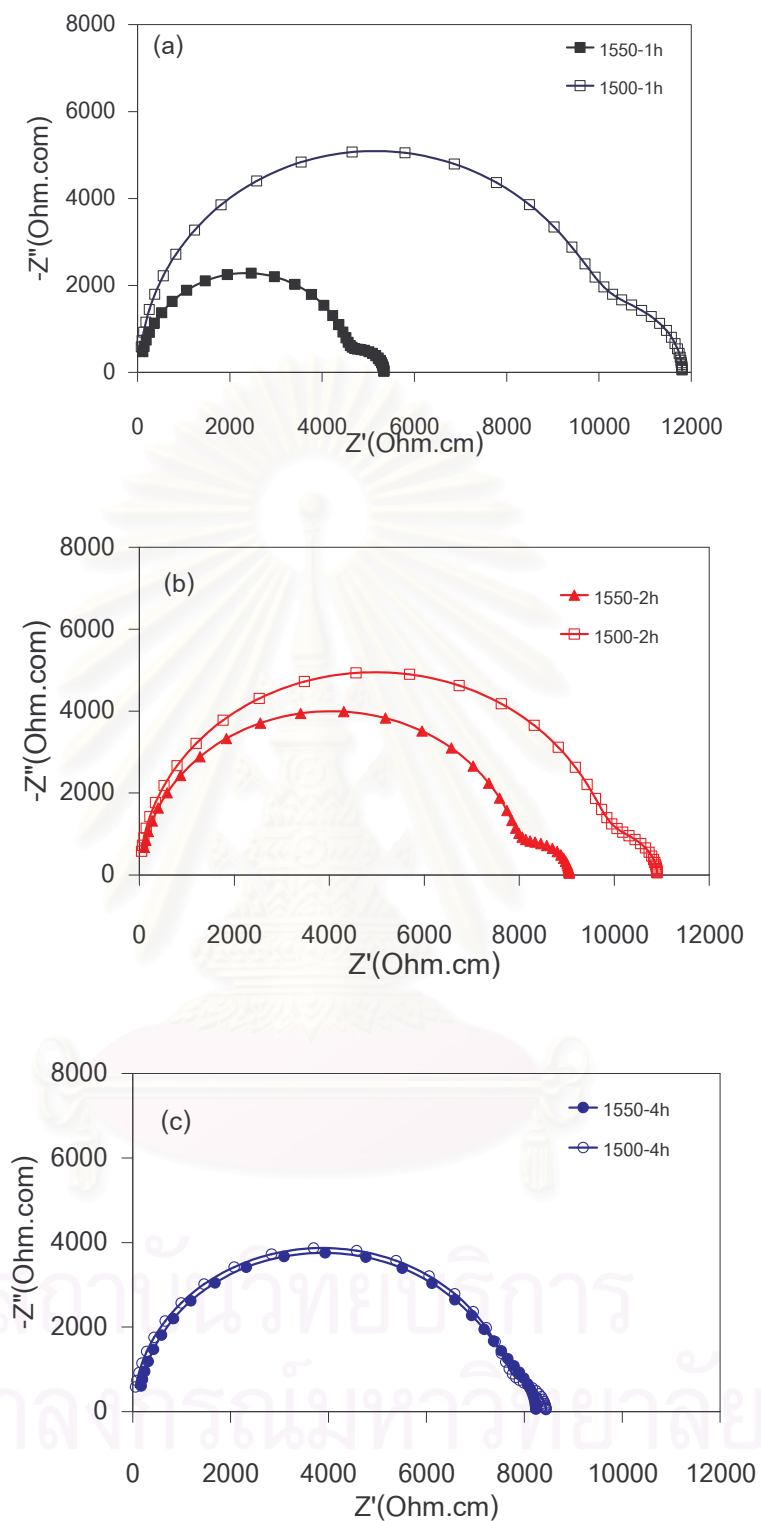


Fig 4.17: Impedance spectra of 8 mol% $\text{Y}_2\text{O}_3\text{-ZrO}_2$ (DAIICHI) electrolyte after sintering for (a) 1 hour, (b) 2 hours, and (c) 4 hour at 1500°C and 1550°C . All the measurements were taken at 400°C

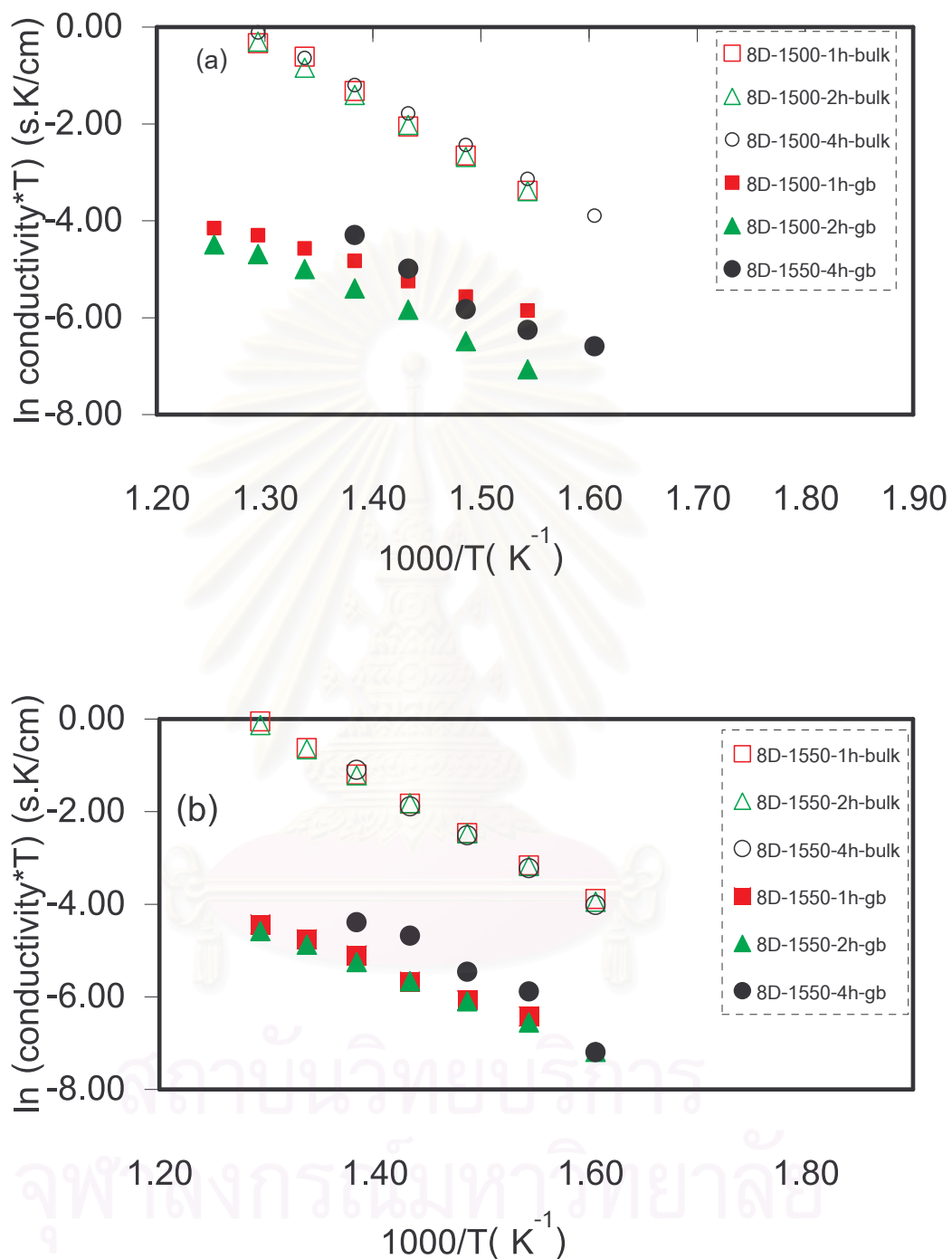


Fig 4.18: Arrhenius plots of the bulk and grain boundary conductivities for 8 mol% $\text{Y}_2\text{O}_3 - \text{ZrO}_2$ (DAIICHI) sintered at 1500°C (a) and 1550°C (b) [for 1 hour, 2 hours, and 4 hours]

Arrhenius plots of 8 mol% $Y_2O_3 - ZrO_2$ (DAIICHI) are shown in Fig 4.18. The gradient of the plotted line for the bulk conductivities was almost the same. This implied the stability of the conductivity with a change of temperature. From these graphs the activation energy was calculated as shown in Table 4.5. The ionic conductivities at 800°C were calculated and extrapolated from linear equation. The specimen that was sintered at 1550°C for 1 hour showed the highest bulk ionic conductivity at 800°C.

Table 4.5: Conductivity and Activation energy at 800°C for 8 mol% $Y_2O_3 - ZrO_2$ (DAIICHI)

Sintering Temperature(°C)	Sintering Time (h)	Conductivity (S/cm)		Activation Energy (eV)	
		bulk	gb	bulk	gb
1500	1	0.0607	0.0001	1.07	0.53
	2	0.0601	0.0002	1.07	0.78
	4	0.0669	0.0002	1.05	0.55
1550	1	0.0726	0.0002	1.06	0.71
	2	0.0688	0.0012	1.06	0.90
	4	0.0597	0.0002	1.02	0.72

4.4.4 Microstructure

The microstructural images of 8 mol% $Y_2O_3 - ZrO_2$ (DAIICHI) sintered at 1500°C for 4 hours are shown in Fig 4.19 (a). There were many pores in the grains and at grain boundaries. The grain sizes were distributed from 1.5 – 10 μm . At high sintering temperature (1550°C), there were fewer amounts of pores than that at lower sintering temperature (1500°C). The abnormal grain growths were presented, which is the process whereby a small number of grain grows rapidly to sizes which are higher than an order of magnitude larger than an average [31].

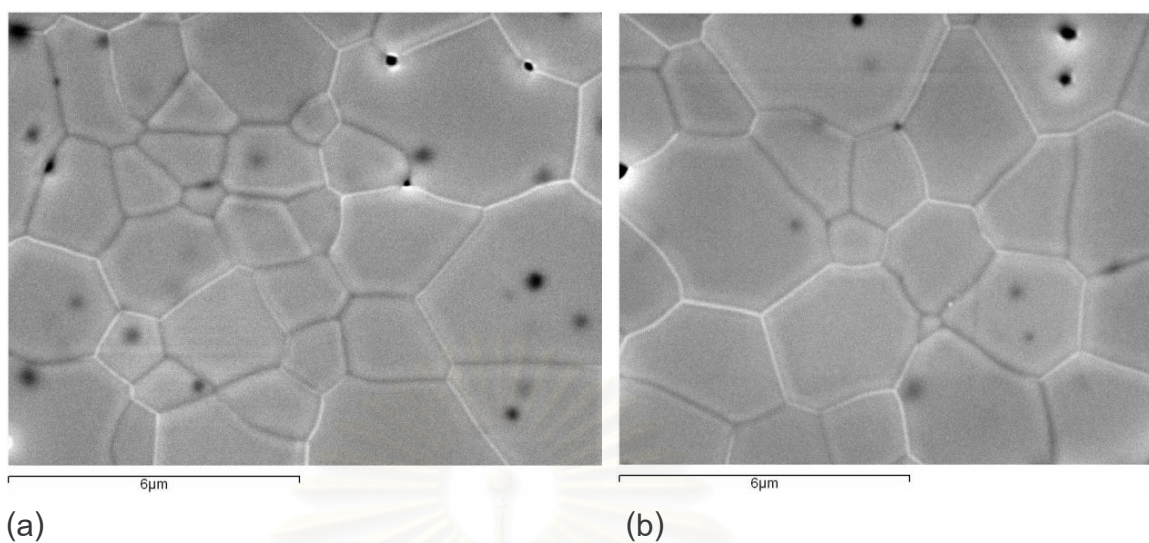


Fig 4.19: SEM micrographs of 8 mol% Y_2O_3 - ZrO_2 (DAIICHI) sintering at 1500°C (a) and 1550°C (b) for 4 hours

4.4.5 Density

The relative density of 8 mol % Y_2O_3 - ZrO_2 (DAIICHI) increases with increasing sintering temperature and sintering time. The relative density increases from 96.3 to 98.2%.

สถาบันวิทยบริการ
จุฬาลงกรณ์มหาวิทยาลัย

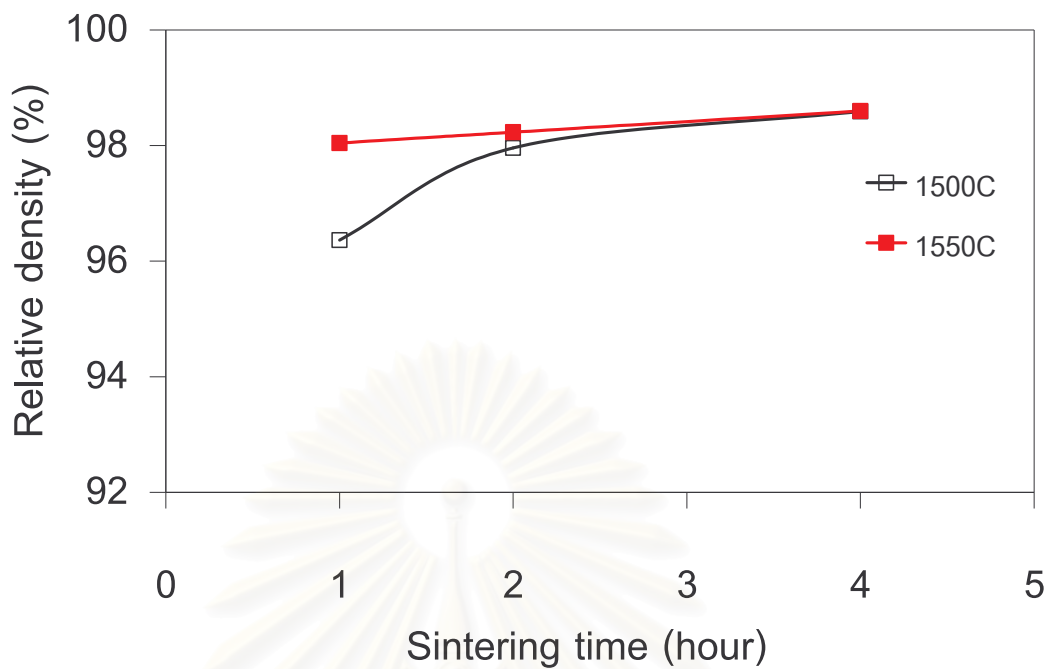


Fig 4.20: The relative density of 8 mol%Y₂O₃-ZrO₂ (DAIICHI) sintering at 1500°C and 1550°C.

4.5 Investigation of 8Y DAIICHI (10 mol%Y₂O₃-ZrO₂ DAIICHI)

4.5.1 Particle size distribution

The mean particle size of 10 mol%Y₂O₃-ZrO₂ (DAIICHI) is 0.35 μm, in the size distribution ranging from 0.12 to 0.64 μm. The curve distribution are shown in APPENDIX A.

4.5.2 X-Ray Fluorescence

The composition of 10 mol% Y₂O₃ – ZrO₂ (DAIICHI) characterized by XRF is shown in Table 4.1. The presence of 1.34 wt % HfO₂ and 0.35 wt % As₂O₃ in the raw powder was detected. The Electrical conductivity of the ceramic electrolyte was influenced by the processing and the purity of raw materials [22-26].

4.5.3 AC-Impedance Spectra

The impedance spectra plots for the 10 mol% Y_2O_3 - ZrO_2 (DAIICHI) measured at $400^\circ C$ are shown in Fig 4.21 and 4.22 for electrolyte pellets after sintering at $1500^\circ C$ and $1550^\circ C$ for 1, 2 and 4 hours. From the impedance spectra there seems to be only one-semicircle at the high frequency for all specimens at all temperatures. The bulk and the grain boundary semicircle were overlapped [6]. The RC circuit was used to fit the impedance spectra showing the bulk and the grain boundary resistances. These results indicated the capacitances of 5×10^{-11} and $5 \times 10^{-9} F$, respectively and presented a small amount of grain boundary resistance. This phenomenon may be caused by the impurity in the powder [32-34]. The bulk resistance is depending on the sintering time. For the 4 hours of sintering time the value of the bulk resistance is the greatest (Fig 4.20). The bulk resistances are decreased when the sintering time is increased. The specimens sintered at $1550^\circ C$ showed the bulk resistance smaller than the specimens being sintered at $1500^\circ C$ (Fig 4.22). The electrical conductivity of the electrolyte pellets is temperature dependent. The electrical conductivities are determined from Eq (3.5). An Arrhenius plot between the conductivity and the reciprocal of absolute temperature is shown in Fig 4.23.

Arrhenius plots of the bulk conductivity are shown in Fig 4.23. The bulk conductivity shows the same trend for all specimens. The activation energies calculated from $\ln\sigma T$ versus $1/T$ plot are presented in Table 4.6.

สถาบันวิทยบริการ
จุฬาลงกรณ์มหาวิทยาลัย

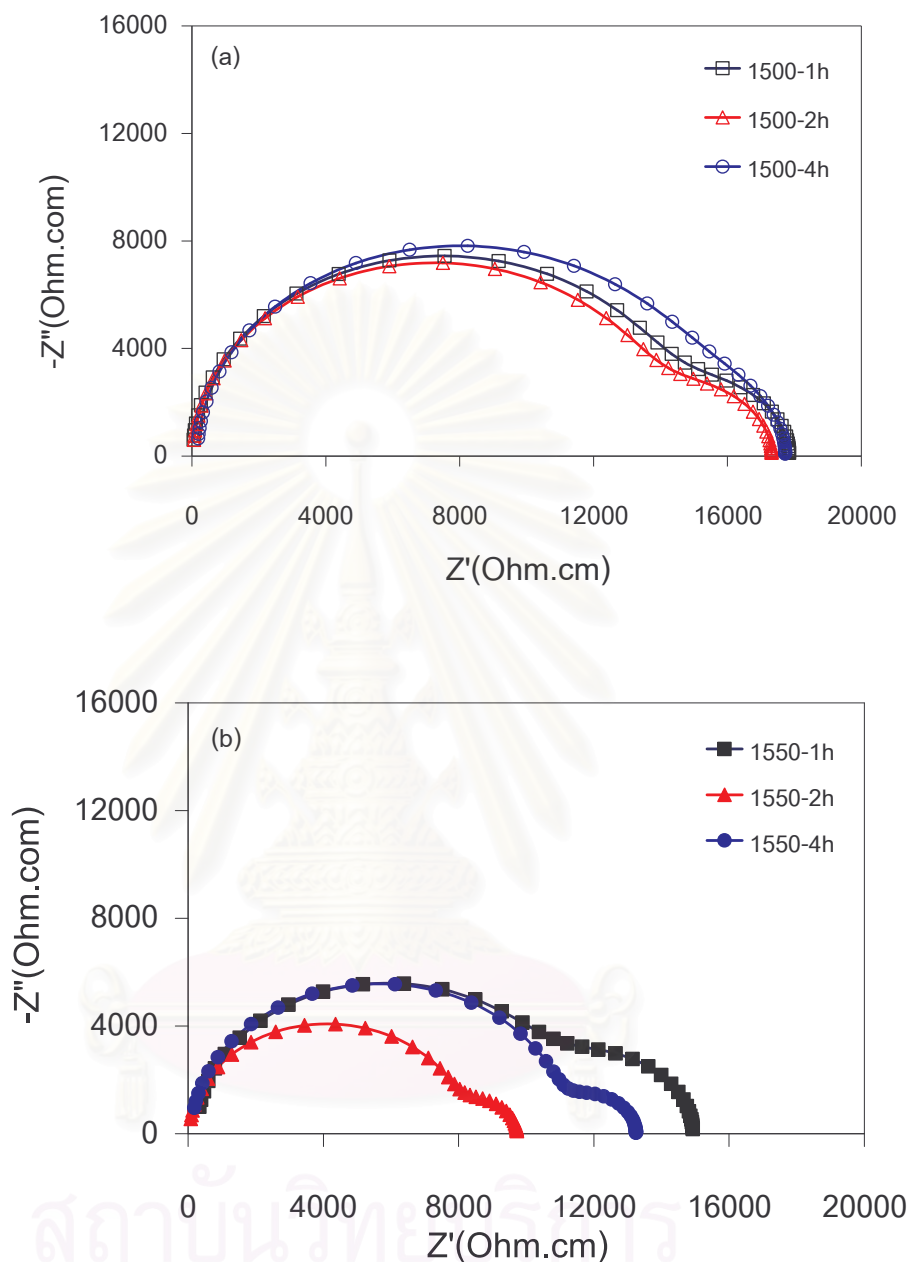


Fig 4.21: Impedance spectra of 10 mol% $\text{Y}_2\text{O}_3\text{-ZrO}_2$ (DAIICHI) electrolyte after sintering at (a) 1500°C and (b) 1550°C for (at various sintering time). All the measurements were taken at 400°C .

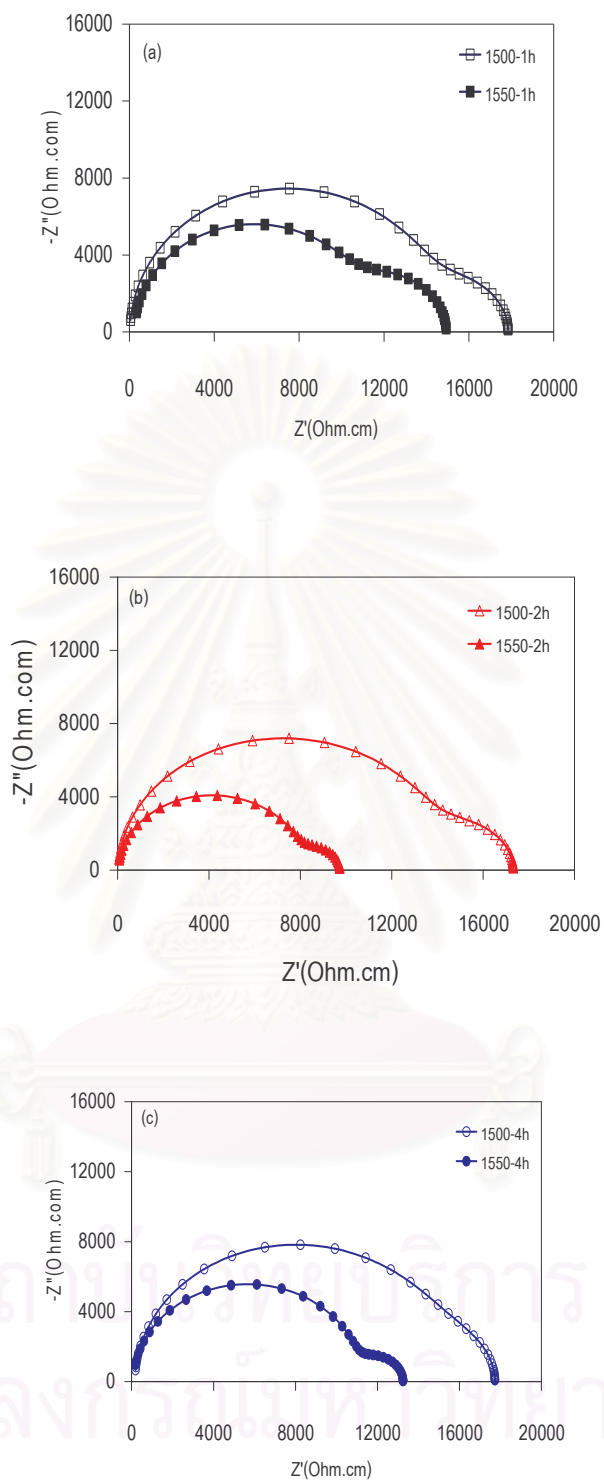


Fig 4.22: Impedance spectra of 10 mol% $\text{Y}_2\text{O}_3\text{-ZrO}_2$ (DAIICHI) electrolyte after sintering for (a) 1 hour, (b) 2 hours, and (c) 4 hours at 1500°C and 1550°C . All the measurements were taken at 400°C .

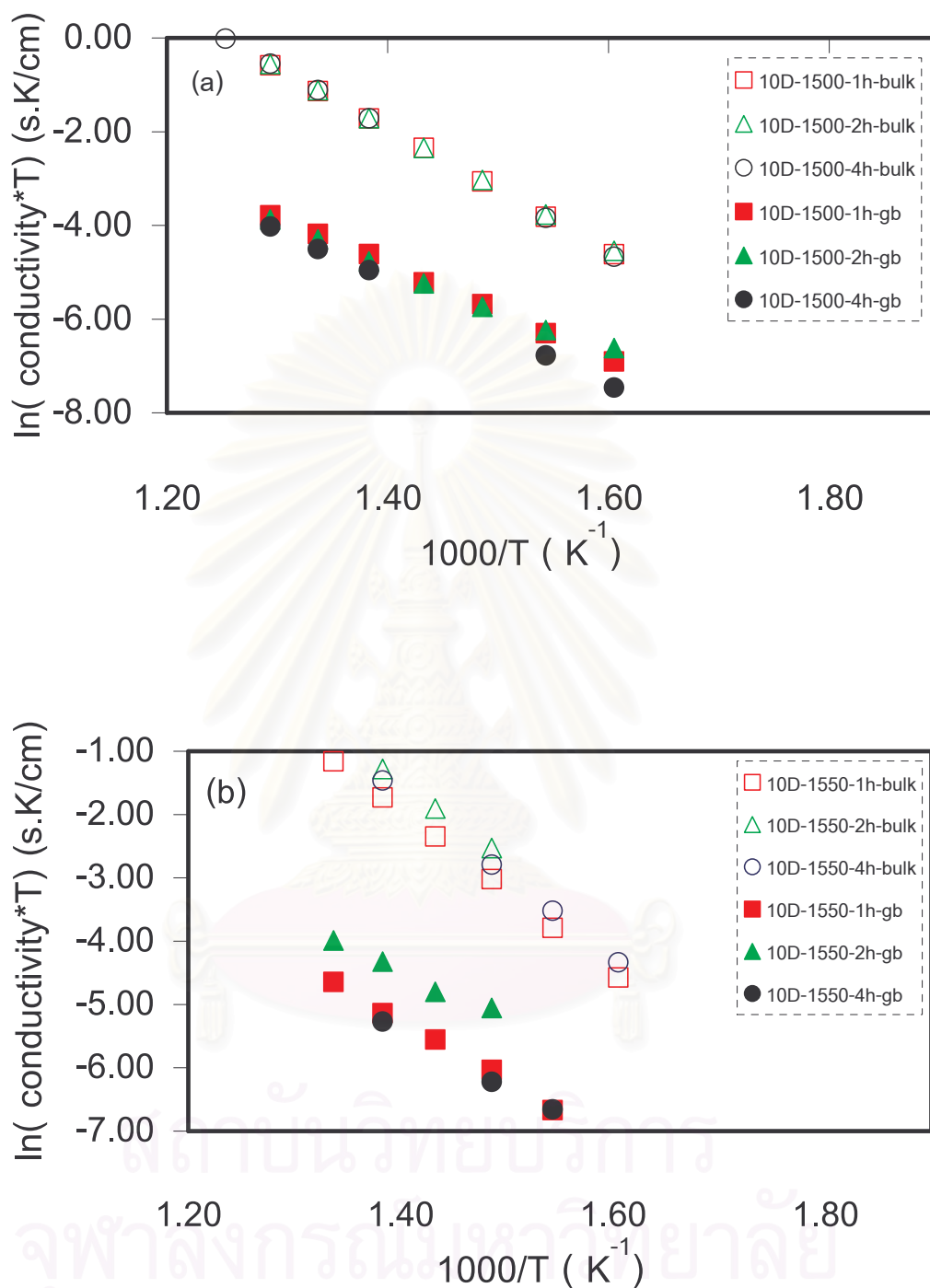


Fig 4.23: Arrhenius plots of the bulk and grain boundary conductivities for 10 mol% $\text{Y}_2\text{O}_3 - \text{ZrO}_2$ (DAIICHI) sintered at 1500°C (a) and 1550°C (b) [for 1 hour, 2 hours, and 4 hours]

Arrhenius plots of the 10 mol% $Y_2O_3 - ZrO_2$ (DAIICHI) are shown in Fig 4.23. The bulk conductivities are higher than the grain boundary conductivities. The conductivities are thermally influenced. The ionic conductivity increases with increasing sintering temperatures. The gradient of the linear plot presents the change in conductivity with temperature. All the Arrhenius plots of the bulk conductivities are similar. The activation energies at 800°C were calculated as shown in Table 4.6.

Table 4.6: Conductivity and Activation energy at 800°C for 10 mol% $Y_2O_3 - ZrO_2$ (DAIICHI).

Sintering temperature(°C)	Sintering time (h)	Conductivity(S/cm)		Activation energy(eV)	
		bulk	gb	bulk	gb
1500	1	0.0573	0.0008	1.12	0.87
	2	0.0548	0.0005	1.11	0.77
	4	0.0645	0.0009	1.14	0.95
1550	1	0.0525	0.0004	1.10	0.81
	2	0.0678	0.0003	1.10	0.64
	4	0.0729	0.0002	1.11	0.73

4.5.4 Microstructure

The microstructural images of 10 mol% $Y_2O_3-ZrO_4$ sintered at 4 hours for 1500°C and 1500°C was depicted in Fig 4.24. The specimens showed many pores in both sintering temperatures (1500°C and 1550°C). The average grain sizes were 2.8 μm and 3.9 μm .

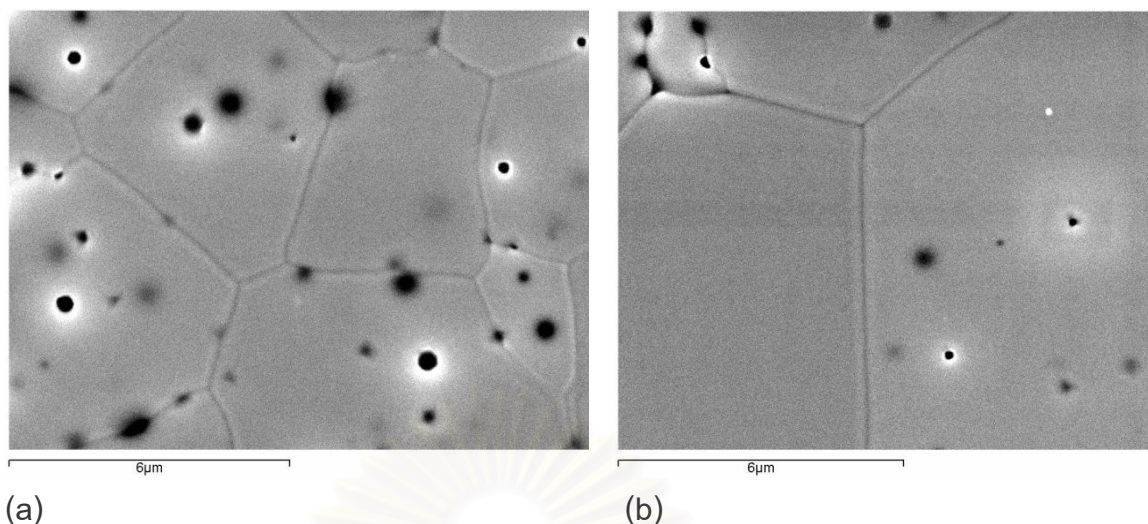


Fig 4.24: SEM micrographs of 10 mol% $\text{Y}_2\text{O}_3\text{-ZrO}_2$ (DAIICHI) sintering at 1500°C (a) and 1550°C (b) for 4 hours

4.5.5 Density

The relative density of the 10 mol% $\text{Y}_2\text{O}_3\text{-ZrO}_4$ DAIICHI increases with increasing sintering temperature and sintering time (at 1500°C and 1550°C for 1 hour to 4 hours)

สถาบันวิทยบริการ
จุฬาลงกรณ์มหาวิทยาลัย

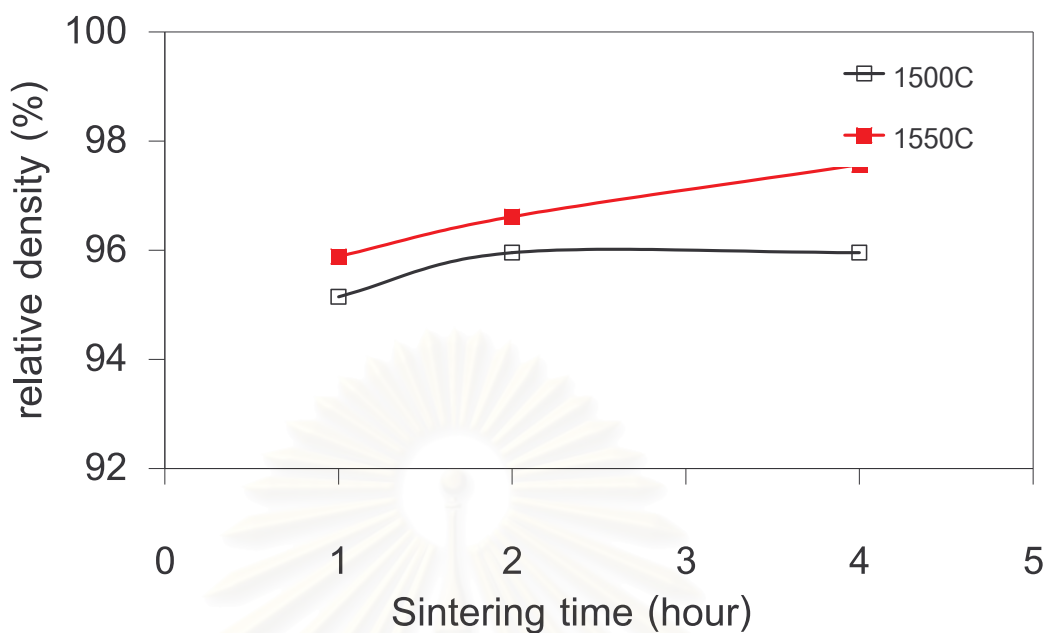


Fig 4.25: The relative density of 10 mol% $\text{Y}_2\text{O}_3\text{-ZrO}_2$ sintering at 1500°C and 1550°C

4.6 Discussion of the pellet impedance spectra

The conductivity of stabilized zirconia initially increased with the dopant content (and vacancy concentration). Upon reaching the maximum value at around 8 mol% Y_2O_3 , the conductivity started to decrease when the amount Y_2O_3 dopant was increased [28-29]. The impedance spectra of 8 mol% Y_2O_3 from various suppliers showed different characteristics, as shown in Fig 4.26. The total resistance is almost the same, but the impedance spectra of 8 mol% $\text{Y}_2\text{O}_3\text{-ZrO}_2$ MEL showed two separate semicircles clearly. While the 8 mol% $\text{Y}_2\text{O}_3\text{-ZrO}_2$ from DAIICHI and TOSOH showed only one semicircle representing the bulk resistance. A careful consideration of the composition of the raw materials powder was made as shown in Table 4.1.

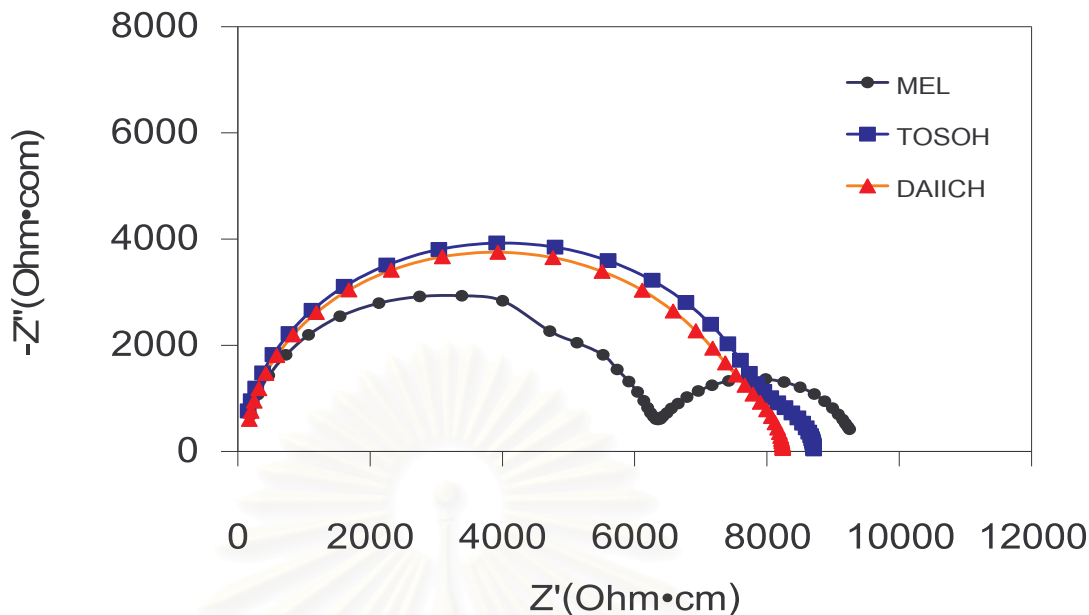


Fig 4.26: Impedance spectra of electrolyte (pellet) from various suppliers (DAIICHI, MEL and TOSOH) after sintering at 1550°C for 4 hours. Impedance spectra were taken at 400°C .

4.7 Characterization of electrolyte materials, prepared by tape casting

Fig 4.27 showed the impedance spectra of electrolyte materials (MEL, TOSOH, and DAIICHI) that were prepared by tape casting and sintered at 1500°C for 4 hours, the impedance spectra were measured at 400°C . The impedance spectra of all specimens exhibited two well-defined semicircles that could be easily separated and resolved. This result was different from the pellet specimens of DAIICHI and TOSOH. The organic binder used in the tape casting process might cause the grain boundary effect. Therefore, the impedance spectra of specimens that prepared by tape casting clearly showed the grain boundary resistance. The first semicircle, in the high frequency domain, represented the contribution of the bulk and the other was related to blocking of conduction by grain boundaries. The grain boundary resistance was smaller than the bulk resistance. Arrhenius plots for bulk and grain boundary conductivity of specimens as shown in the Fig 4.28, the results indicated that the conductivity of the MEL specimen was the highest and the slopes of both specimens were quite similar.

The microstructural images of those specimens are shown in Fig 4.29. The grain size of MEL specimen was smaller than the TOSOH and DAIICHI specimens. However, the microstructure of TOSOH was different from other specimens that it was not dense as others. This phenomenon might be affected from the impurity which occurred during fabrication. The other possibility is that the sintering was not completed that led to very high bulk resistance.

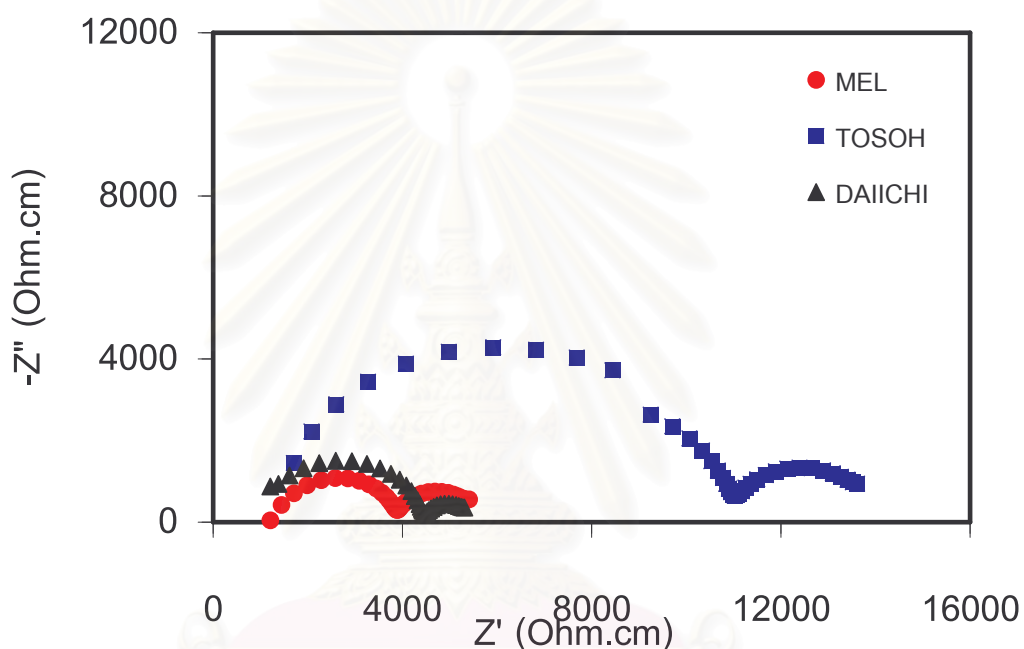


Fig 4.27: Impedance spectra of 8 mol% Y_2O_3 - ZrO_2 MEL, TOSOH and DAIICHI electrolyte (tape casting) after sintering for 4 hours at $1500^\circ C$. All the measurements were taken at $400^\circ C$.

สถาบันวิทยบริการ
จุฬาลงกรณ์มหาวิทยาลัย

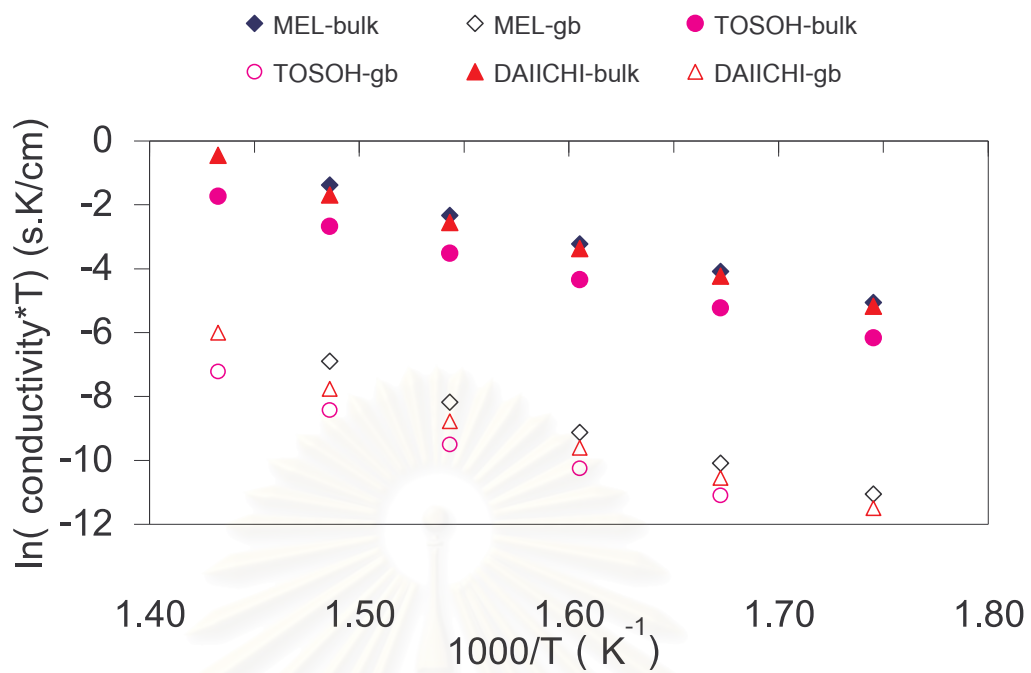


Fig 4.28: Arrhenius plots of the bulk and grain boundary conductivities for 8 mol% Y_2O_3 - ZrO_2 (tape casting) sintered at $1500^\circ C$ for 4 hours

สถาบันวิทยบริการ
จุฬาลงกรณ์มหาวิทยาลัย

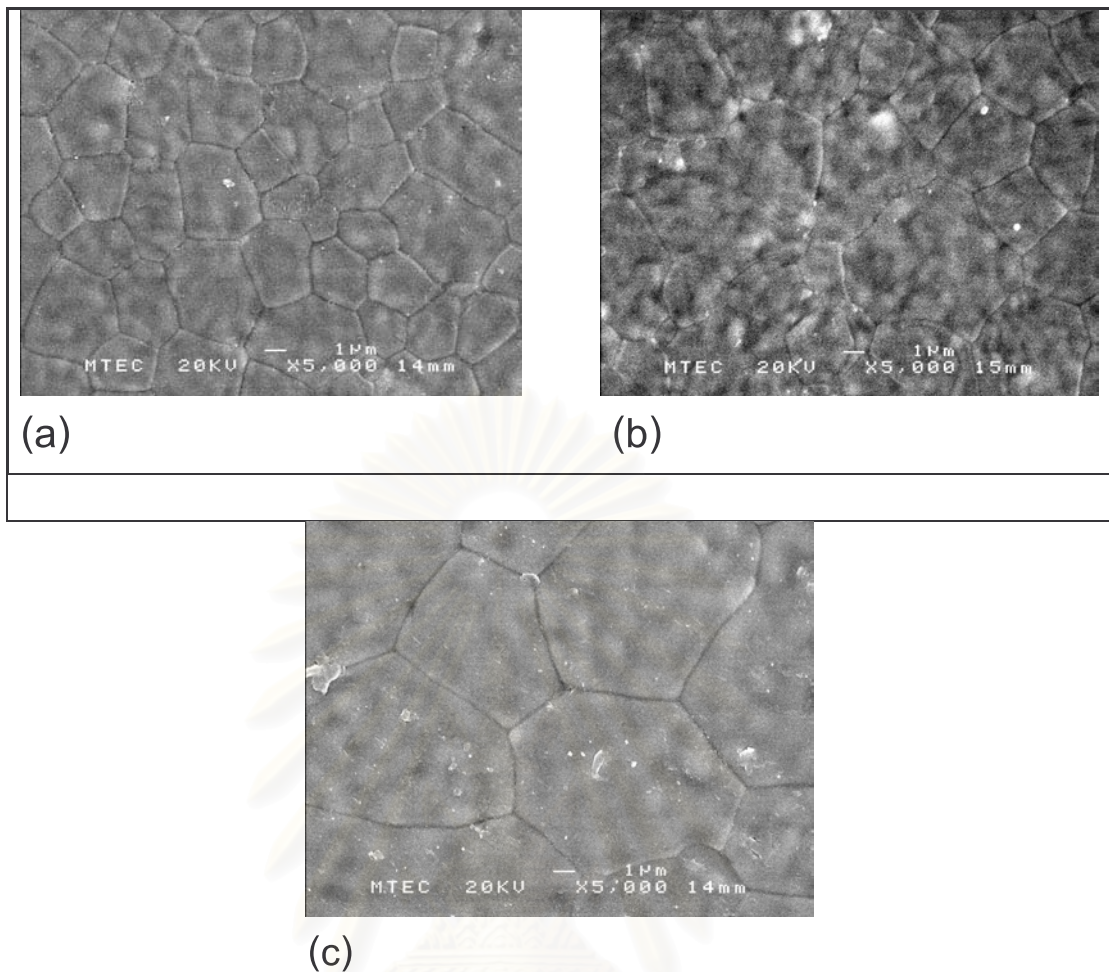


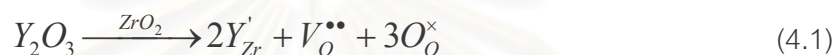
Fig 4.29: Microstructures of 8 mol% Y_2O_3 - ZrO_2 (tape casting) sintering at $1500^\circ C$ for 4 hours, [MEL (a), TOSOH (b), and DAIICHI (c)]

4.8 Summary

The electrical conductivity is greatly influenced by the concentration of defects and their interactions [26]. An increase in conductivity is due to the increase of the amount of charge carriers, i.e., the oxygen vacancies, at low dopant content. At a concentration of vacancies approximately between 3 and 7 mol% Y_2O_3 , the electrostatic interactions among defects take place, which results in an increase of the activation energy. At 8 mol% Y_2O_3 , there is equilibrium between the increase of oxygen vacancies and the increase of electrostatic interactions between the created defects, i.e., the vacancies and the substituted dopant cations. Therefore, a maximum in conductivity will be observed for a specimen with 8 mol% Y_2O_3 . On further increase of the dopant

concentration (>8 mol% Y_2O_3), the interaction among the defects becomes the dominating factor giving rise to a gradual decrease in the electrolyte conductivity [26], because the mobility of the oxygen ions is hindered.

The curvature of Arrhenius plots of the electrical conductivity is consistent with the dissociation of the oxide ion vacancy from the dopant Y^{3+} ion [10]. It is well known that doping of ZrO_2 with Y_2O_3 results in substitution incorporation of Y^{3+} on the Zr^{4+} cation sublattice with the concomitant formation of oxygen vacancies as charge compensating defects. The defect formation reaction can be written in Kröger and Vink notation as



Due to Coulombic and elastic attractive forces between Y'_{Zr} and $V_O^{\bullet\bullet}$ the existence of two associates can be postulated as;



and



Manning et al [36] suggested that $(Y_{Zr}V_O)^{\bullet}$ is more likely to occur because of the expected random distribution of Y'_{Zr} . The effect of the binding enthalpy of an associate can be significant after the population of free vacancies at low temperature. At lower temperatures the association is almost complete, therefore,

$$[(Y_{Zr}V_O)^{\bullet}] \gg [V_O^{\bullet\bullet}] \quad (4.4)$$

And

$$[V_o^{**}] = \frac{A}{T} \text{EXP}\left(-\frac{Ea}{RT}\right) \quad (4.5)$$

Where Ea is the association binding enthalpy, R is the gas constant, T is the absolute temperature, and A is a pre-exponential constant. The conductivity (σ) can be explained by Eq.(4.6)

$$\sigma = e\mu[V_o^{**}] \quad (4.6)$$

where μ is the mobility. And e is an effective charge. The mobility is given by

$$\mu = \frac{B}{T} \exp\left(-\frac{Em}{RT}\right) \quad (4.7)$$

Where Em is the enthalpy for motion and B is a pre-exponential constant. The conductivity can be explained by the oxygen vacancy concentration (Eq.4.5) and the mobility (Eq. 4.7)

$$\sigma = e \frac{C}{T^2} \exp\left[\frac{-(Ea + Em)}{RT}\right] \quad (4.8)$$

where C is a pre-exponential constant. The activation energy for conduction (Ec) is expressed as

$$Ec = Ea + Em \quad (4.9)$$

At higher temperatures the complex of $(Y_{Zr}V_o)^{\cdot}$ dissociates completely to free V_o^{**} and $V_o^{**} = Y'_{Zr}$. The concentration of free V_o^{**} is independent of the temperature and equal to the total concentration of dopant Y^{3+} . Therefore, the migration enthalpy, Em , could be estimated from the slope of the temperature dependence for conduction in high temperature range. The association enthalpy could be calculated from the difference of the slopes in a lower temperature range and in a high temperature one.

Fig 4.30 showed the impedance spectra of 8 mol % $Y_2O_3 - ZrO_2$ that were prepared from different routes. The impedance spectra depend on the fabrication, impurities and the microstructure. All of these affect the electrical property of specimens. The electrical conductivity of 8YSZ from MEL was higher than TOSOH and DAIICHI.

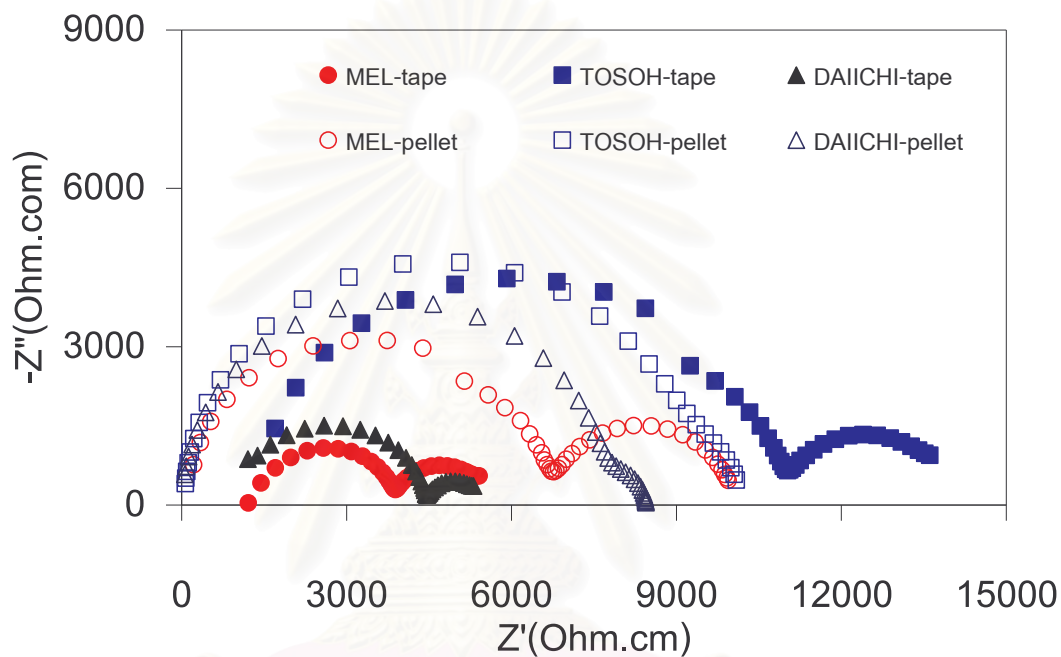


Fig 4.30: Impedance spectra of 8 mol% $Y_2O_3 - ZrO_2$ MEL, TOSOH and DAIICHI electrolyte after sintering for 4 hours at $1500^\circ C$ (prepared by pellet and tape casting). All the measurements were taken at $400^\circ C$.

สถาบันวิจัยวัสดุ
จุฬาลงกรณ์มหาวิทยาลัย

CHAPTER V

CONCLUSIONS

AC-Impedance Spectroscopy is a very attractive and powerful technique in fuel cells research and development. It can be used as an in situ technique. The interpretation and modeling of impedance data still remains a complicated technique. An investigation of the electrical property of electrolyte material can be provided using AC Impedance Technique. Three typical compositions of Y_2O_3 doped ZrO_2 electrolyte (3, 8 and 10 mol% Y_2O_3) powders from various suppliers were investigated. The microstructures of sintered specimens were significantly related to the electrical properties of the electrolyte.

- For 3 mol% $Y_2O_3 - ZrO_2$, the conductivity variation in sintered ceramic prepared from MEL was significant with sintering conditions. The specimen sintered at $1500^\circ C$ for 4 hours showed the highest conductivity. The impedance spectra showed separate bulk and grain boundary resistances semicircle clearly. The average grain size is between 0.7 to 0.8 μm .
- For 8 mol% $Y_2O_3 - ZrO_2$, the grain size distribution is large. The conductivity was highest in comparison with 3 and 10 mol% Y_2O_3 contents.
- The Impedance Spectra of 8 mol% $Y_2O_3 - ZrO_2$ MEL showed two semicircles, representing clearly the bulk and grain boundary resistances. The bulk and the grain boundary resistance decreased with increasing the measuring temperature.
- Although using the same amount of Y_2O_3 contents but impedance spectra show different shapes of impedance spectra. These phenomena depend on the impurity content and sintering conditions.
- 8 mol% $Y_2O_3 - ZrO_2$ from MEL showed the highest conductivity at $800^\circ C$ when sintered at $1550^\circ C$ for 4 hours. From the Impedance Spectra the bulk resistance was larger than the grain boundary resistance.

- The impedance spectra showed only the bulk resistance for 8 mol% Y_2O_3 – ZrO_2 from DAIICHI and TOSOH. This Phenomenon is the same as 10 mol% Y_2O_3 – ZrO_2 from DAIICHI.
- The capacitance of each semicircle is used to differentiate between the bulk and the grain boundary resistances.



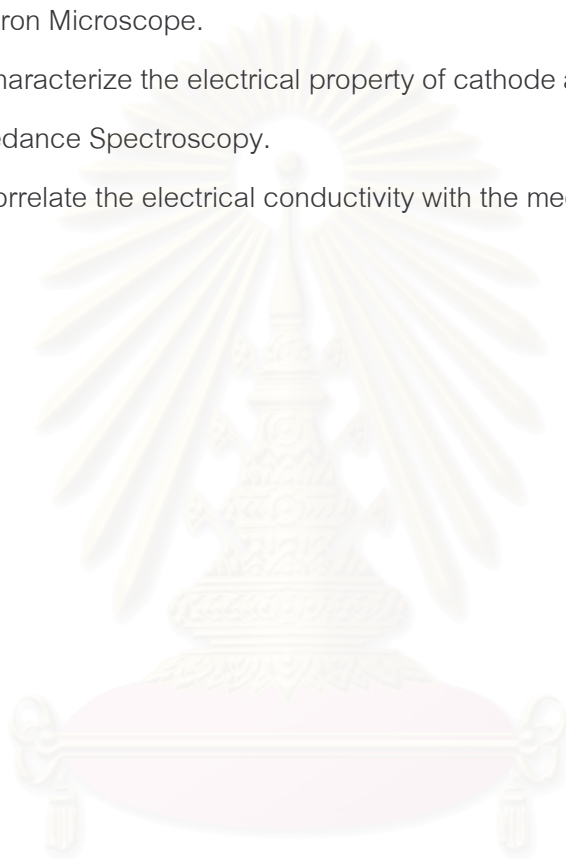
สถาบันวิทยบริการ
จุฬาลงกรณ์มหาวิทยาลัย

CHAPTER VI

SUGGESTIONS FOR THE FUTER WORK

The future work from this thesis is proposed as follows;

1. To investigate the microstructure of grain boundary using Transmission Electron Microscope.
2. To characterize the electrical property of cathode and anode using AC-Impedance Spectroscopy.
3. To correlate the electrical conductivity with the mechanistic model.



สถาบันวิทยบริการ
จุฬาลงกรณ์มหาวิทยาลัย

REFERENCES

1. Haile, S.M. Fuel cells Materials and components. Acta Materialia. 55 (2003): 5981-6000.
2. Minh, N.Q., and Takahashi, T. Science and Technology of Ceramic Fuel Cells. Elsevier, 1995.
3. Minh, N.Q. Ceramic Fuel Cells. J. of American Ceramic Society. 76 [3] (1993): 563-588.
4. Larmirie, J., and Dicks, A. Fuel Cells System Explain. New York: John Wiley & Sons, 2000.
5. Singhal, S.C., and Kendall, K. High Temperature Solid Oxide Fuel Cells. Elsevier, 2003.
6. Macdonald, J.R. Impedance Spectroscopy. New York: John Wiley & Sons, 1987.
7. Badwal, S.P.S. Stability of solid oxide fuel cell components. Solid State Ionics 143 (2001): 39-46.
8. Skinner, S.J., and Kilner, J.A. Oxygen ions conductor. Materialstoday. (2003): 30 – 36.
9. Stevens, R. Zirconia and Zirconia ceramics. Magnesium Elektron, 1986.
10. Arachi, Y., Sakai, H., Yamamoto, O., Takeda, Y., and Imanishai, N. Electrical conductivity of the $ZrO_2 - Ln_2O_3$ (Ln = lanthanides) system. Solid State Ionics. 121 (1999): 133–139.
11. Haering, C., Roosen, A. and Schichl, H. Degradation of the electrical conductivity in stabilized zirconia systems Part I: yttria stabilized zirconia. Solid State Ionics. 176 (2005): 253–259.
12. Graaf van de, M.A.C.G., and Burggraaf, A.J. Science and Technology of Zirconia II. In Claussen, N., Rühle, M. and Heuer, A.H. (eds.), Americanceramic Society. OH, 1984.
13. Bard, A.J., and Foukner, L.R. Electrochemical Methods Fundamentals and Applicatins. John Wiley & Sons, 1980

14. Bauerle, J.E. Study of solid electrolyte polarization by complex admittance method. J. Physics Chemistry Solids. 30 (1969): 2657 – 2670.
15. Kurumada, M., Hara, H., and Iguchi, E. Oxygen vacancies contributing to intragranular electrical conduction of yttria-stabilized zirconia (YSZ) ceramics. Acta Materialia. 53 (2005): 4839-4846.
16. Guo, X. and Zhang, Z. Grain Size dependent grain boundary defect structure: case of zirconia. Acta Materialia. 51 (2003): 2539–2547.
17. Guo, X. and Maier, J. Grain Boundary Blocking Effect in Zirconia: A Schottky Barrier Analysis. J. of Electrochem Socociety. 148 (2001): E121-E126.
18. ASTM. Designation C 373 -88,115-116.
19. Chinn, R.E. Ceramography. USA: ASTM International, 2002.
20. Abram, E.J., Sinclair, D.C., and West, A.R. Electrode – Contact Spreading Resistance Phenomena in Doped-Lanthanum Gallate Ceramics. J. of Electrochem Socociety. (2001): 179-188.
21. Bruce, P.G. Solid State Electrochemistry. United Kingdom: Cambridge University Press, 1995.
22. He, T., et al. Characterization of YSZ electrolyte membrane tubes presented by a vacuum casting method. J. of Alloys and Compounds. 337 (2002): 231-236
23. Mondal, P., Klein, A., Jaegermann, W., and Hahn, H. Enhanced specific grain boundary conductivity in nanocrystalline Y_2O_3 – stabilized zirconia. Solid State Ionics. 118 (1999): 331-339.
24. Chen, X.J., Khor, K.A., Chan, S.H., and Yu, L.G. Preparation yttria-stabilized zirconia electrolyte by spark-plasma sintering. Materials Science and Engineering. A341 (2003): 43-48.
25. Kumar, M., and Kulandainathan, M.A., Raj, I.A., Chandrasekaran, R., and Pattabiraman, R. Electrical and sintering behaviour of $Y_2Zr_2O_7$ (YZ) pyrochlore-based materials- the influence of bismuth. Materials Chemistry and Physics. 92 (2005): 295-302.

26. Vladikova, D. Electrical Properties in Yttria Stabilized Zirconia Investigated by Impedance Spectroscopy. (n.d.) Available from: <http://accessimpedance.iusi.bas.bg>
27. Kleitz, M., Dessemond, L., and Steil, M.C. Model for ion-blocking at interfaces in zirconias. Solid State Ionics. 75 (1995): 107-115.
28. Aoki, M., and et al. Solute Segregation and Grain boundary Impedance in High-Purity Stabilized Zirconia. J. of American Ceramics Society. 79 [5] (1996): 1169 -1180.
29. Badwal, S.P.S., Caicchi, F.T., Giampietro, K.M., Lawie V., and Skala, R.D. Zirconia – Yttrai Electrolyte Materials for Solid Oxide Fuel Cells, In Huijsmas, J. (ed), proceeding of the 5th European Solid Oxide Fuel cells Forum, pp.199-206. European Fuel Forum, 2002.
30. Kingery, W.D., Woven, H.K., and Uhlmann, D.R. Introduction to Ceramics. 2nded. New York: John Wiley & Sons, 1991.
31. Barsoum, M.W. Fundamentals of Ceramics. New York: McGraw-Hill, 1997.
32. Florio de, D.Z., and Muccillo, R., Sintering of Zirconia – yttria ceramics studied by impedance spectroscopy. Solid State Ionics. 123 (1999): 301 – 305.
33. Kayan, A., Tarcan, E., Kadiloglu, U., and Esmer, K. Electrical and dielectrical properties of the MnO doped with As₂O₃ and SnO. Materials Letters. 58 [16] (2004): 2170-2174.
34. Feighery, A.J., and Irvine, J.T.S. Effect of alumina additions upon electrical properties of 8 mol% yttria – stabilized zirconia. Solid State Ionics. 121(1999): 209 – 216.
35. Hattori, M., et al. Effect of annealing on electrical conductivity of the Y₂O₃-ZrO₂ system. J. of Power Sources. 131 (2004): 247 – 250.
36. Manning, P.S., Sirman, J.D., De Souza, R.A., and . Kilner, J.A. The kinetics of oxygen transport in 9.5 mol % single crystal yttria stabilized zirconia. Solid State ionics. 100 (1997): 1-10.



APPENDICES

สถาบันวิทยบริการ
จุฬาลงกรณ์มหาวิทยาลัย

APPENDIX A

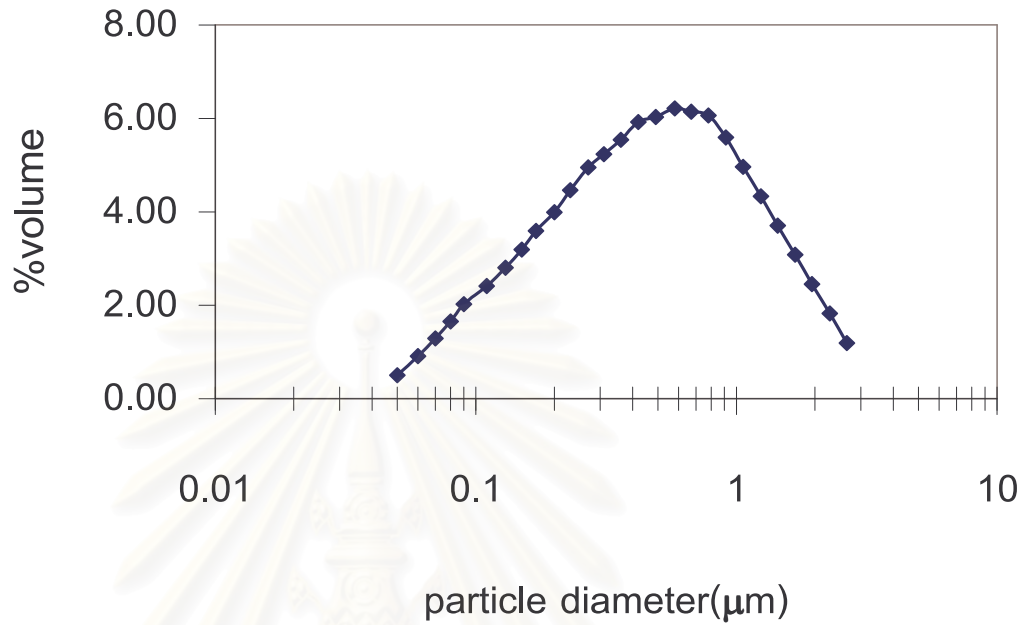


Fig A1: The particle size distribution of 3 mol % $Y_2O_3-ZrO_2$ powder [MEL].

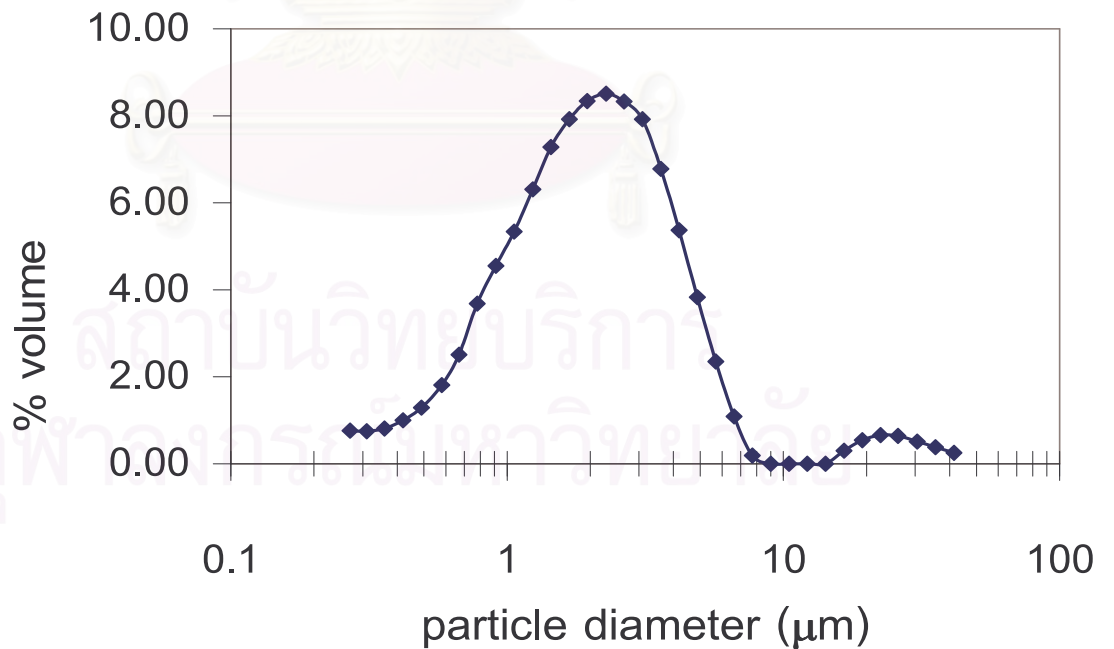


Fig A2: The particle size distribution of 8 mol % $Y_2O_3-ZrO_2$ powder [MEL].

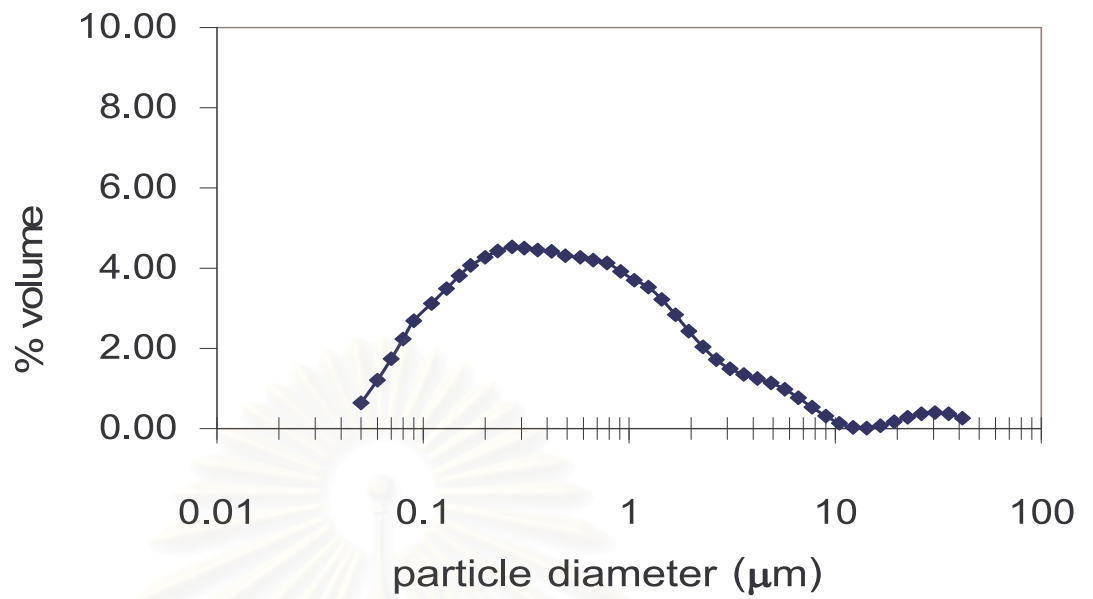


Fig A3: The particle size distribution of 8 mol % $Y_2O_3-ZrO_2$ powder [TOSOH].

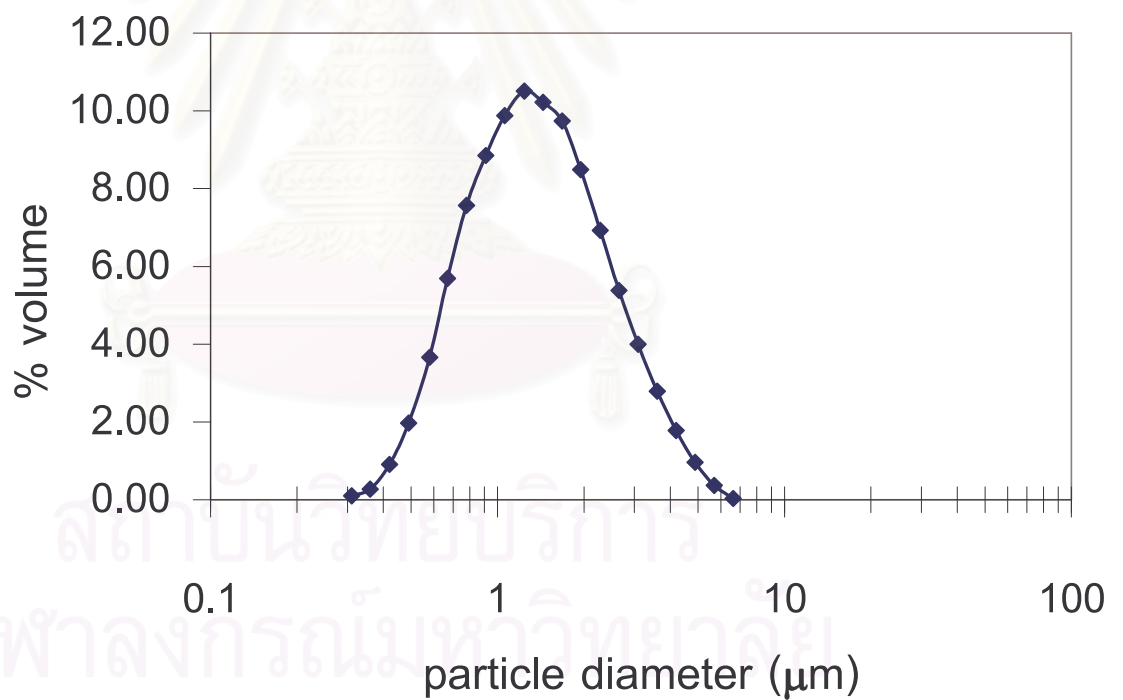


Fig A4: The particle size distribution of 8 mol % $Y_2O_3-ZrO_2$ powder [DAIICHI].

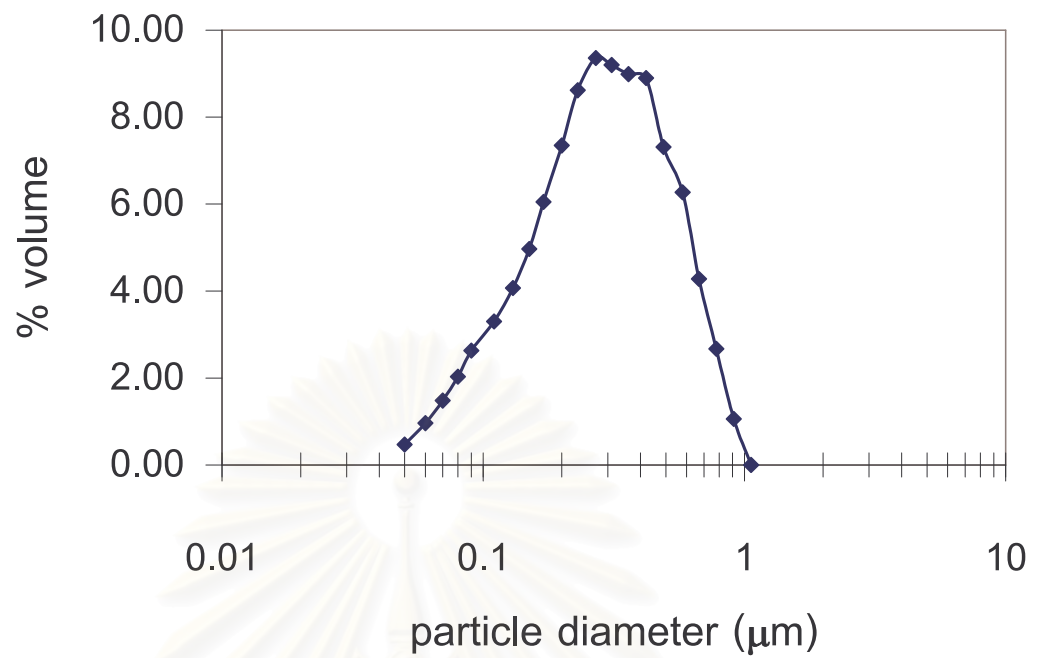


Fig A5: The particle size distribution of 10 mol % Y₂O₃-ZrO₂ powder [DAIICHI].

สถาบันวิทยบริการ
จุฬาลงกรณ์มหาวิทยาลัย

APPENDIX B

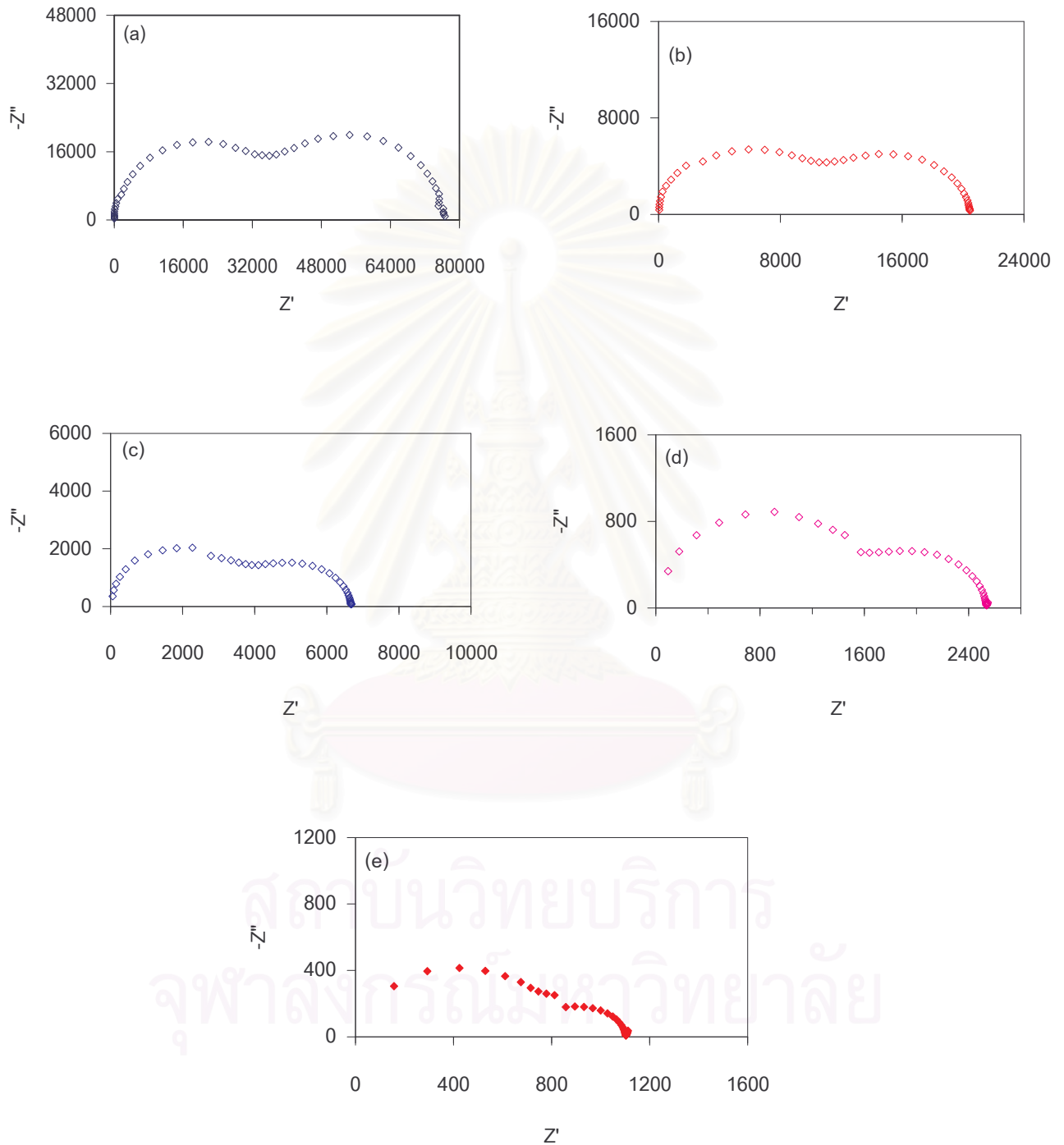


Fig B1: The Impedance Spectra of 3mol% $Y_2O_3-ZrO_2$ (MEL) after sintering at $1500^\circ C$ for 1 hour.

The measurements were taken at $350^\circ C$ (a), $400^\circ C$ (b), $450^\circ C$ (c), $500^\circ C$ (d), and $550^\circ C$ (e).

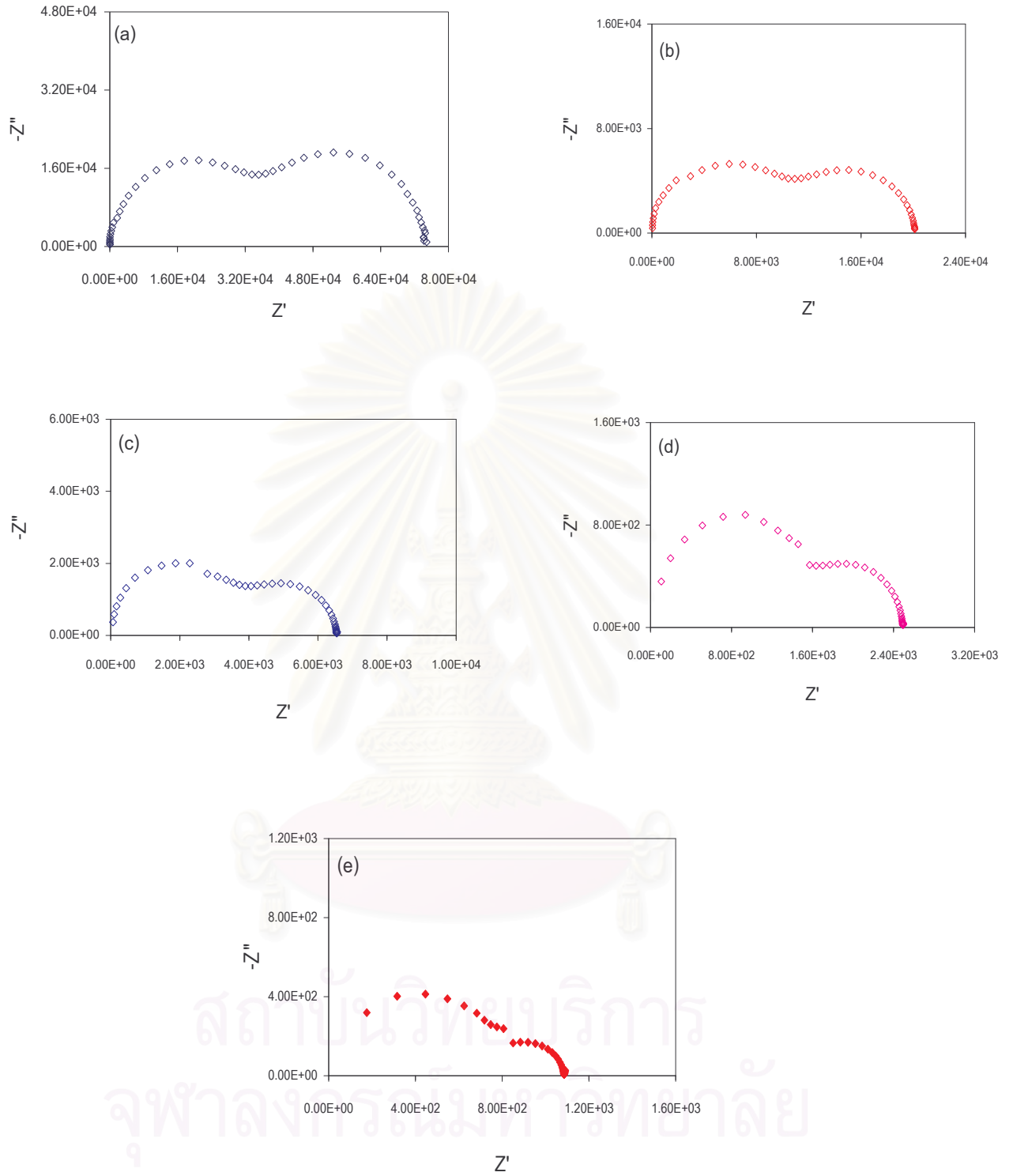


Fig B2: The Impedance Spectra of 3mol% $\text{Y}_2\text{O}_3\text{-ZrO}_2$ (MEL) after sintering at 1500°C for 2 hours. The measurements were taken at 350°C (a), 400°C (b), 450°C (c), 500°C (d), and 550°C (e).

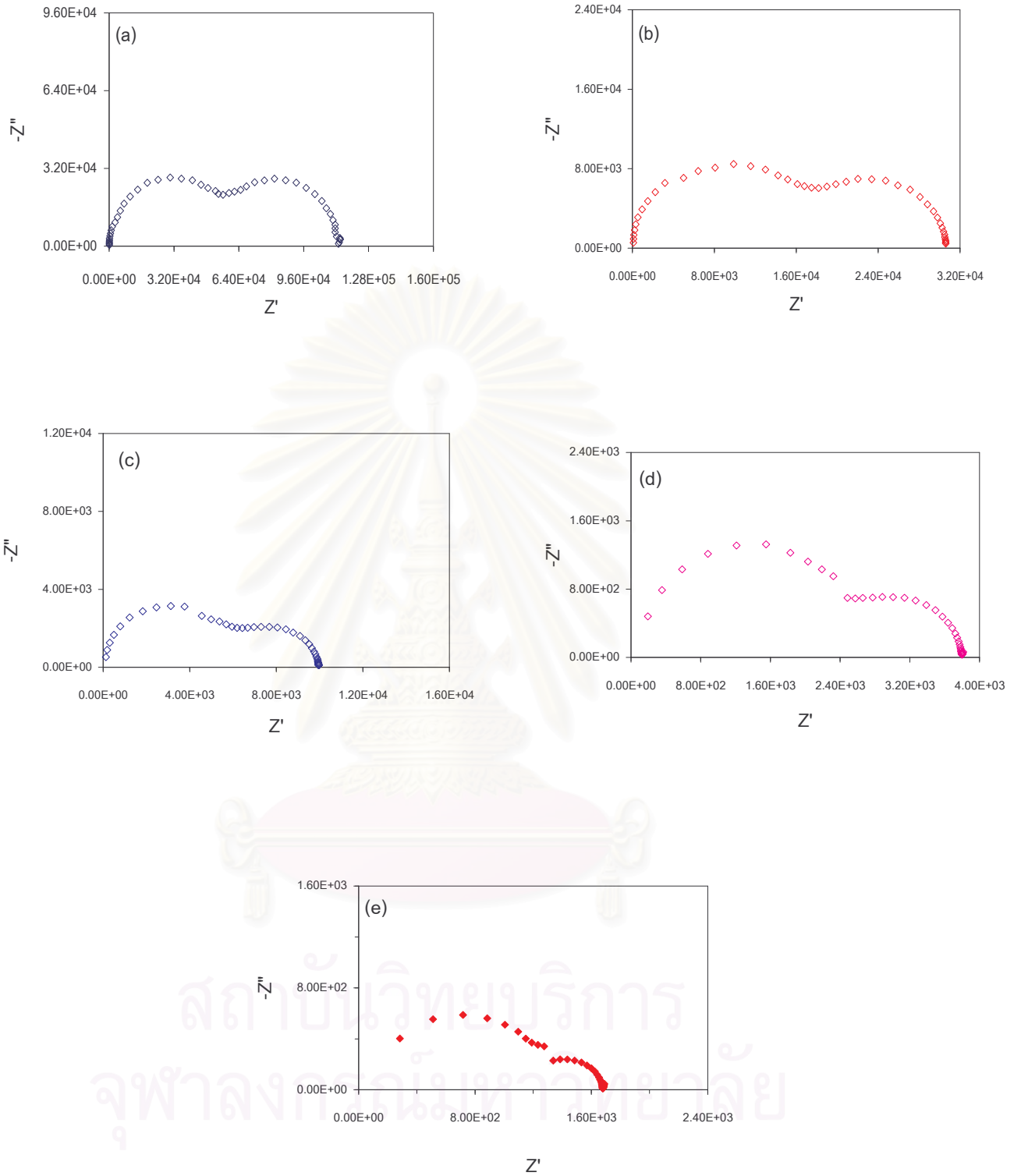


Fig B3: The Impedance Spectra of 3 mol% $\text{Y}_2\text{O}_3\text{-ZrO}_2$ (MEL) after sintering at 1500°C for 4 hours. The measurements were taken at 350°C (a), 400°C (b), 450°C (c), 500°C (d), and 550°C (e).

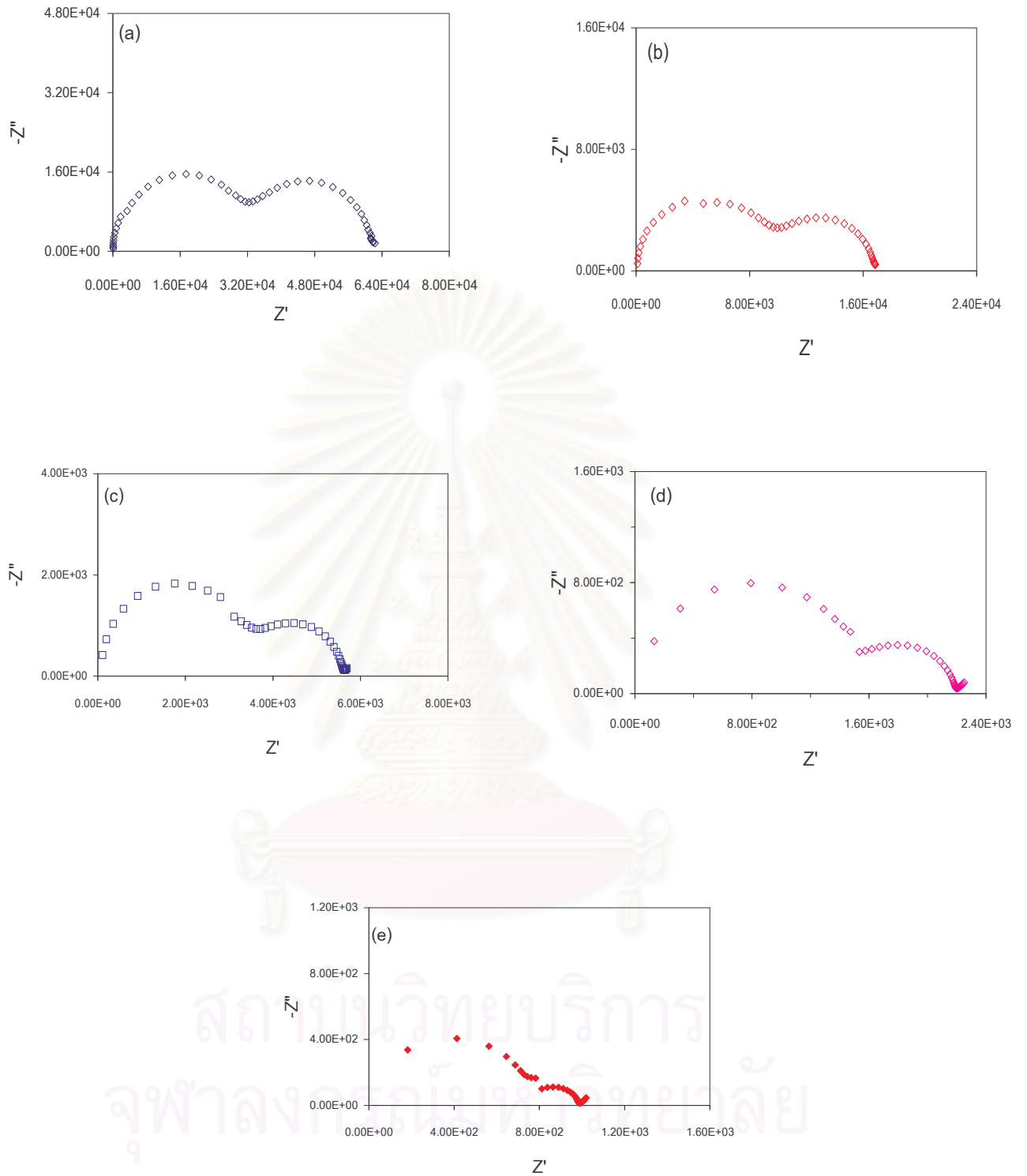


Fig B4: The Impedance Spectra of 3mol% $\text{Y}_2\text{O}_3\text{-ZrO}_2$ (MEL) after sintering at 1550°C for 1 hour. The measurements were taken at 350°C (a), 400°C (b), 450°C (c), 500°C (d), and 550°C (e).

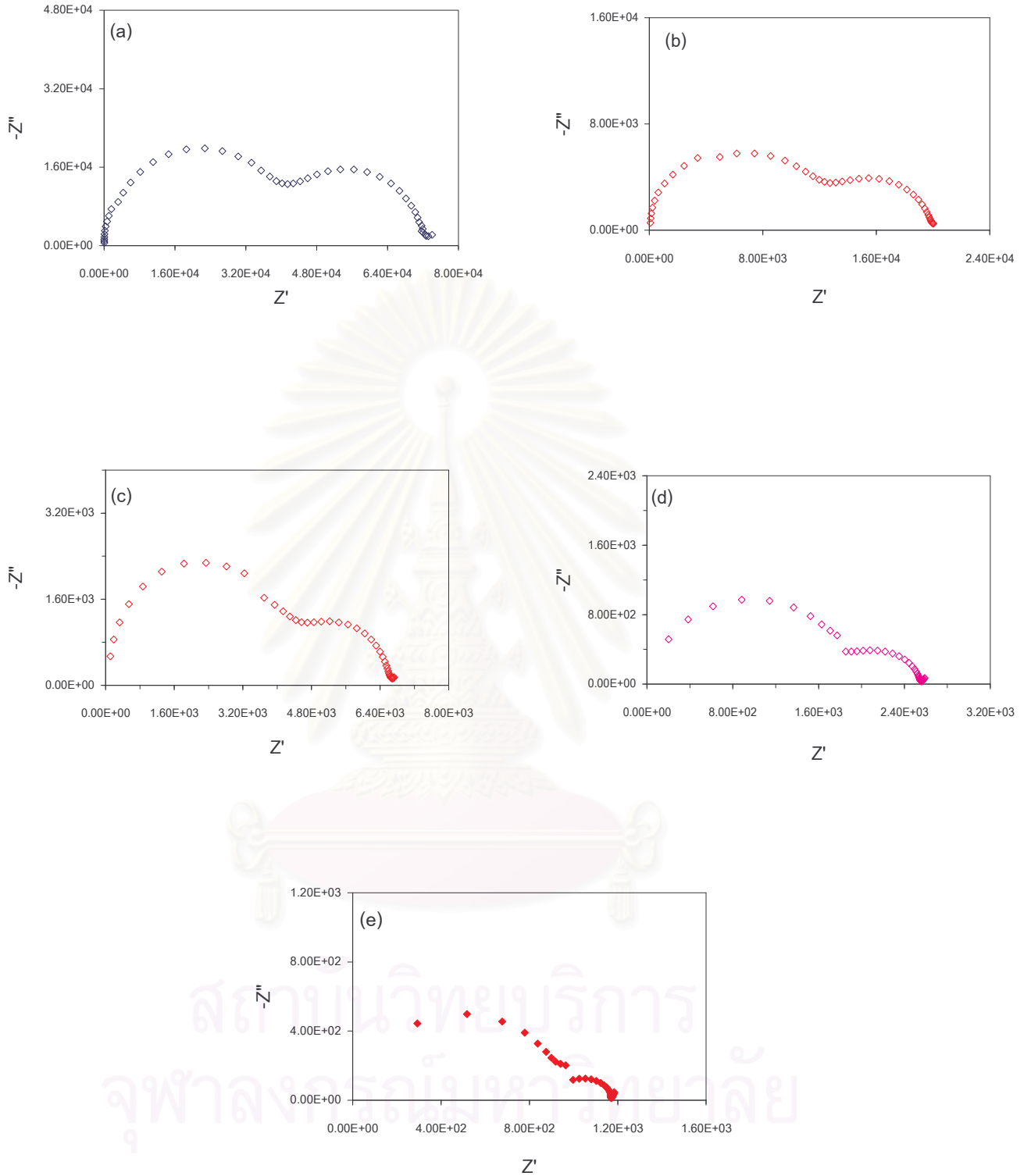


Fig B5: The Impedance Spectra of 3mol% Y_2O_3 - ZrO_2 (MEL) after sintering at 1550°C for 2 hours. The measurements were taken at 350°C (a), 400°C (b), 450°C (c), 500°C (d), and 550°C (e).

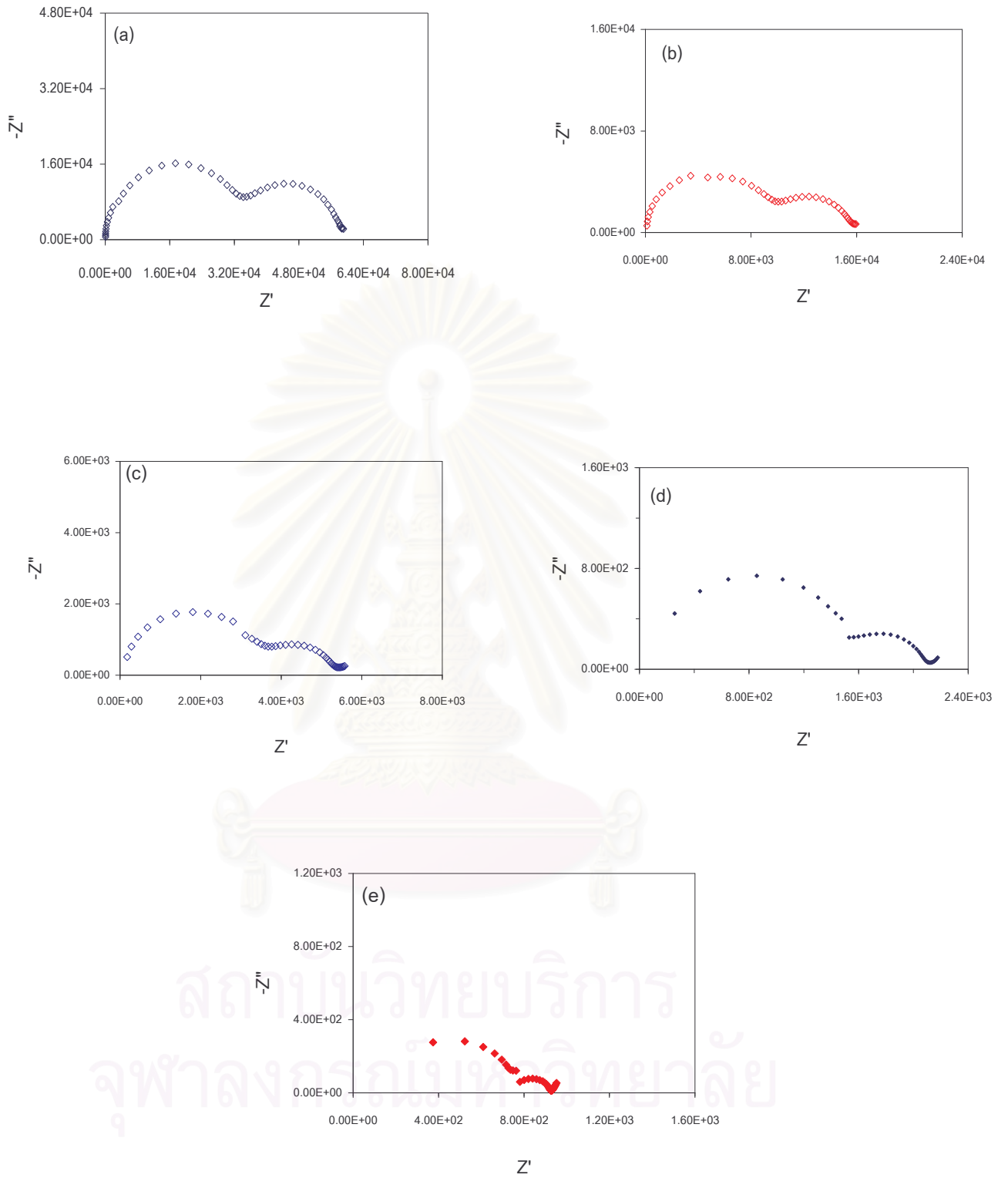


Fig B6: The Impedance Spectra of 3 mol% $\text{Y}_2\text{O}_3\text{-ZrO}_2$ (MEL) after sintering at 1550°C for 4 hours. The measurements were taken at 350°C (a), 400°C (b), 450°C (c), 500°C (d), and 550°C (e).

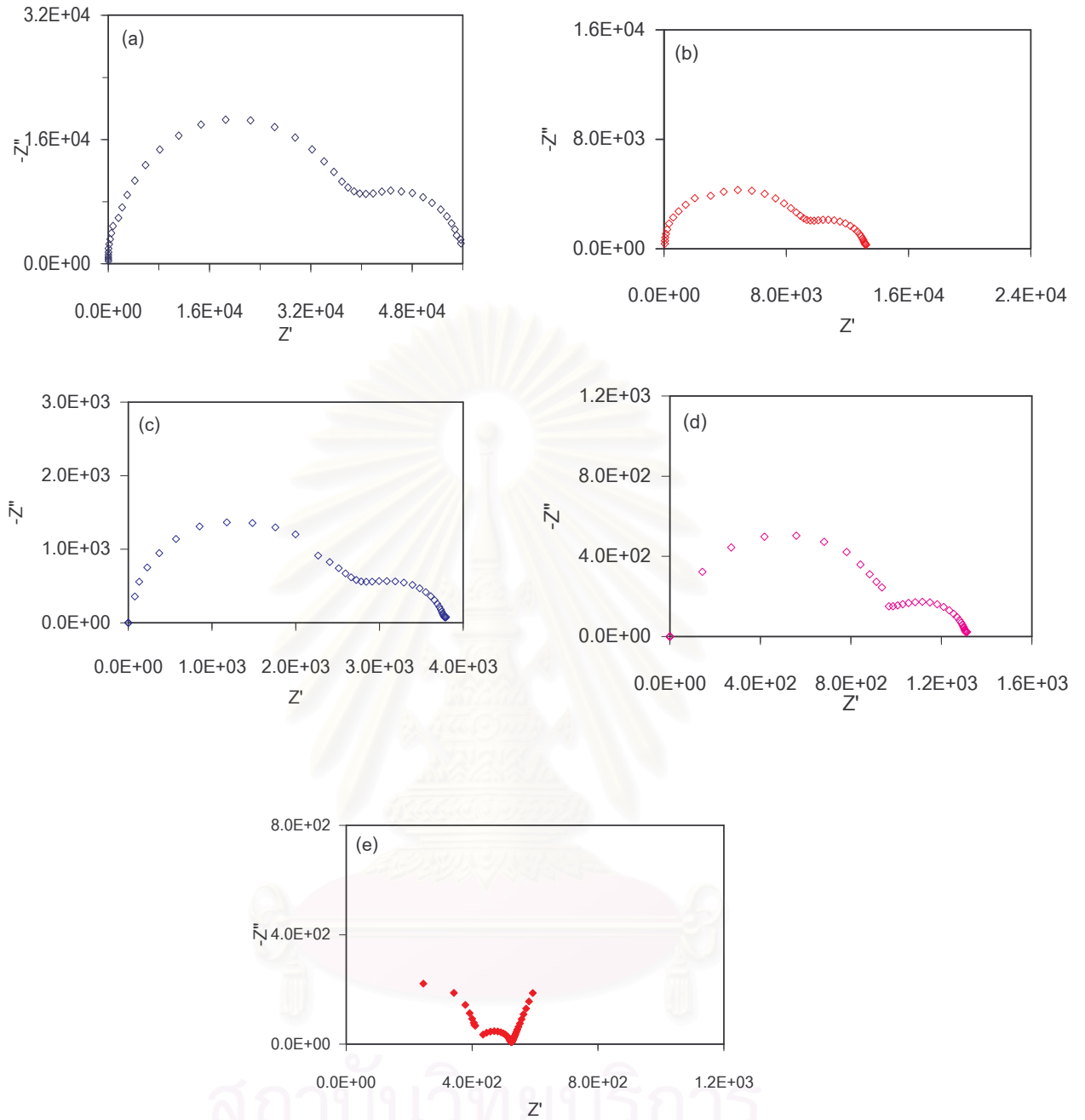


Fig B7: The Impedance Spectra of 8 mol% Y_2O_3 - ZrO_2 (MEL) after sintering at $1500^\circ C$ for 1 hour. The measurements were taken at $350^\circ C$ (a), $400^\circ C$ (b), $450^\circ C$ (c), $500^\circ C$ (d), and $550^\circ C$ (e).

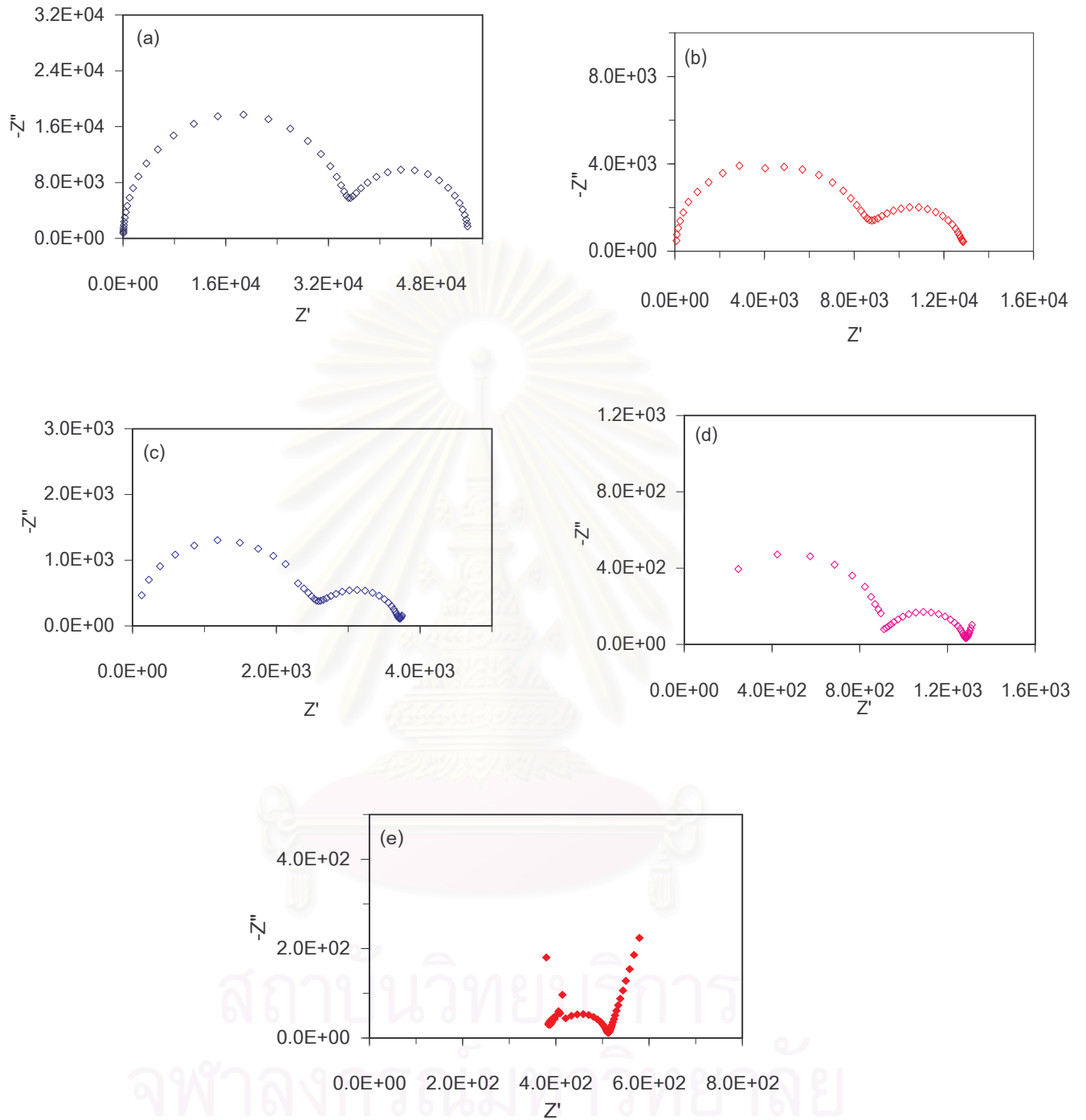


Fig B8: The Impedance Spectra of 8 mol% Y_2O_3 - ZrO_2 (MEL) after sintering at 1500°C for 2 hours. The measurements were taken at 350°C (a), 400°C (b), 450°C (c), 500°C (d), and 550°C (e).

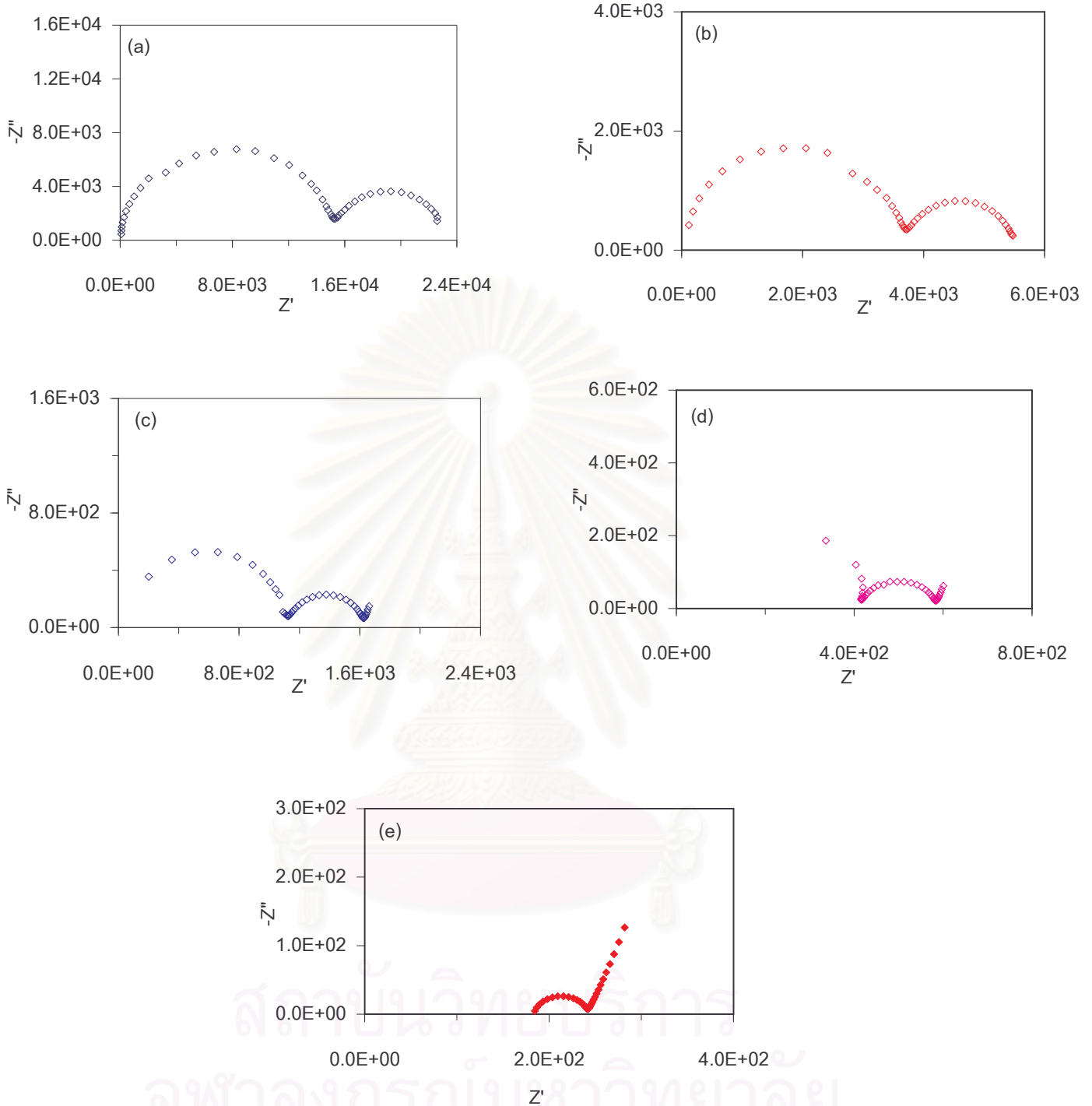


Fig B9: The Impedance Spectra of 8 mol% Y_2O_3 - ZrO_2 (MEL) after sintering at 1500°C for 4 hours.

The measurements were taken at 350°C (a), 400°C (b), 450°C (c), 500°C (d), and 550°C (e).

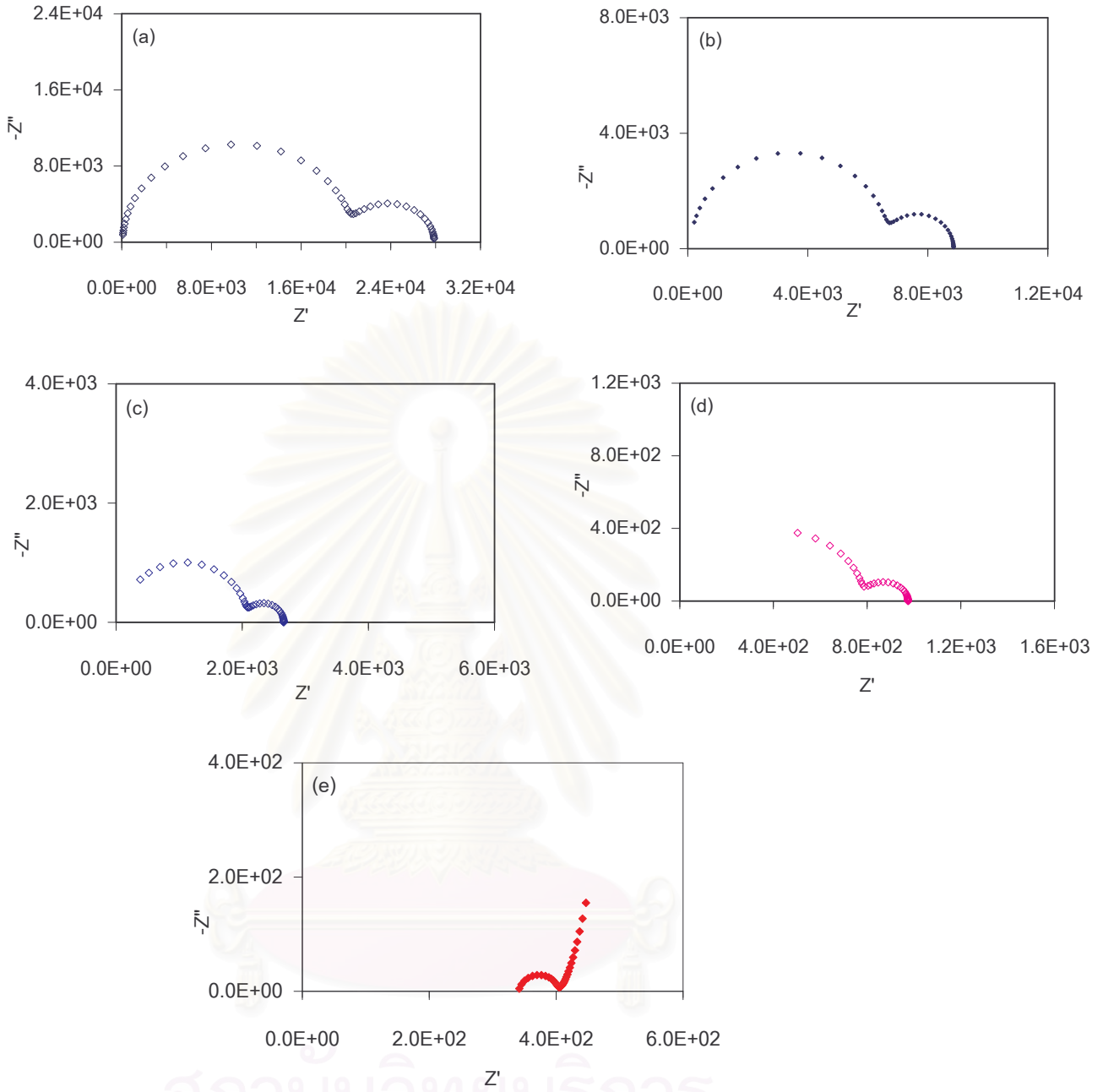


Fig B10: The Impedance Spectra of 8 mol% $Y_2O_3-ZrO_2$ (MEL) after sintering at 1550°C for 1 hour. The measurements were taken at 350°C (a), 400°C (b), 450°C (c), 500°C (d), and 550°C (e).

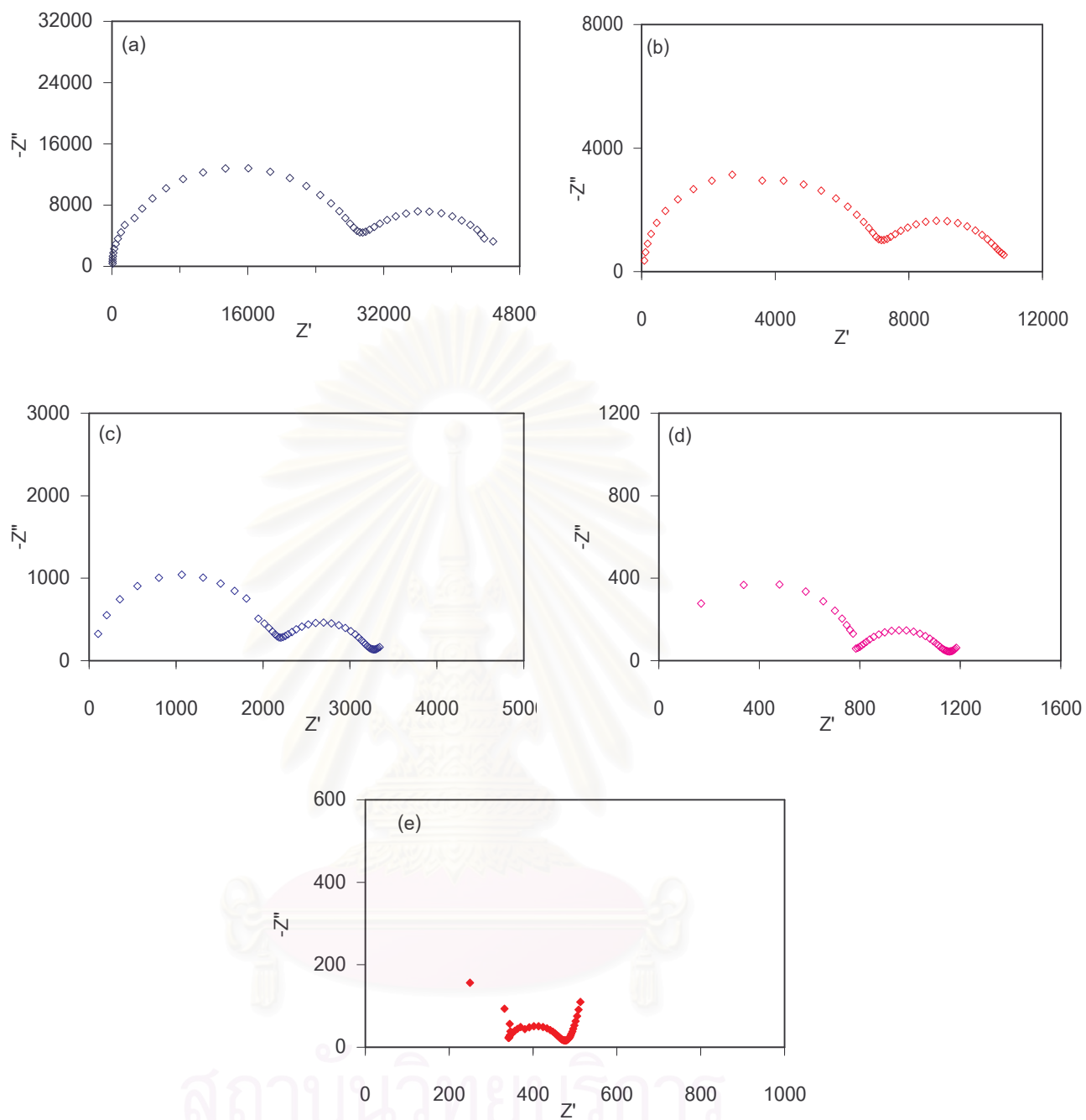


Fig B11: The Impedance Spectra of 8 mol% $\text{Y}_2\text{O}_3\text{-ZrO}_2$ (MEL) after sintering at 1550°C for 2 hours. The measurements were taken at 350°C (a), 400°C (b), 450°C (c), 500°C (d), and 550°C (e).

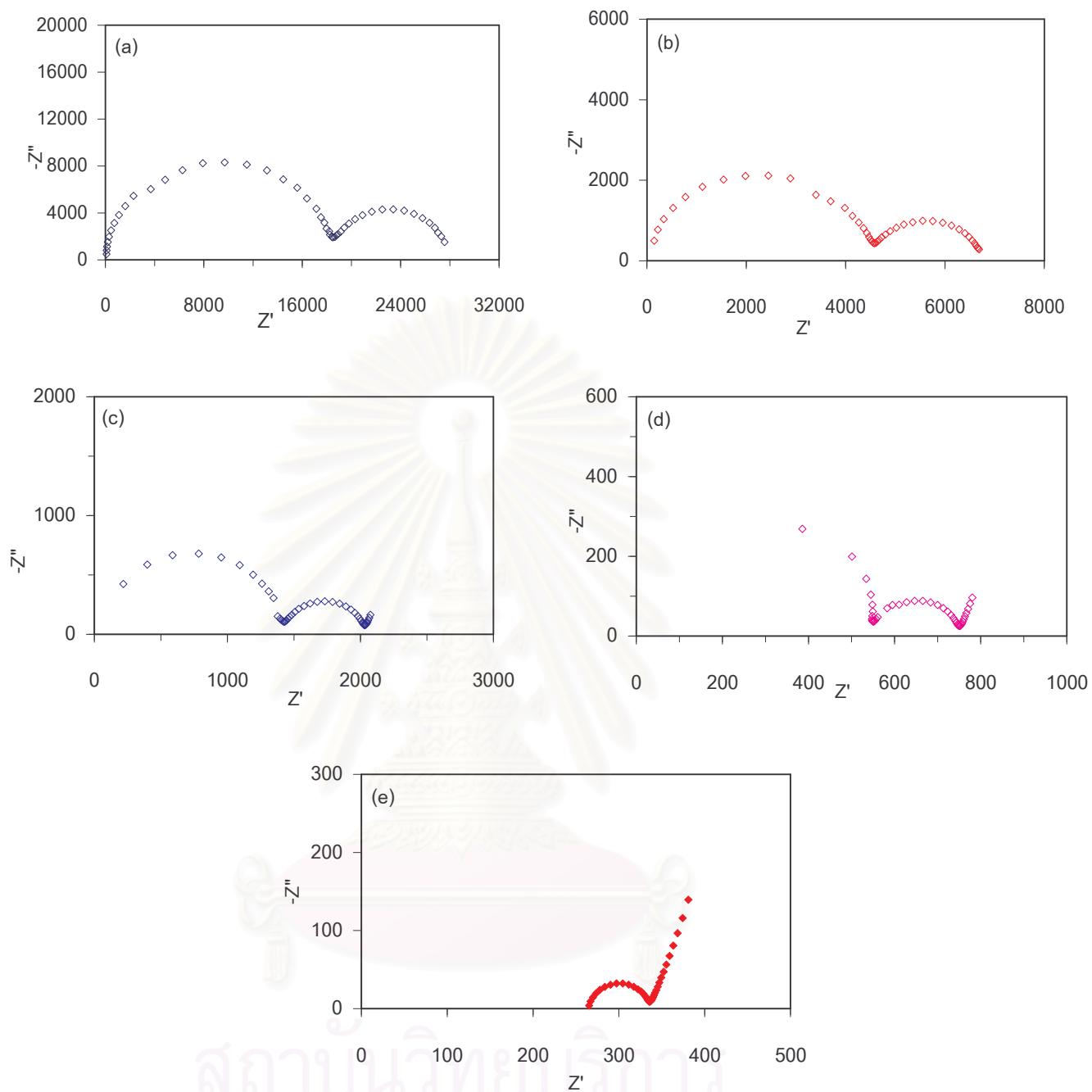


Fig B12: The Impedance Spectra of 8 mol% $\text{Y}_2\text{O}_3\text{-ZrO}_2$ (MEL) after sintering at 1550°C for 4 hours.

The measurements were taken at 350°C (a), 400°C (b), 450°C (c), 500°C (d), and 550°C (e).

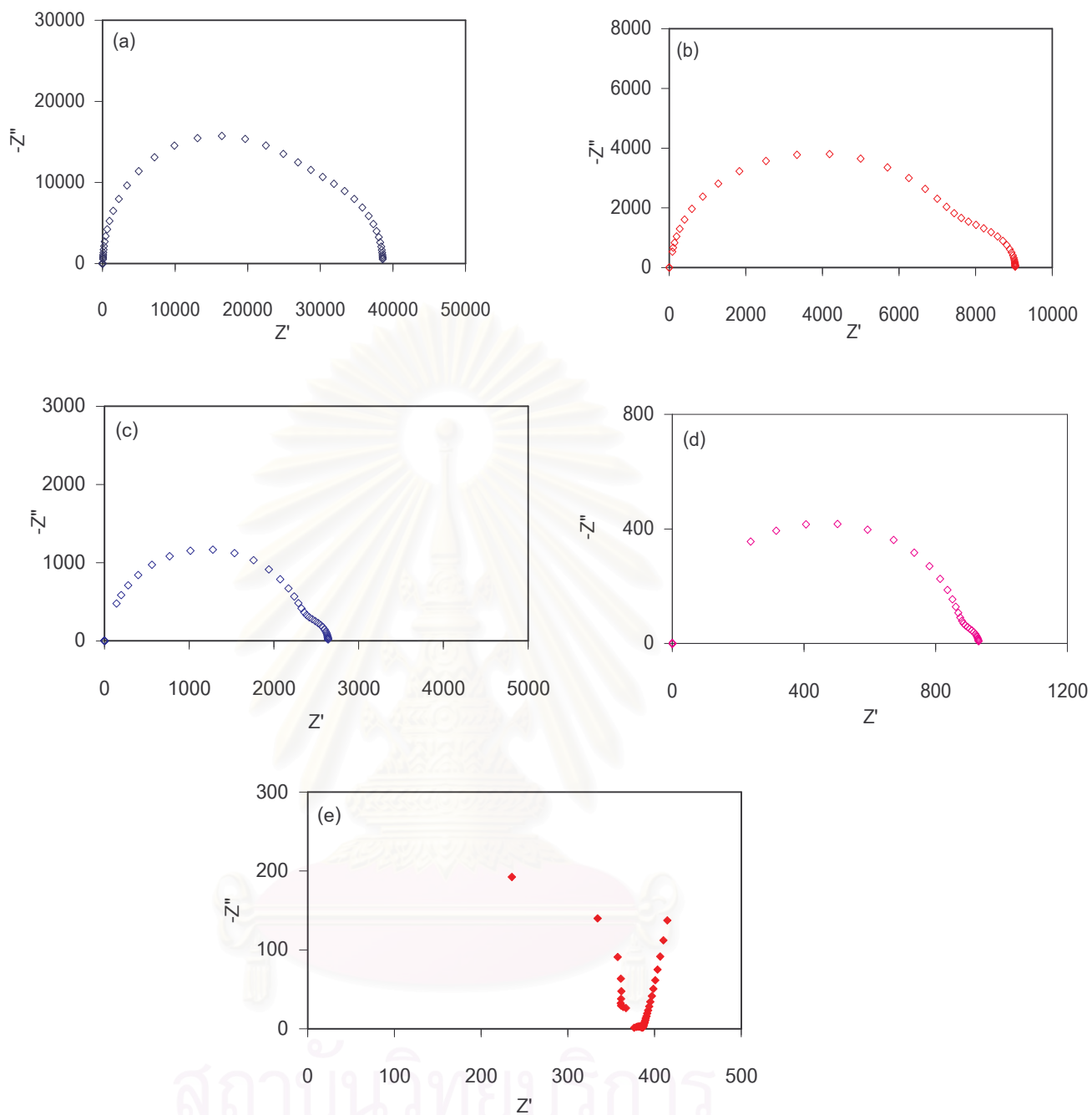


Fig B13: The Impedance Spectra of 8 mol% $Y_2O_3-ZrO_2$ (Tosoh) after sintering at $1500^\circ C$ for 1 hour.

The measurements were taken at $350^\circ C$ (a), $400^\circ C$ (b), $450^\circ C$ (c), $500^\circ C$ (d), and $550^\circ C$ (e).

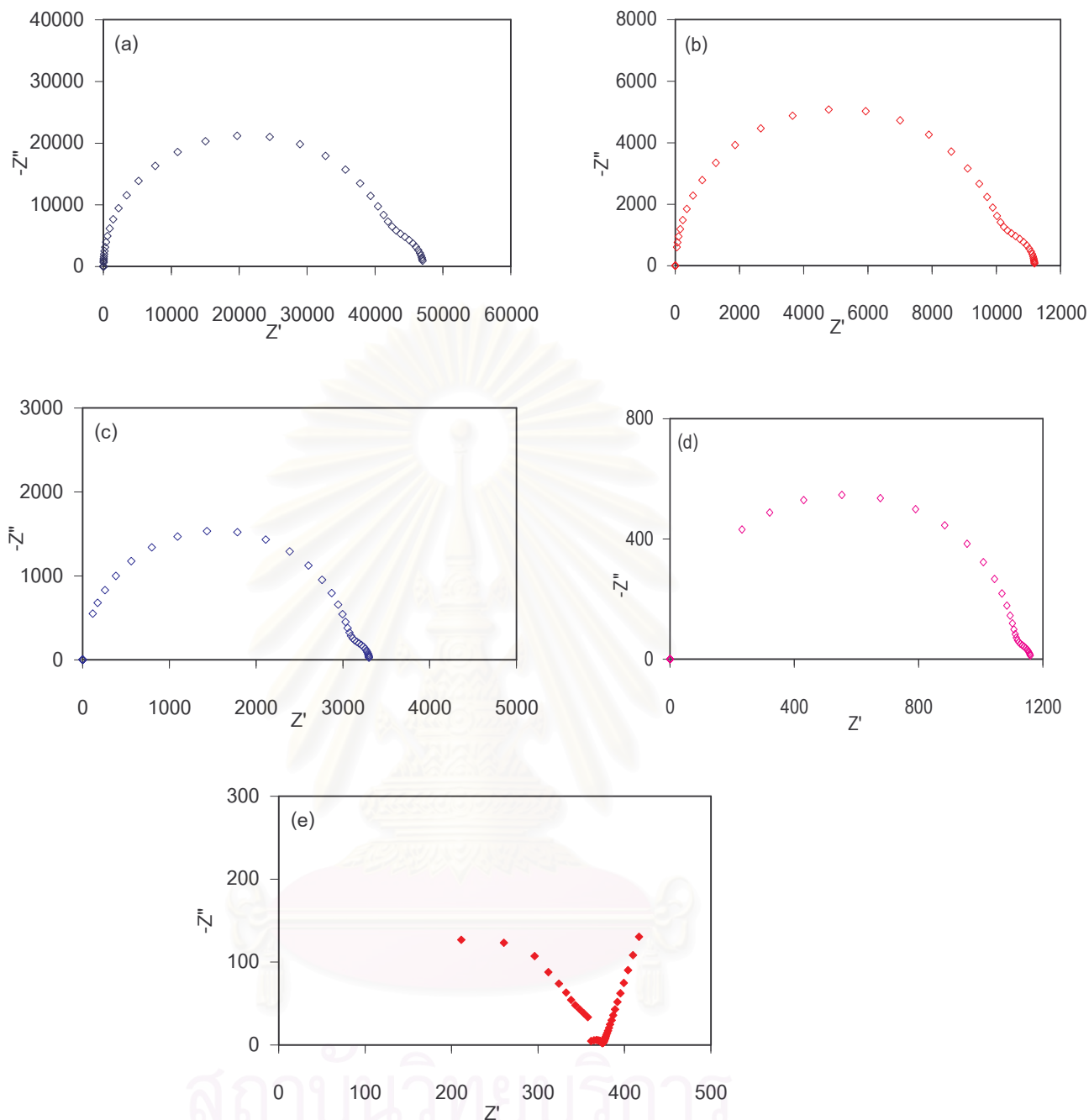


Fig B14: The Impedance Spectra of 8 mol% $\text{Y}_2\text{O}_3\text{-ZrO}_2$ (Tosoh) after sintering at 1500°C for 2 hours. The measurements were taken at 350°C (a), 400°C (b), 450°C (c), 500°C (d), and 550°C (e).

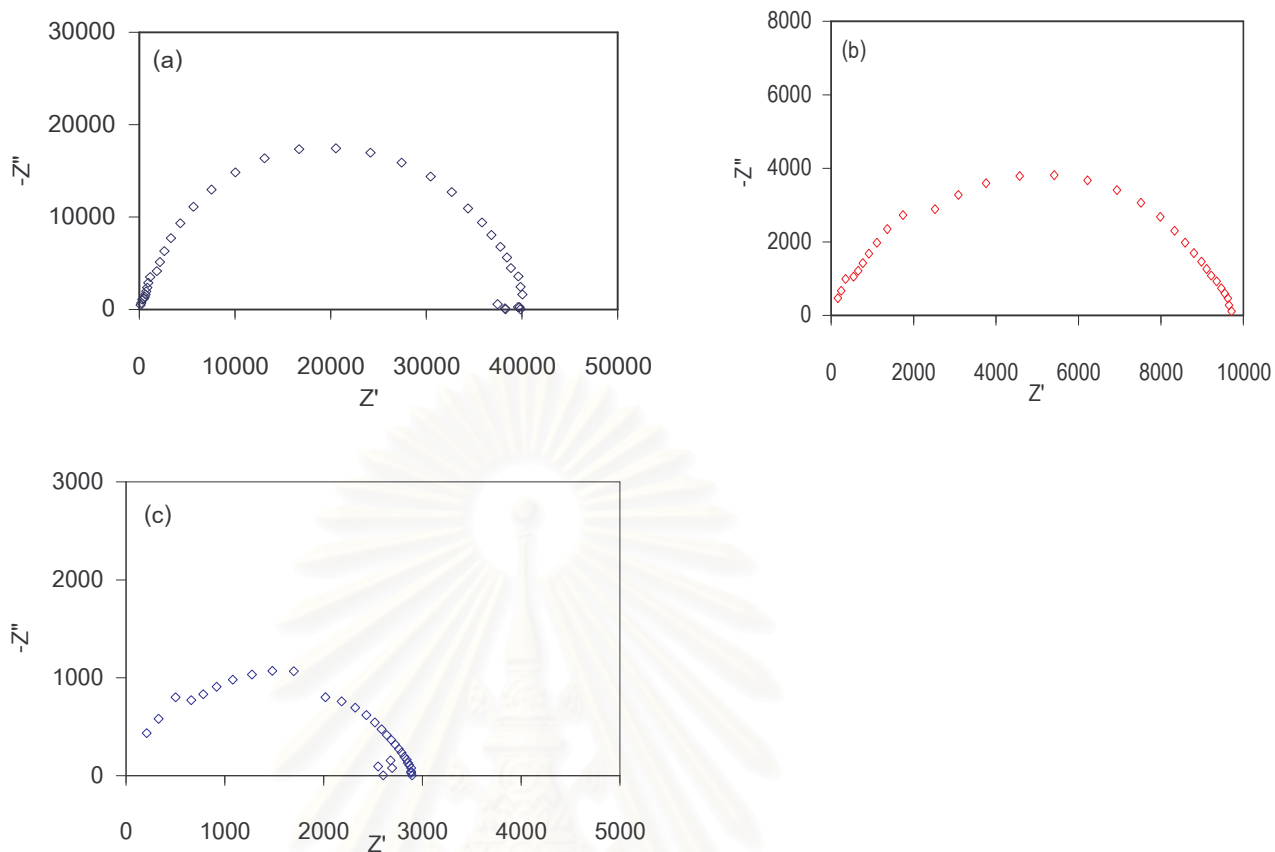


Fig B15: The Impedance Spectra of 8 mol% $\text{Y}_2\text{O}_3\text{-ZrO}_2$ (Tosoh) after sintering at 1500°C for 4 hours. The measurements were taken at 350°C (a), 400°C (b), and 450°C (c)

สถาบันวิทยบริการ
จุฬาลงกรณ์มหาวิทยาลัย

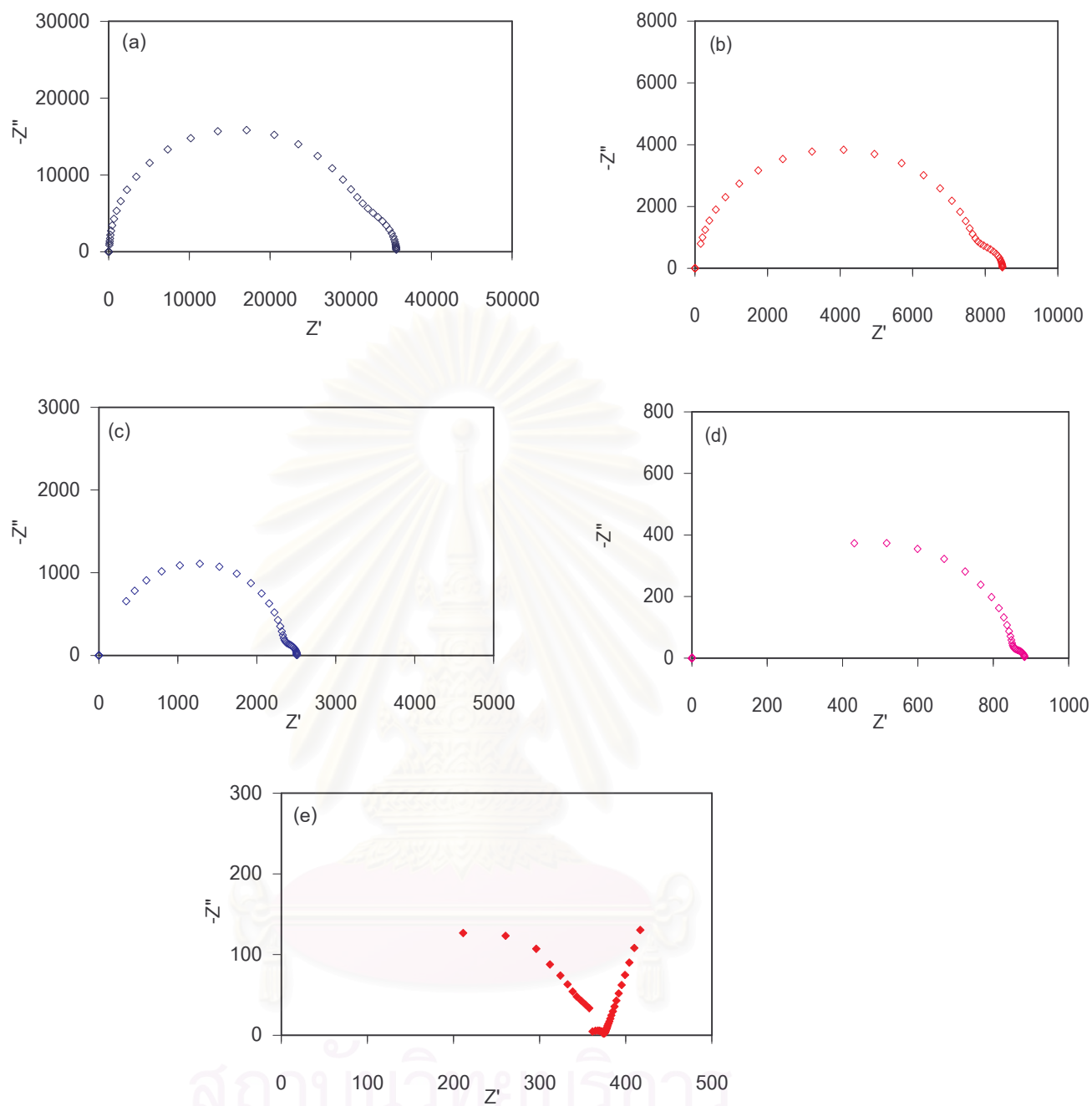


Fig B16: The Impedance Spectra of 8 mol% $\text{Y}_2\text{O}_3\text{-ZrO}_2$ (Tosoh) after sintering at 1550°C for 1 hour. The measurements were taken at 350°C (a), 400°C (b), 450°C (c), 500°C (d), and 550°C (e).

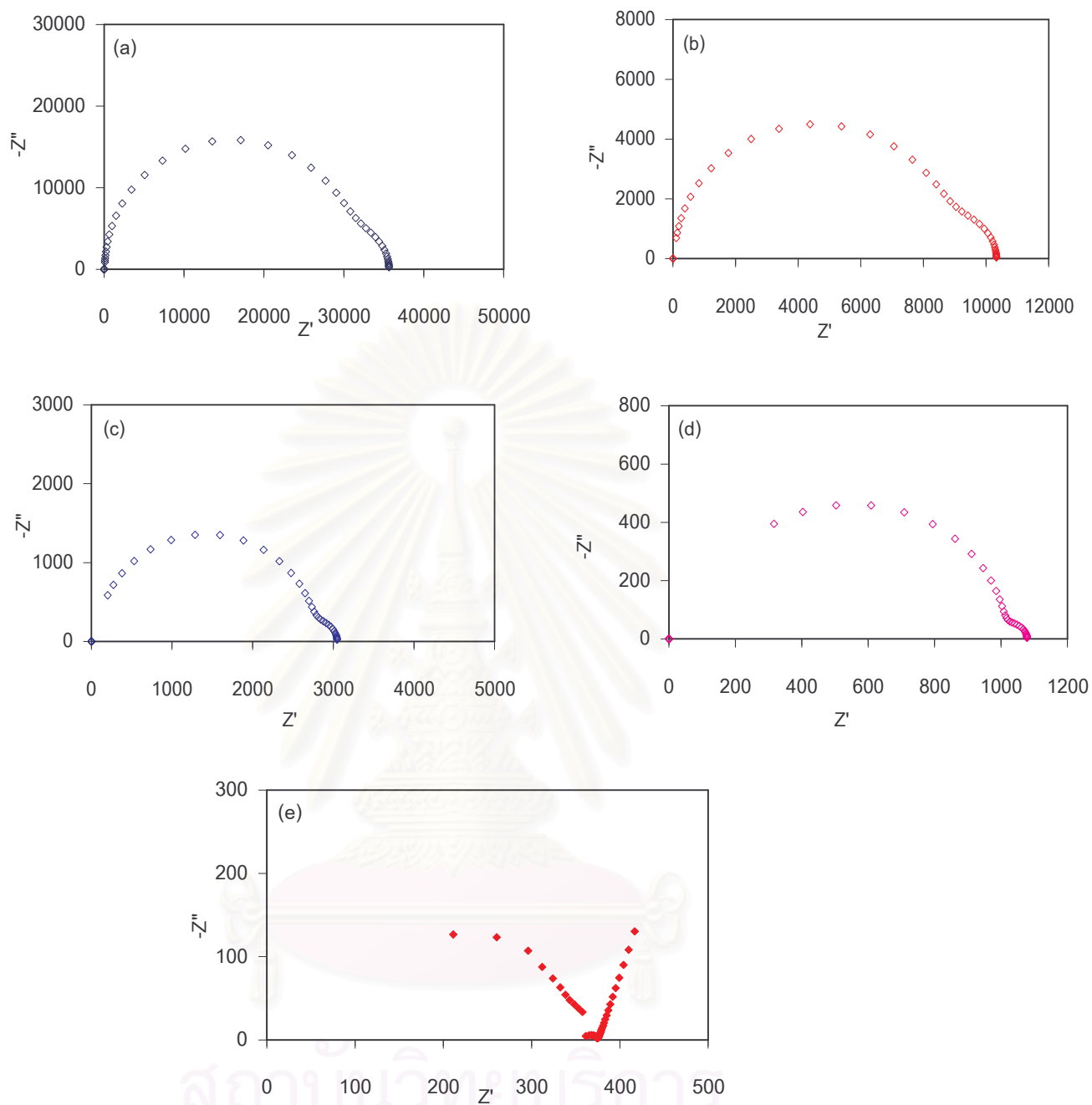


Fig B17: The Impedance Spectra of 8 mol% $\text{Y}_2\text{O}_3\text{-ZrO}_2$ (Tosoh) after sintering at 1550°C for 2 hours. The measurements were taken at 350°C (a), 400°C (b), 450°C (c), 500°C (d), and 550°C (e).

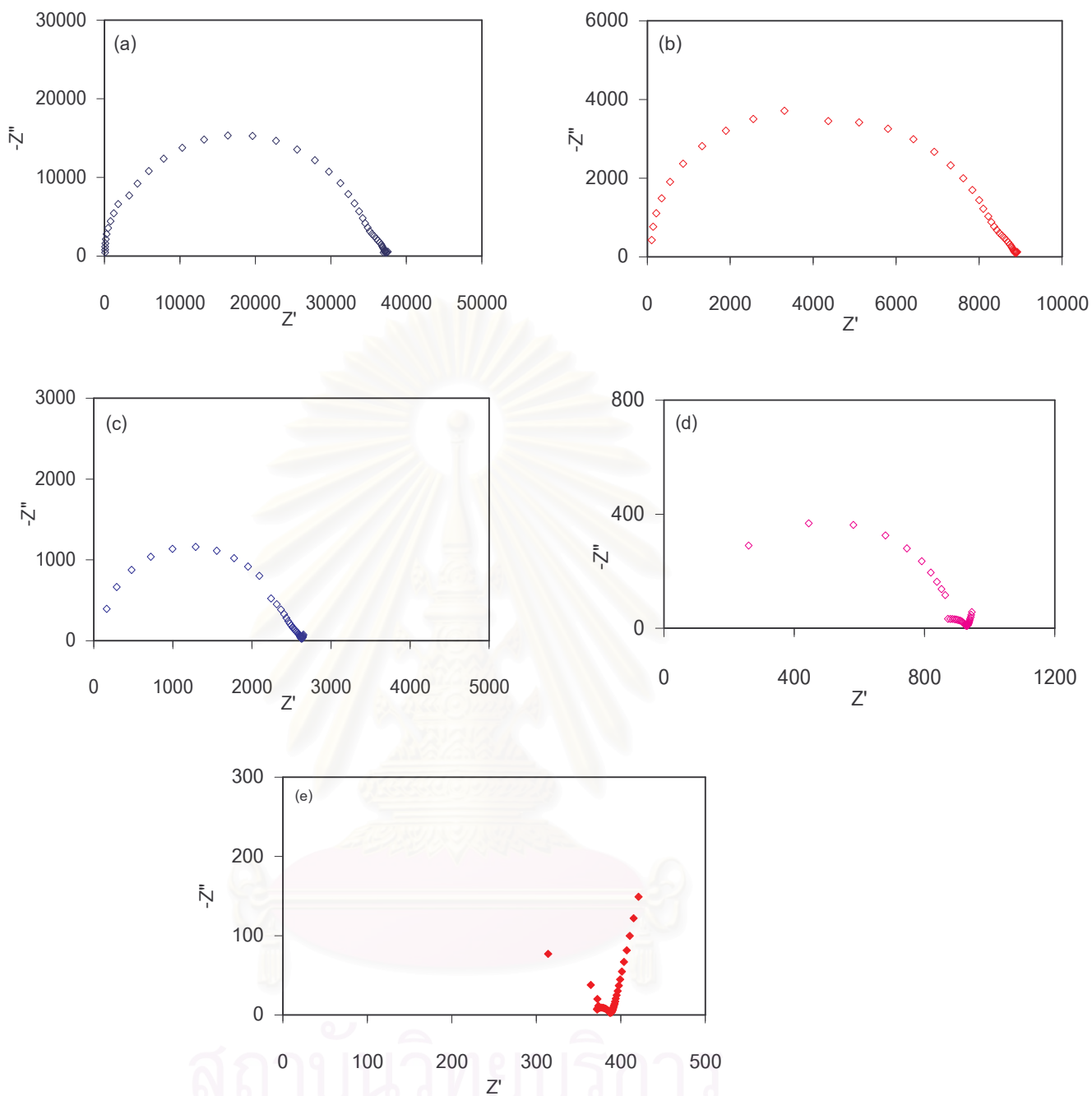


Fig B18: The Impedance Spectra of 8 mol% $\text{Y}_2\text{O}_3\text{-ZrO}_2$ (Tosoh) after sintering at 1550°C for 4 hours. The measurements were taken at 350°C (a), 400°C (b), 450°C (c), 500°C (d), and 550°C (e).

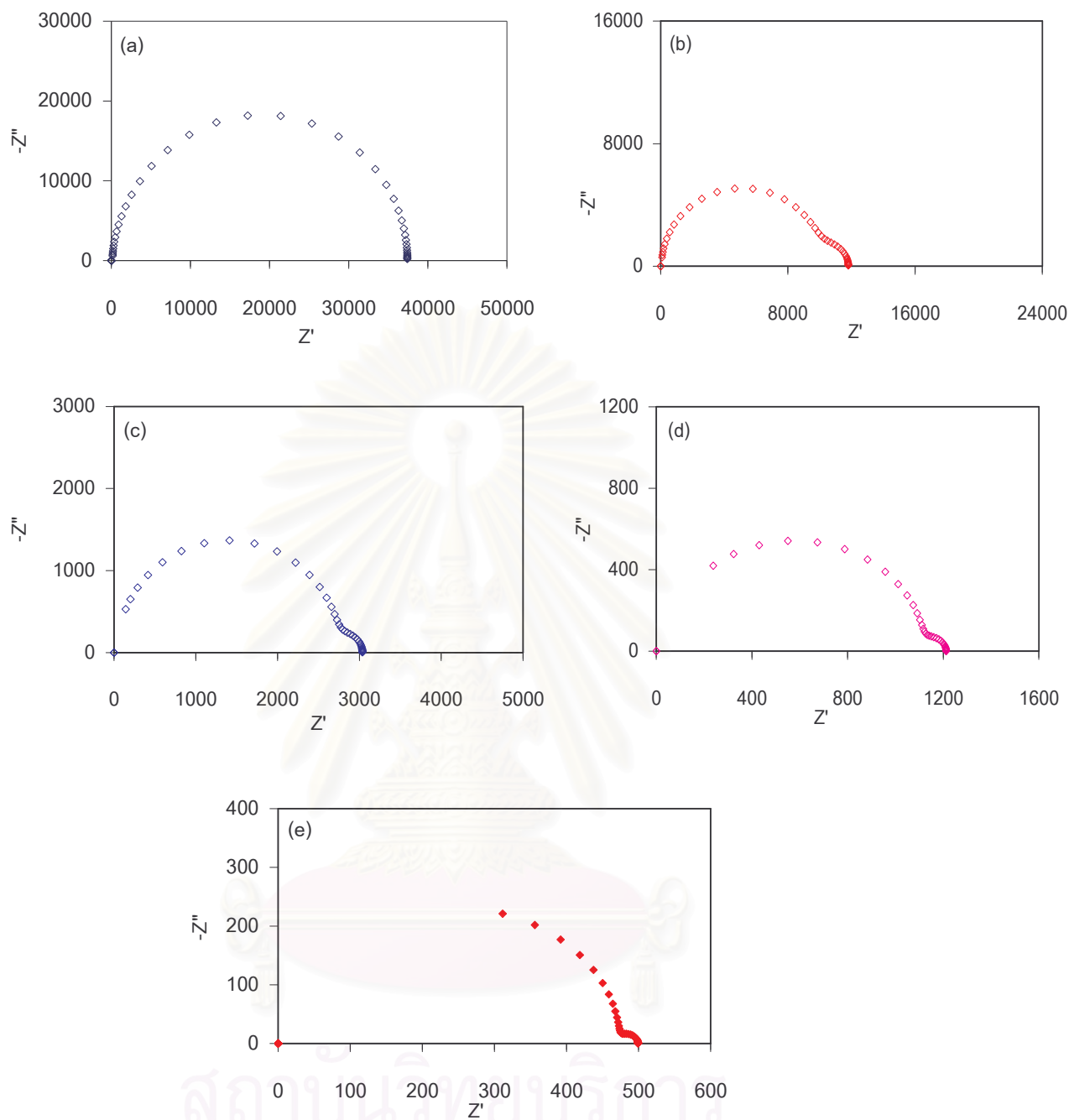


Fig B19: The Impedance Spectra of 8 mol% $\text{Y}_2\text{O}_3\text{-ZrO}_2$ (Daiichi) after sintering at 1500°C for 1 hour. The measurements were taken at 350°C (a), 400°C (b), 450°C (c), 500°C (d), and 550°C (e).

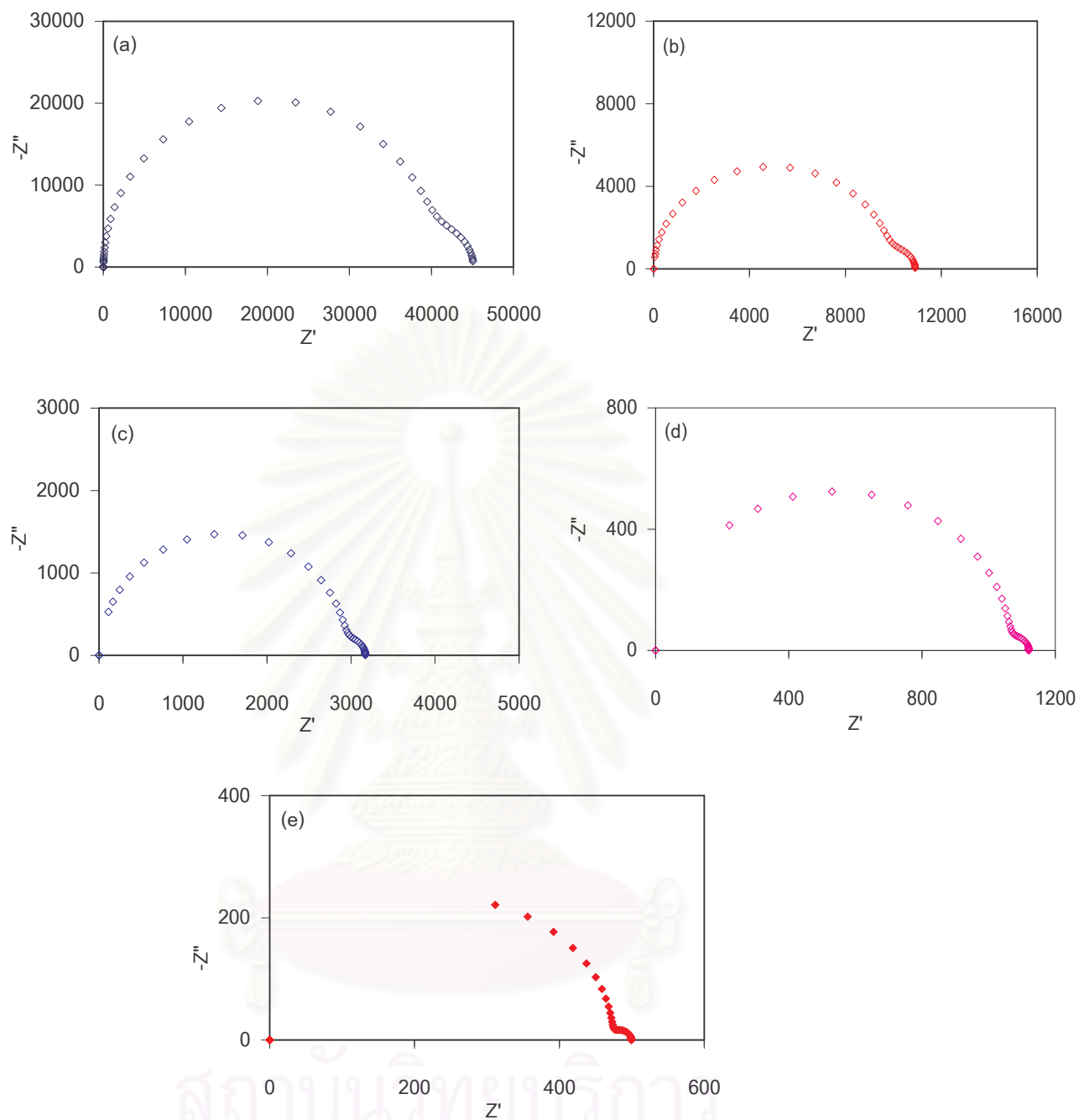


Fig B20: The Impedance Spectra of 8 mol% $\text{Y}_2\text{O}_3\text{-ZrO}_2$ (Daiichi) after sintering at 1500°C for 2 hours. The measurements were taken at 350°C (a), 400°C (b), 450°C (c), 500°C (d), and 550°C (e).

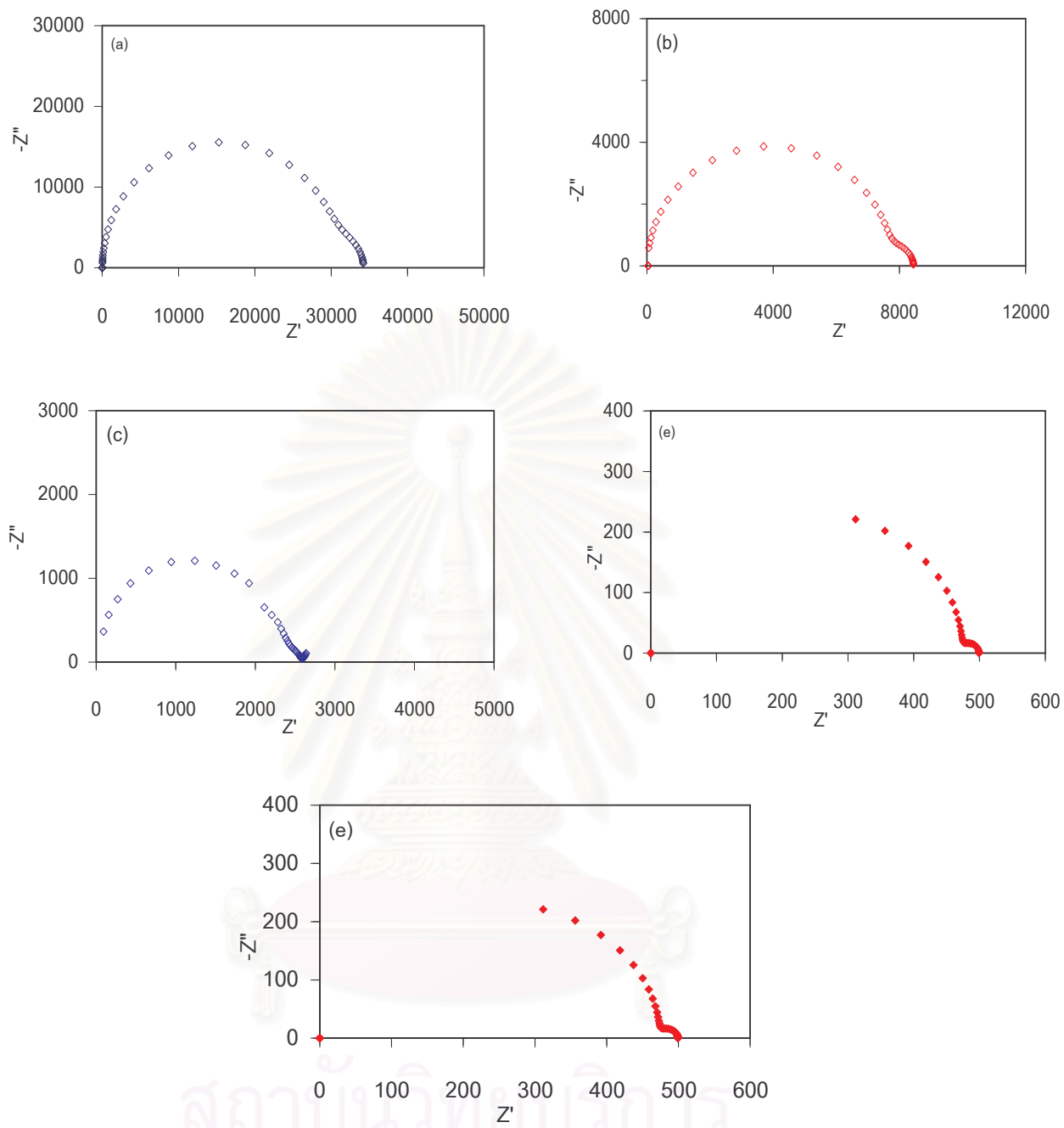


Fig B21: The Impedance Spectra of 8 mol% $\text{Y}_2\text{O}_3\text{-ZrO}_2$ (Daiichi) after sintering at 1500°C for 4 hours.

The measurements were taken at 350°C (a), 400°C (b), 450°C (c), 500°C (d), and 550°C (e).

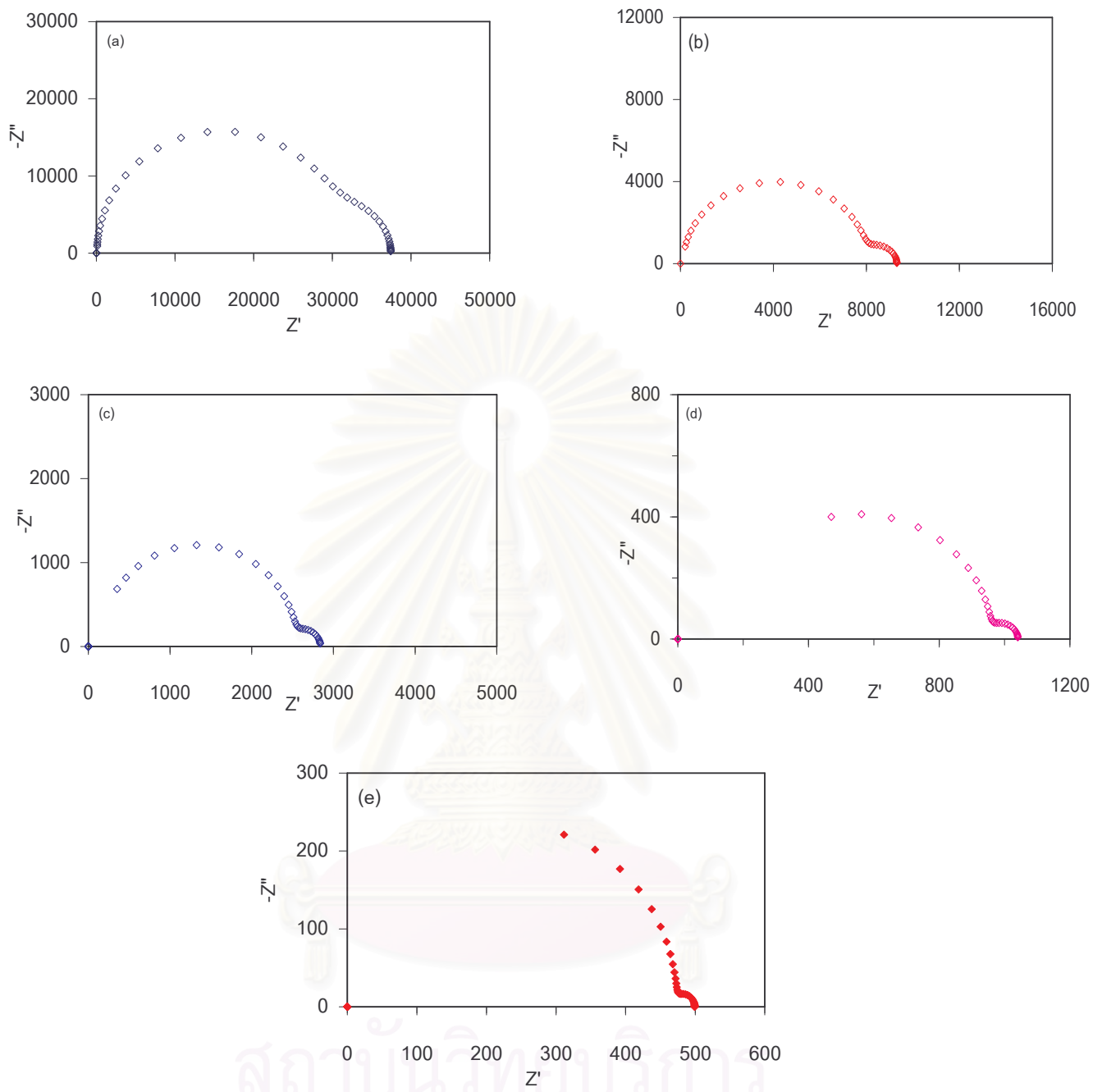


Fig B22: The Impedance Spectra of 8 mol% $\text{Y}_2\text{O}_3\text{-ZrO}_2$ (Daiichi) after sintering at 1550°C for 1 hour. The measurements were taken at 350°C (a), 400°C (b), 450°C (c), 500°C (d), and 550°C (e).

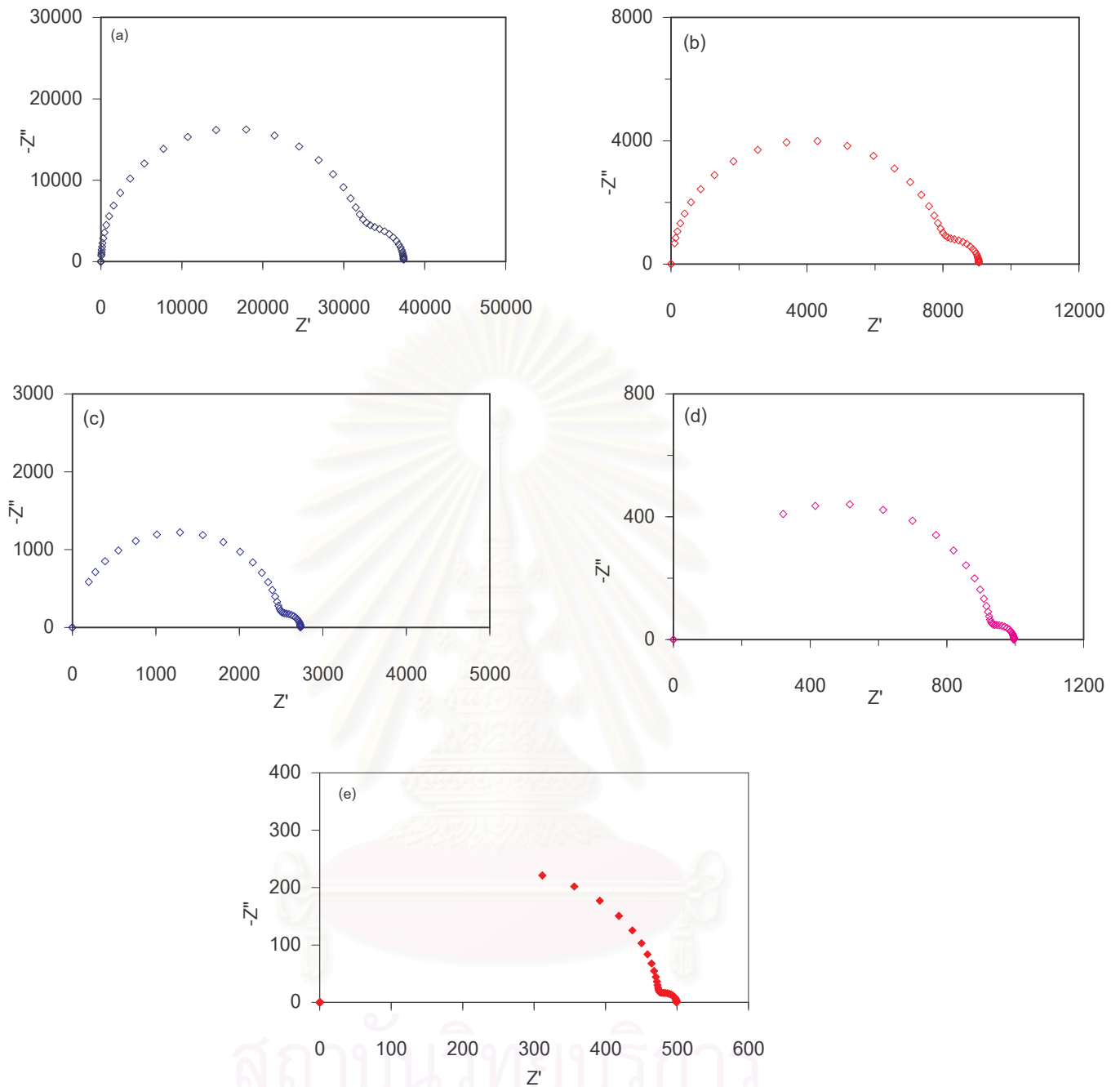


Fig B23: The Impedance Spectra of 8 mol% $\text{Y}_2\text{O}_3\text{-ZrO}_2$ (Daiichi) after sintering at 1550°C for 2 hours. The measurements were taken at 350°C (a), 400°C (b), 450°C (c), 500°C (d), and 550°C (e).

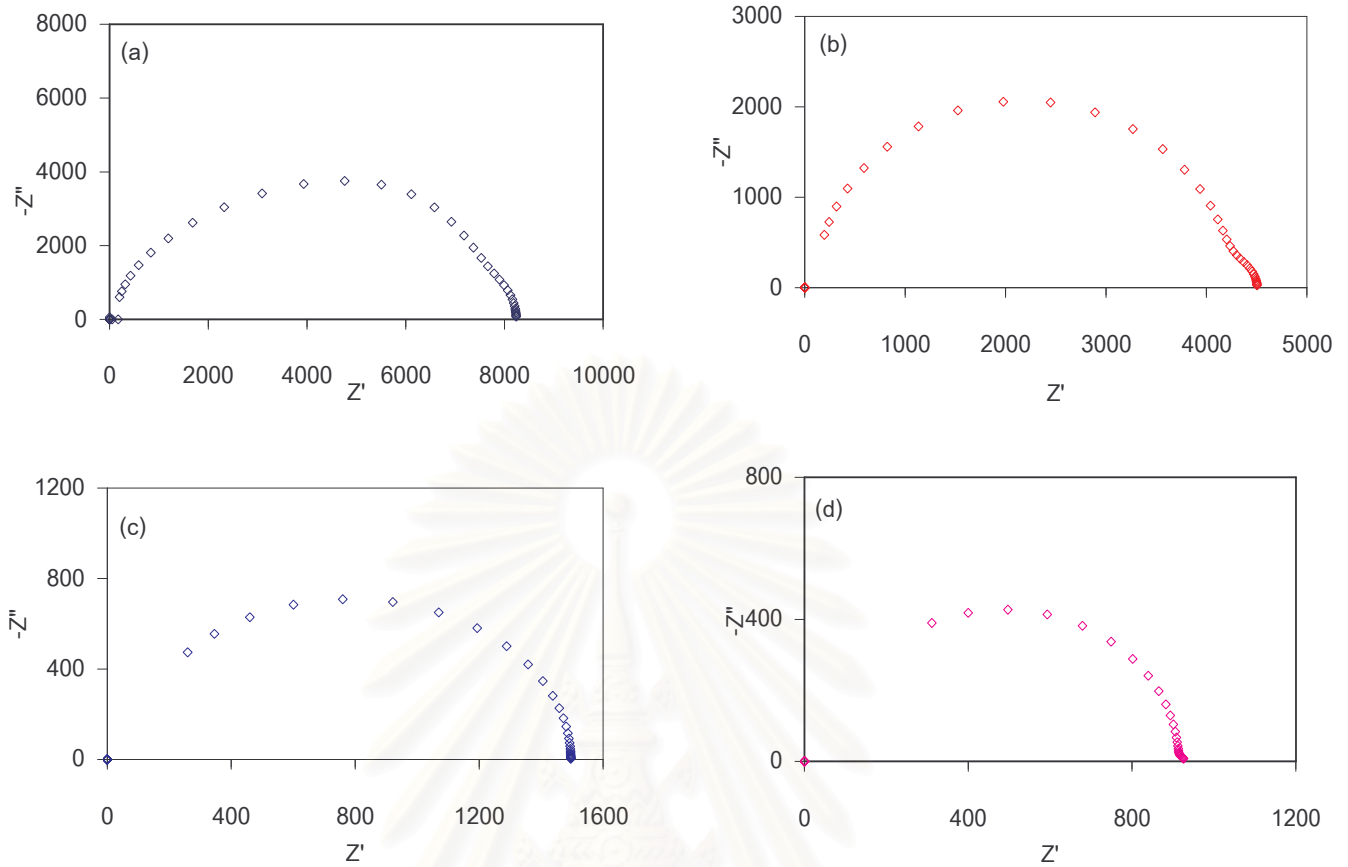


Fig B24: The Impedance Spectra of 8 mol% $\text{Y}_2\text{O}_3\text{-ZrO}_2$ (Daiichi) after sintering at 1550°C for 4 hours. The measurements were taken at 400°C (a), 425°C (b), 475°C (c), and 500°C (d).

สถาบันวิทยบริการ
จุฬาลงกรณ์มหาวิทยาลัย

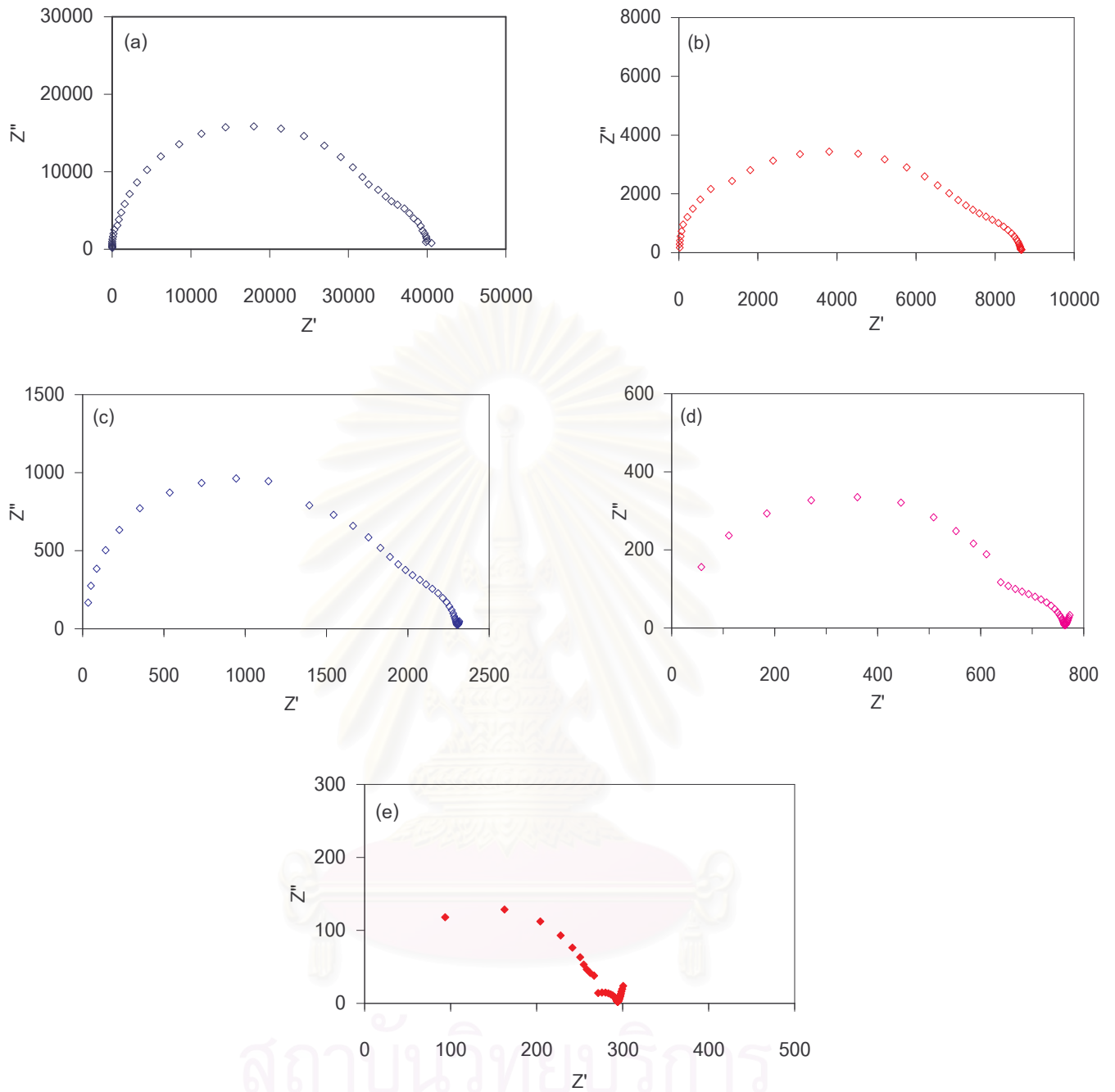


Fig B25: The Impedance Spectra of 10% $\text{Y}_2\text{O}_3\text{-ZrO}_2$ (Daiichi) after sintering at 1500°C for 1 hour. The measurements were taken at 350°C (a), 400°C (b), 450°C (c), 500°C (d), and 550°C (e).

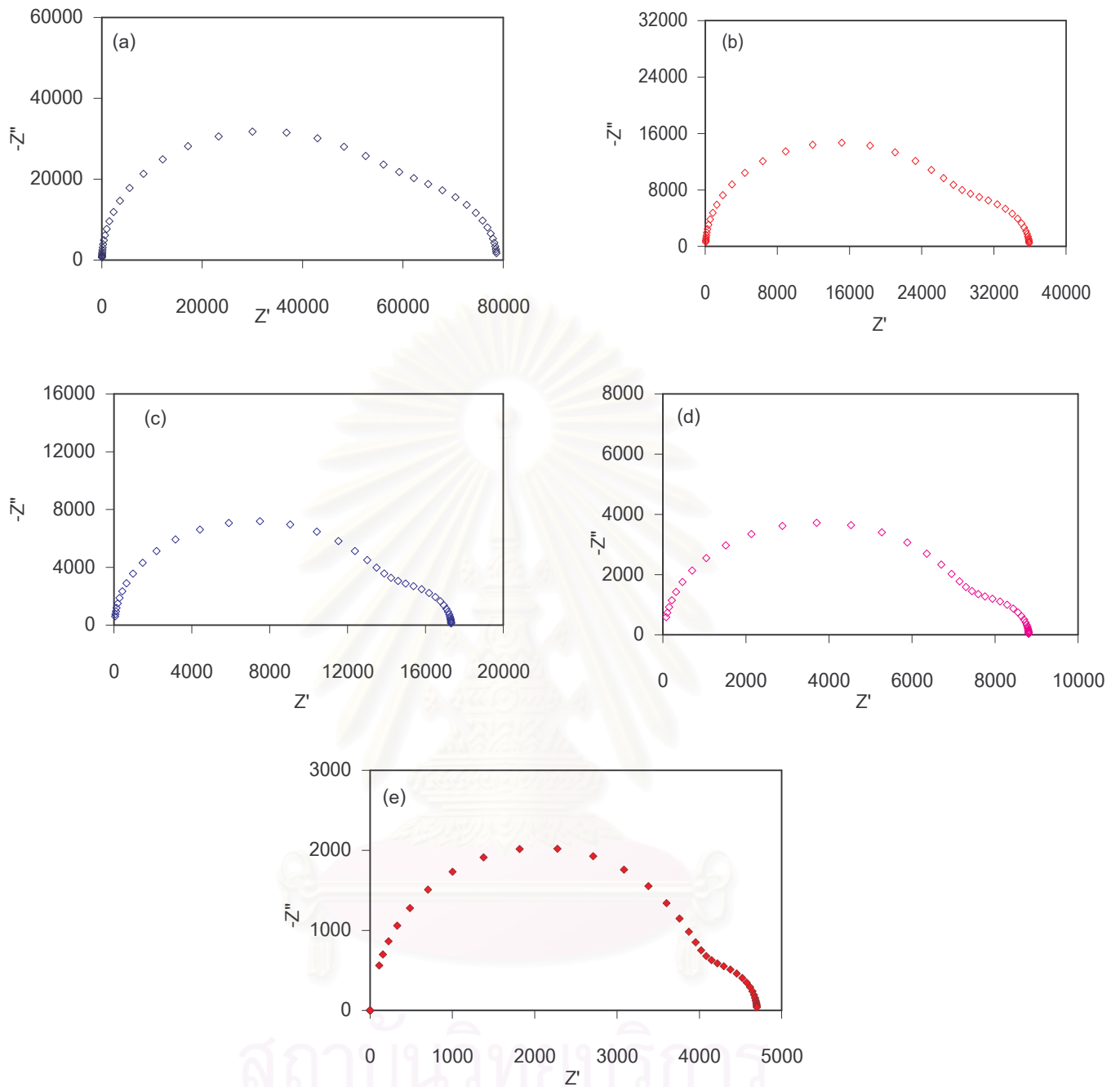


Fig B26: he Impedance Spectra of 10 % $\text{Y}_2\text{O}_3\text{-ZrO}_2$ (Daiichi) after sintering at 1500C for 2 hours. The measurements were taken at 350°C (a), 400°C (b), 450°C (c), 500°C (d), and 550°C (e).

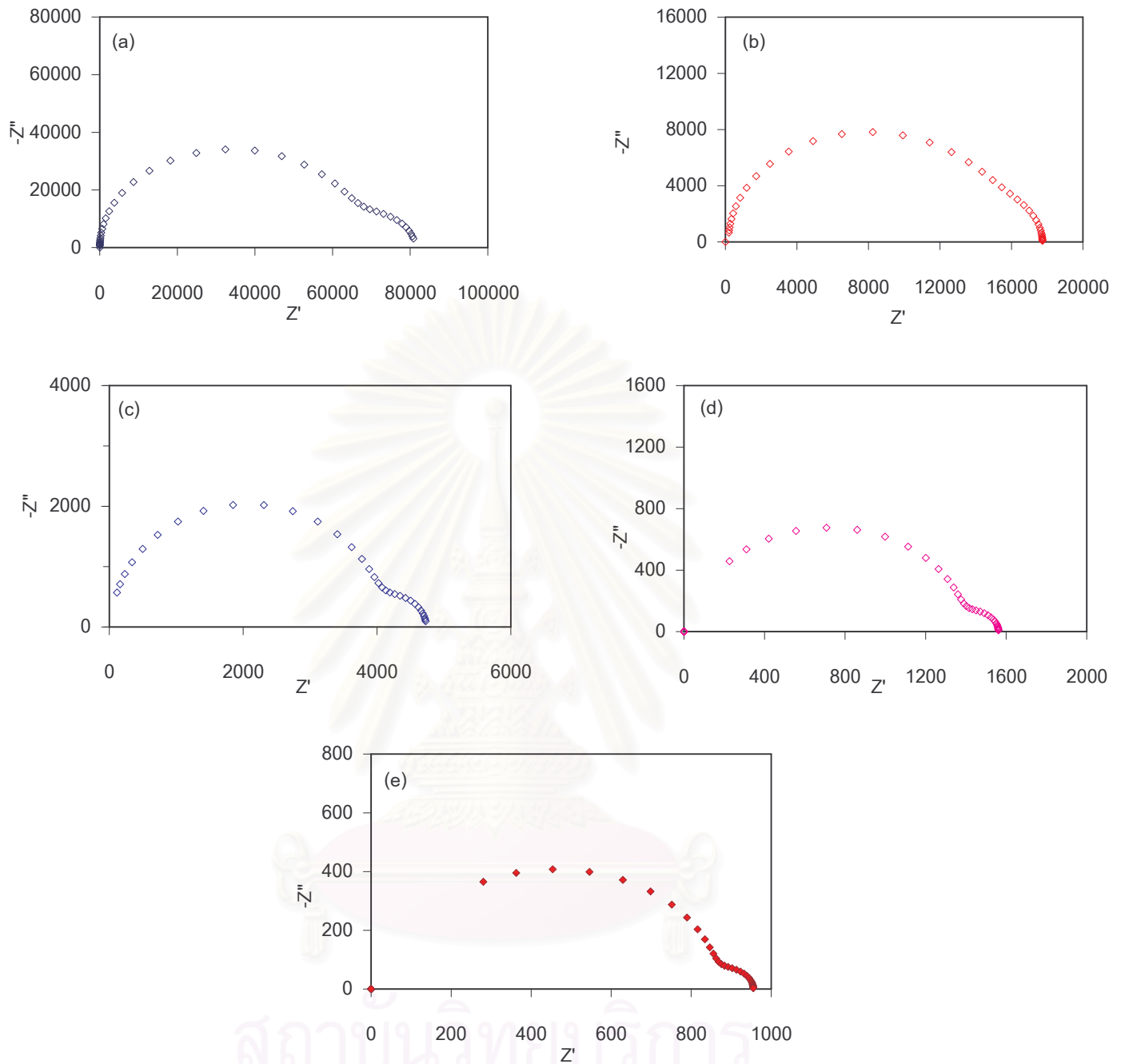


Fig B27: he Impedance Spectra of 10 % $\text{Y}_2\text{O}_3\text{-ZrO}_2$ (Daiichi) after sintering at 1500°C for 4 hours. The measurements were taken at 350°C (a), 400°C (b), 450°C (c), 500°C (d), and 550°C (e).

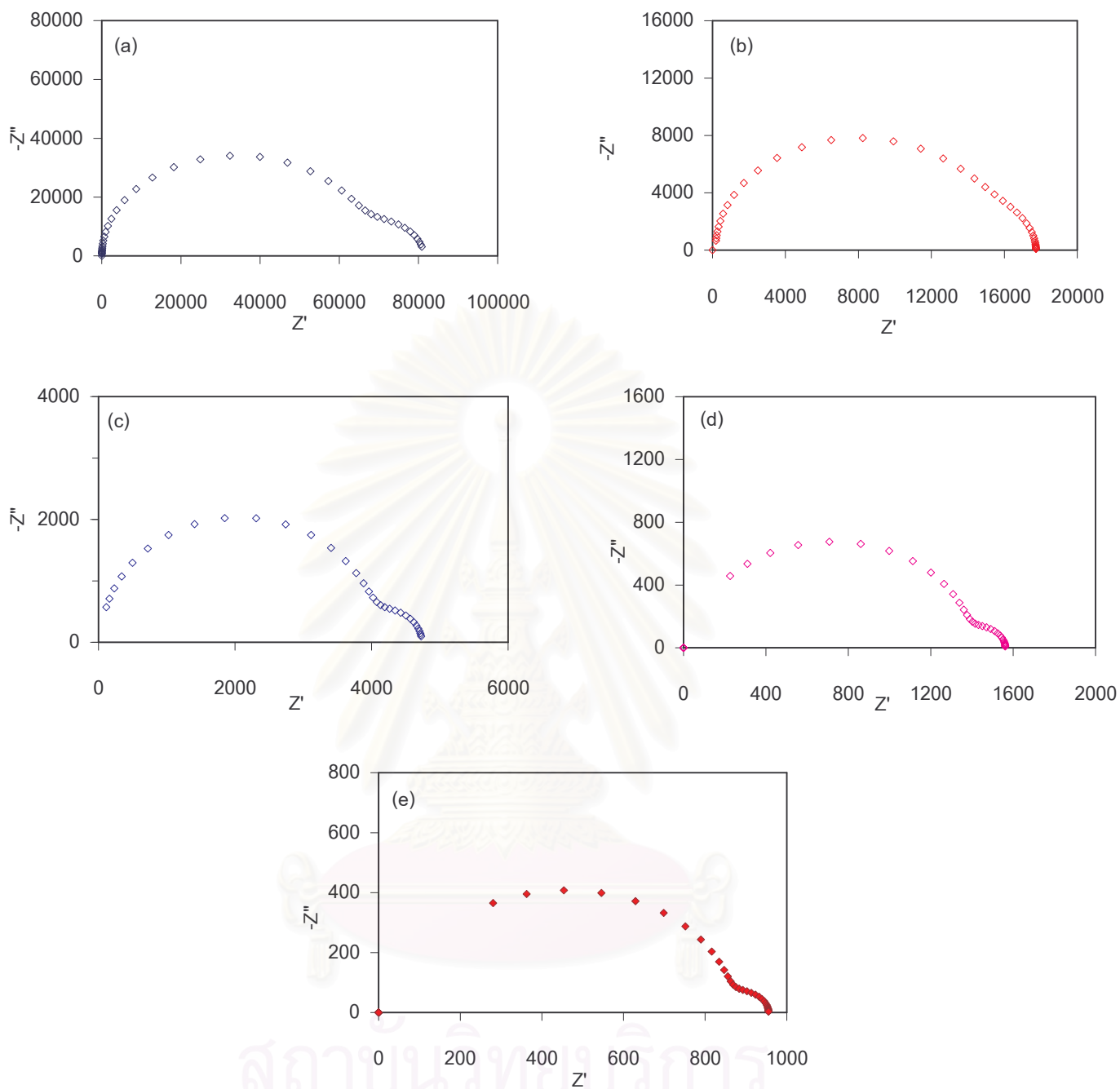


Fig B28: Impedance Spectra of 10 % $\text{Y}_2\text{O}_3\text{-ZrO}_2$ (Daiichi) after sintering at 1550°C for 1 hour. The measurements were taken at 350°C (a), 400°C (b), 450°C (c), 500°C (d), and 550°C (e).

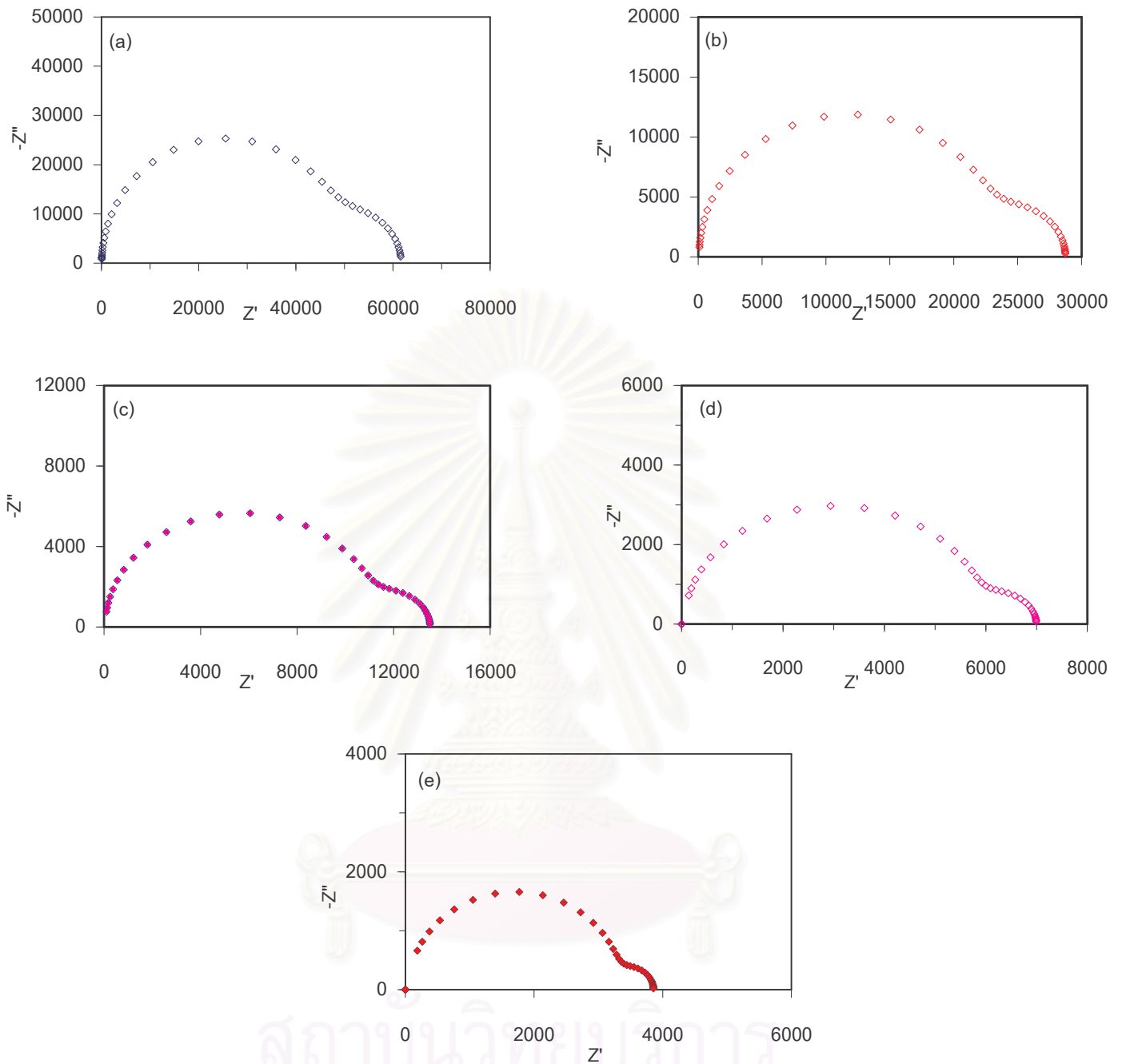


Fig B29: Impedance Spectra of 10 % Y_2O_3 - ZrO_2 (Daiichi) after sintering at 1550°C for 2 hours. The measurements were taken at 350°C (a), 375°C (b), 400°C (c), 450°C (d), and 550°C (e).

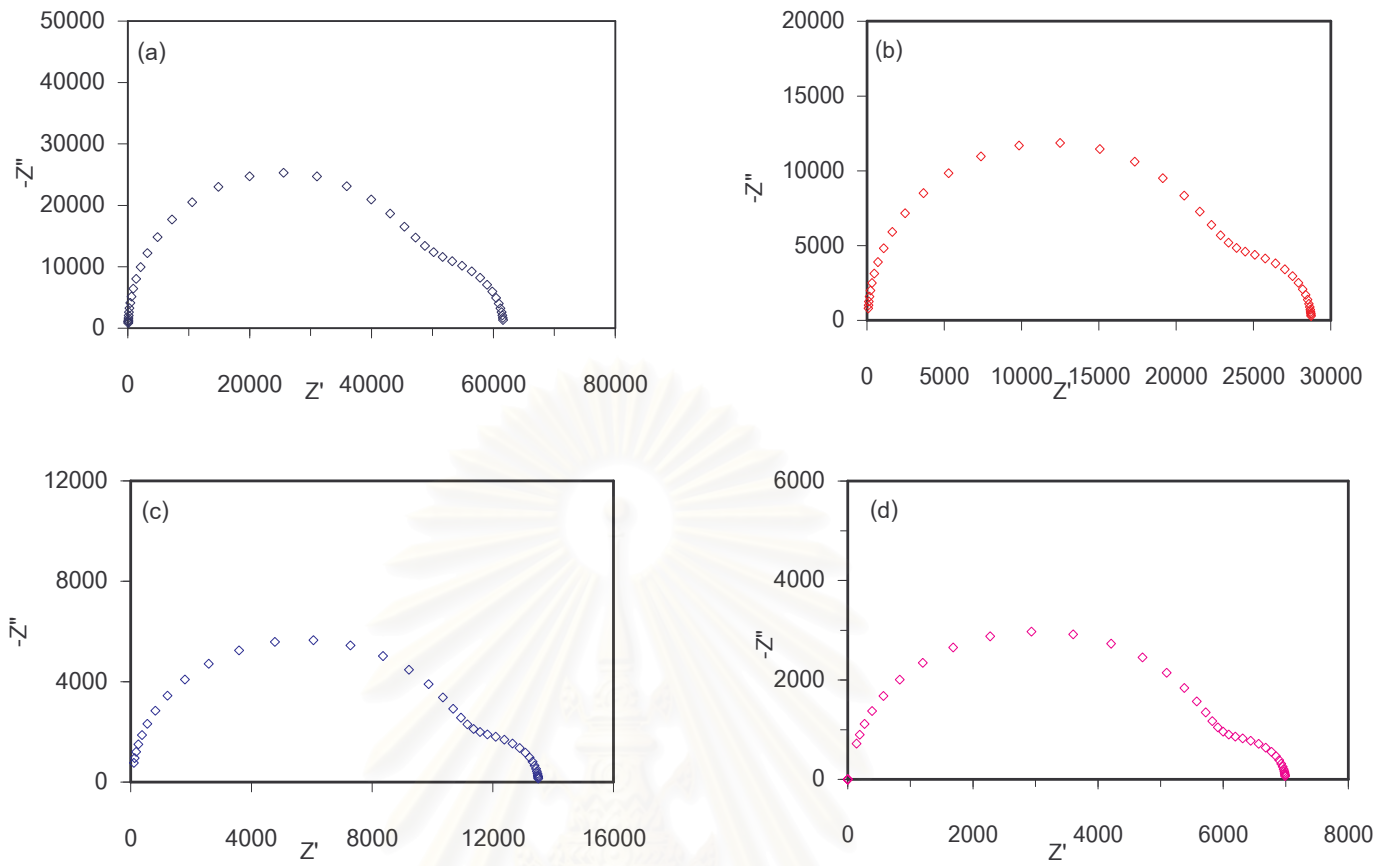


Fig B30: The Impedance Spectra of 10 % $\text{Y}_2\text{O}_3\text{-ZrO}_2$ (Daiichi) after sintering at 1550°C for 4 hours.

The measurements were taken at 350°C (a), 375°C (b), 400°C (c), and 450°C (d).

สถาบันวิทยบริการ
จุฬาลงกรณ์มหาวิทยาลัย

BIOGRAPHY

Miss Areerak Khamnoi was born on April 15th, 1975. She graduated from Chaingmai University with bachelor degree of Science in 1998. After graduation, she has been working as a nuclear chemist at the Office of Atomic for Peace. In 2003, she joined the faculty of Science, Chulalongkorn University and graduated with a Master Degree in Materials Science in 2006.



สถาบันวิทยบริการ
จุฬาลงกรณ์มหาวิทยาลัย